ADVANCES IN THE OPERATING CONDITION DESIGN ANALYSIS OF AIR BASED PHOTOVOLTAIC THERMAL SOLAR ROOF SYSTEMS

BY

HO-SUNG KIM

DISSERTATION

Submitted in partial fulfillment of the requirements
for the degree of Doctor of Philosophy in Architecture
in the Graduate College of the
University of Illinois at Urbana-Champaign, 2013

Urbana, Illinois

Doctoral Committee:

Associate Professor Richard K. Strand, Chair
Associate Professor Emeritus Michael T. McCulley
Associate Professor Scott C. Murray
Associate Professor Xinlei Wang

Abstract

Air based photovoltaic thermal (PV/T) solar systems combine the technologies of electricity generating PV cells and active solar energy to supplement the electricity and heating loads of buildings and potentially reduce energy consumption. There has been a significant amount of research on these systems over the past 30 years in which many researchers have investigated the merits of these systems. However, there is a lack of research on the energy efficiency of the proposed air based PV/T solar energy system when applied to buildings in various climates.

This study provides information on the analysis of the energy efficiency of an air based PV/T solar roof system when integrated with a building's existing HVAC system in various climates within the United States. Specifically, this study utilizes a computational and numerical analysis program that incorporates computational fluid dynamics (CFD) to investigate detailed fluid flow and heat transfer. The CFD simulations were carried out over a wide range of conditions to compute the inlet mass flow rate, momentum fluxes, fluxes of energy, and ultimately the thermal effectiveness of the solar roof system. The results showed that thermal conversion efficiency greater than 70% can be achieved with proper air channel depth, air mass flow rate, and a longer air channel length. Additionally, the results showed that performance of the proposed air based PV/T solar roof system eventually hits a maximum and that the level of incident solar radiation does not play a significant role once the system's thermal efficiency is near the maximum range. Together,

the findings suggest that the proposed air based PV/T solar roof system can be effective in various climates.

In addition to the CFD simulations, this study performed whole building annual energy simulations, using the EnergyPlus program, to obtain comprehensive insight in the understanding of the performance of an air based PV/T solar roof system for various climates within the United States. Two computational case study models, a small commercial office building and a quick-service restaurant were selected for this study. These were chosen because they are both designed with a Gable roof which can potentially expose half of the roof area to the sun depending on the roof configuration and orientation. Six different climatic zones within the United States were developed based on by the amount of insolation and the need for space heating. Local weather information of 28 cities was used in the simulations and analysis.

The findings from the annual building energy simulations demonstrated that climatic Zones 1 and 2, which have the highest mean daily total insolation, achieved the highest energy savings. In Zones 1 and 2, the small commercial office building showed an average of 31.1% in heating gas consumption savings and an average of 277.4 GJ in annual PV electricity production. As for the quick-service restaurant, an average of 40.7% of heating gas consumption was saved and an average of 230.9 GJ in PV electricity was produced in Zones 1 and 2. Results further show that the gas energy savings is proportional to the mean daily winter insolation and that energy saving of gas and electricity can be achieved in various climates within the United States using the air based PV/T solar roof system. It is also important to note, however, that the air based PV/T solar roof system is

not able to handle the entire heating load of a building but rather can supplement the existing HVAC system. Finally, a cost benefit analysis was also performed to evaluate the economic merit of the proposed air based PV/T solar roof system. Calculations showed that the estimated payback period in Flagstaff, AZ (Zone 1), Atlanta, GA (Zone 3), and Minneapolis, MN (Zone 6) are all less than six years.

Acknowledgements

First and foremost I would like to express my gratitude to my advisor, Professor Richard K. Strand, for his essential guidance and insight throughout my graduation student career. It has been an honor to be one of your students and thank you for being extremely supportive, constantly motivating and encouraging me throughout my Ph.D. pursuit.

Sincere appreciation is due to Professor Michael T. McCulley, Professor Scott C. Murray, and Professor Xinlei Wang, for your encouragement, expertise, insightful ideas, and for many intriguing questions and stimulating discussions.

I would also like to thank Daeho Kang, Daejin Kim, Dho Heon Jun, Harvey Jacobs, Heayoung Won, Heedon Choi, Junshik Um, Kangwook Jung, Kwang Ho Lee, Kyungrok Do, Kyuwan Kim, Moonhoon Hwang, Sangkoo Park, Sarah Jacobs, Seungjun Lee, Susan Jacobs, Taejin Ju, Useon Choi, Wonwoo Shon, Wooyoung Choi, Wooyoung Kang, and Young Tae Chae for providing support and friendship while as a graduate student at UIUC.

Finally, I would like to thank and dedicate this thesis to my lovely wife, Yoon Ju Kang, our beautiful daughter, Claire Jiwon Kim, my parents, Dal-Yong Kim and Young-Hee Lee, and my sister, So-Yeon Kim. This thesis would not have been possible without all of you. Thank you for your constant support and unconditional love.

Table of Contents

Chapter 1. Introduction

The use of solar energy has been gaining much interest given the concern related to climate change. Governments around the world including the United States consider climate change the greatest long-term challenge that will affect the human race and the environment. Efforts to reduce greenhouse gas emissions are increasing as it can be seen by a rise in the awareness of energy conservation and the development of new technologies. The reduction of greenhouse gas emissions resulting from buildings is a significant part of protecting the climate since buildings consume nearly 40% of all energy (of which approximately 20% relates to space heating) produced in the United States according to the U.S. Department of Energy's (DOE) 2008 Building Energy Data Book [1] and energy consumption is linked with the emission of greenhouse gases. Moreover, the U.S. Energy Information Administration (EIA) reports that in 2009, the Building Sector used 77% of all the electricity produced in the United States just to operate buildings and was responsible for nearly half (47%) of the United States carbon dioxide emissions [2]. Despite the fact that buildings are the largest source of emissions and energy consumption, they have tremendous potential for reducing energy usage through the implementation of energy efficiency measures and the application of renewable energy technologies. Although there are various technologies available for building applications, the sharp increase in the cost of fossil fuels and the high risk of the demand for energy exceeding the supply of electricity has resulted in energy optimization and research in renewable energy becoming a subject of intense interest.

The Sun is a source of renewable energy and it is ultimately responsible for most of the energy used by the Earth. The Sun is the power source for plants, the cause of air and water flow, and the source of warmth which makes the Earth habitable. Solar energy technologies also benefit the environment since they produce less air pollutants and do not emit greenhouse gases into the atmosphere.

Active solar energy is one potential solar building application. According to the U.S. Department of Energy (DOE), there are two different types of active solar energy systems based on the type of energy transfer fluid – liquid vs. air – that is heated in the solar energy collectors [3]. Solar radiation heats the fluid in the collector and then transfers the fluid directly to an interior space or to a storage system from which the heat is distributed. In most cases, active solar energy systems are auxiliaries or back-up systems to the central HVAC system of a building. The system is referred to as active as pumps or fans are used to move the fluid which is being used to transfer energy.

Photovoltaic (PV) materials and devices are another source of solar building applications. PV cells convert sunlight into electrical energy [4]. The popularity of PV is growing and the manufacturing of PV cells has advanced considerably in recent years, improving efficiency and reducing costs. PV is considered the third most important renewable energy source, following hydro and wind power, in terms of globally installed capacity. PV can be installed ground-mounted or integrated into walls or rooftops of buildings. In recent years, PV has come to be considered reliable and emission free and is gaining popularity worldwide.

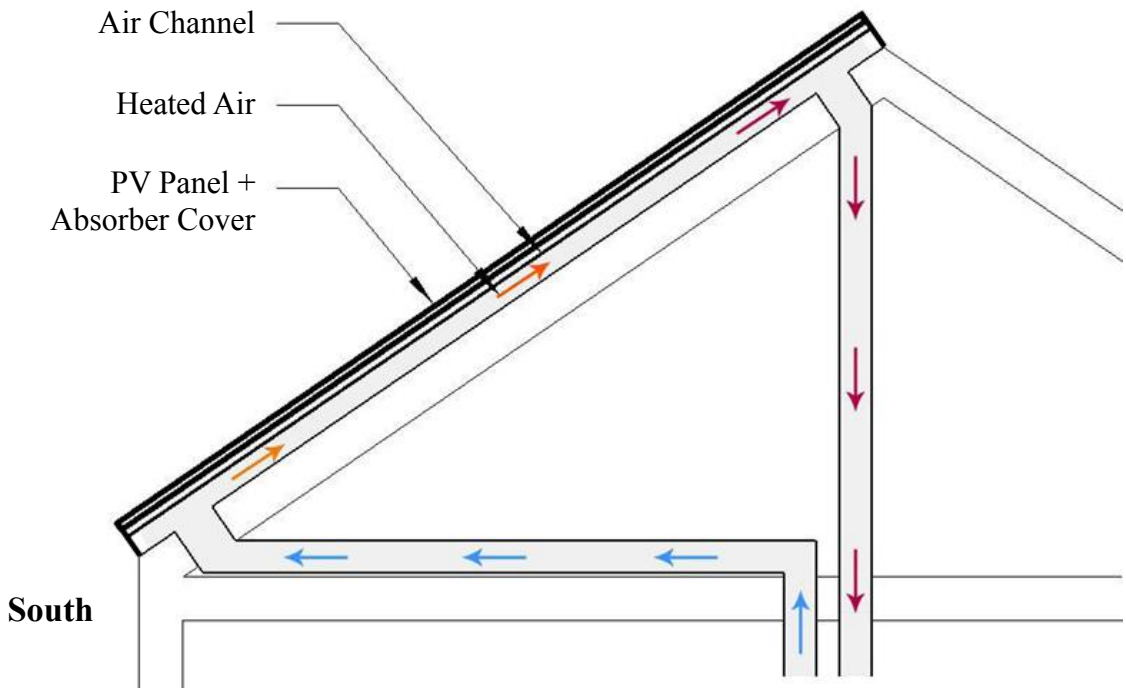

Figure 1.1 – Schematic airflow diagram of the air based PV/T solar roof system

One type of PV system that combines the technologies of air based solar energy systems and PV cells is commonly known as the 'air based photovoltaic thermal (PV/T) solar energy systems'. Air based systems are considered more durable than liquid based systems as they are not subject to corrosion, freezing, or overheating problems, weigh less, and are generally lower in construction cost [5]. One downside is that air has a lower heat capacity than water, thereby requiring the ducts to be sized significantly larger than comparable water pipes. Moreover, fan energy is higher than pump energy due to the much lower specific heat of air. This can impact the efficiency of an air system negatively. However, most buildings in the United States are already equipped with forced air HVAC

systems. Therefore, the need for ductwork is not necessarily a significant problem and enables a substantially simpler and safer system.

Air based PV/T systems are typically incorporated into a building's roof as shown in Figure 1.1. The roof is one of the most important elements in protecting the building against various weather conditions. The roof acts as an insulator to protect against the extremes of heat and cold while controlling the accompanying problems of air leakage and water vapor condensation. In most cases, the roof is exposed to the Sun more than any other surface of a building and is vital to the sheltering function of a building. One air based PV/T solar energy system which is integrated as part of the building's roof is called an 'air based photovoltaic thermal (PV/T) solar roof system'.

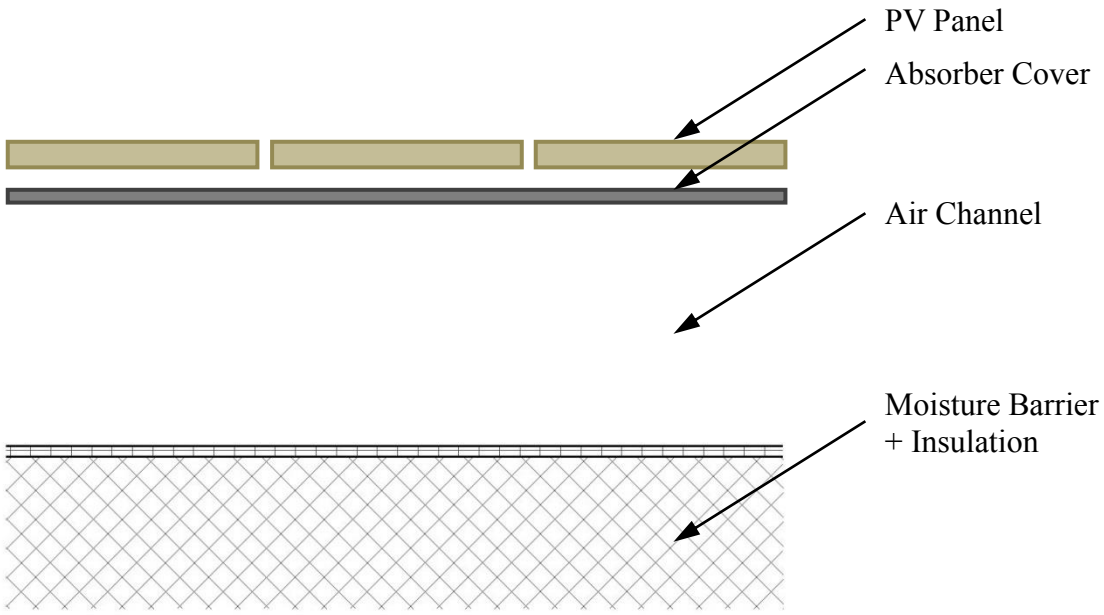

Figure 1.2 – Cross sectional diagram of the air based PV/T solar roof system

This configuration of the air based PV/T solar roof system consists of the PV panel, a metallic absorber cover (copper or aluminum), an air channel, and the insulation of the roof as shown in Figure 1.2. This configuration is the most common type of active PV/T solar collectors and is based on standards that have been established by the American Society of Heating, Refrigerating and Air Conditioning Engineers (ASHRAE) for testing the performance of solar collectors [6][7], and the Solar Rating and Certification Corporation [8].

There has been a significant amount of research on air based PV/T solar energy systems over the past 30 years including analytical and numerical models, experimental work, and the qualitative evaluation of thermal output [9][10][11]. Previous work shows significant energy savings may be possible with the utilization of air based PV/T solar energy systems when used correctly in various environmental settings. Despite such asserted benefits, there are no studies regarding the energy efficiency of this air based PV/T solar energy system when applied as a building application in various climates. Furthermore, there is a lack of annual building energy simulation data for these systems which is very important to configure the overall energy savings and payback period.

Predicting the performance of an air based PV/T solar roof system before they are actually manufactured and installed as part of the building's energy system is an important issue for the optimization of a design and minimizing energy consumption. This dissertation investigates this important issue using a computational and numerical analysis technique that is widely adopted in engineering, architectural design, and natural environmental analysis. Specifically, this study utilizes a tool called computational fluid

dynamics (CFD) that is often used for HVAC design and indoor thermal environment. This technique has the potential to assist investigations of detailed fluid flow and heat transfer analysis as well as allowing the incorporation of realistic boundary conditions and obstructions. Analyzing and optimizing the proposed air based PV/T solar roof system through numerical CFD studies can be accomplished in terms of thermal efficiency, which can be defined as the ratio of the useful heat gain of the entire air system versus total incident solar radiation on the gross surface area of the PV/T solar roof.

In addition to using a CFD analysis tool, this study will also perform whole building annual energy simulations using the EnergyPlus program to examine the energy efficiency of the air based PV/T solar roof system and obtain a comprehensive insight towards understanding its performance for various climates within the United States. The numerical analysis of the CFD studies will be incorporated into the whole building energy simulations to determine how the system responds to building thermal loads under different building circumstances and establish what limitations the system has if it is to be implemented into buildings from the perspective of building energy consumption and occupants' thermal comfort. Two buildings types, a quick-service restaurant and a small commercial office building, will be used to compare the proposed system to conventional mechanical air conditioning system and the thermal performances will be assessed for both heating/cooling design days as well as annual energy calculations. Furthermore, overall impacts or benefits of the air based PV/T solar roof system will be presented in terms of energy consumptions/savings and CO_2 emissions.

In this chapter, the background of active solar energy systems and the overall scope and methodologies of this study are presented. Chapter 2 reviews the past work in the existing literature relevant to the study and provides definitions and parameters affecting air based PV/T solar energy systems. Chapter 3 presents the theoretical backgrounds and numerical equations in the modeling of the air based PV/T solar roof system within a whole building annual energy simulation program. Chapter 4 presents the properties of the case study models used for the CFD and whole building annual energy simulations. Chapter 5 presents the modeling process of the air based PV/T solar roof system in Fluent (a CFD analysis program) and describes the parametric studies for the performance improvement of the air based PV/T solar roof system. Chapter 6 presents the modeling process in EnergyPlus (whole building annual energy simulation program), the results, and findings from annual building energy simulations for various climates. Finally, Chapter 7 provides the conclusions of this study and proposes some suggestions for future research.

Chapter 2. Literature Review

An air based photovoltaic (PV/T) solar collector is attractive as it can achieve a higher overall efficiency for converting sunlight into useful energy compared to either a PV collector or a conventional solar thermal collector. Zondag et al. [14] found that the electrical and thermal performances of PV/T solar collectors are lower than that of separate PV collector and solar thermal collector. However, placing two PV/T collectors next to each other produced more energy per unit surface area than of one PV collector and one solar thermal collector next to each other. This indicates that PV/T solar collectors have higher energy conversion efficiency per unit surface area than the total efficiency of a PV collector and a solar thermal collector side by side due to the utilization of a greater fraction of the incident solar radiation. This can be an important design element where the availability of a surface area can be limited, such as the roof of a building.

This chapter presents a review of the available literature on air based PV/T solar collectors. It is presented in a thematic way, in order to enable an easier comparison of the findings obtained by various researchers, especially on parameters affecting the performance and efficiency of the air based PV/T solar collectors.

2.1 Parametric Studies Affecting Performance

Important control parameters or main design considerations affecting the performance of the air based PV/T solar energy system can be identified as the air mass flow rate, the dimensions of air the channel, and the use of a glass cover. The air mass flow rate and the dimensions of the air channel dictate the heat transfer from the absorber to the

air within the air channel. The use of a glass cover influences how much solar radiation absorbs on the PV panel and acts as a thermal barrier to reduce heat loss from the top of the air based PV/T solar energy system. However, the insulating effect of the glass cover causes the PV panel to operate at a higher temperature, which results in a lower electrical efficiency [15][16][17]. Comparisons of thermal and electrical performances of glazed and unglazed PV/T solar energy systems are explained further below.

2.1.1 Heat Transfer Air Mass Flow Rate

The air mass flow rate is a critical parameter in determining the performance and efficiency of an air based PV/T solar energy system since the convective heat transfer coefficient is dependent on the air mass flow rate. Bhargava et al. [18], Sopian et al. [19], Garg et al. [20], Hegazy [21], Tonui et al. [22], and Sarhaddi et al. [23] investigated the thermal, electrical, and overall performances of air based PV/T solar energy systems under steady state conditions. All of these studies examined different configurations of air based PV/T solar energy systems and the effects of air mass flow rate as well as the selectivity of the absorber plate.

As an example of the different configuration and parameter studies, Hegazy [21] investigated the thermal, electrical, hydraulic, and overall performance of four different types of PV/T air collectors which the fluid is either flowing over or under the absorber, on both sides of the absorber in a single or double pass, as shown in Figure 2.1. Numerical analysis was performed for each model determining the effects of air mass flow rate on collector's performance. Hegazy [21] mentions that Model III (with air flowing on both sides of the absorber in a single pass) followed by Model IV (with air flowing on both sides

of the absorber in a double pass) has the highest overall performance and is suitable design for converting solar radiation into thermal and electrical energy.

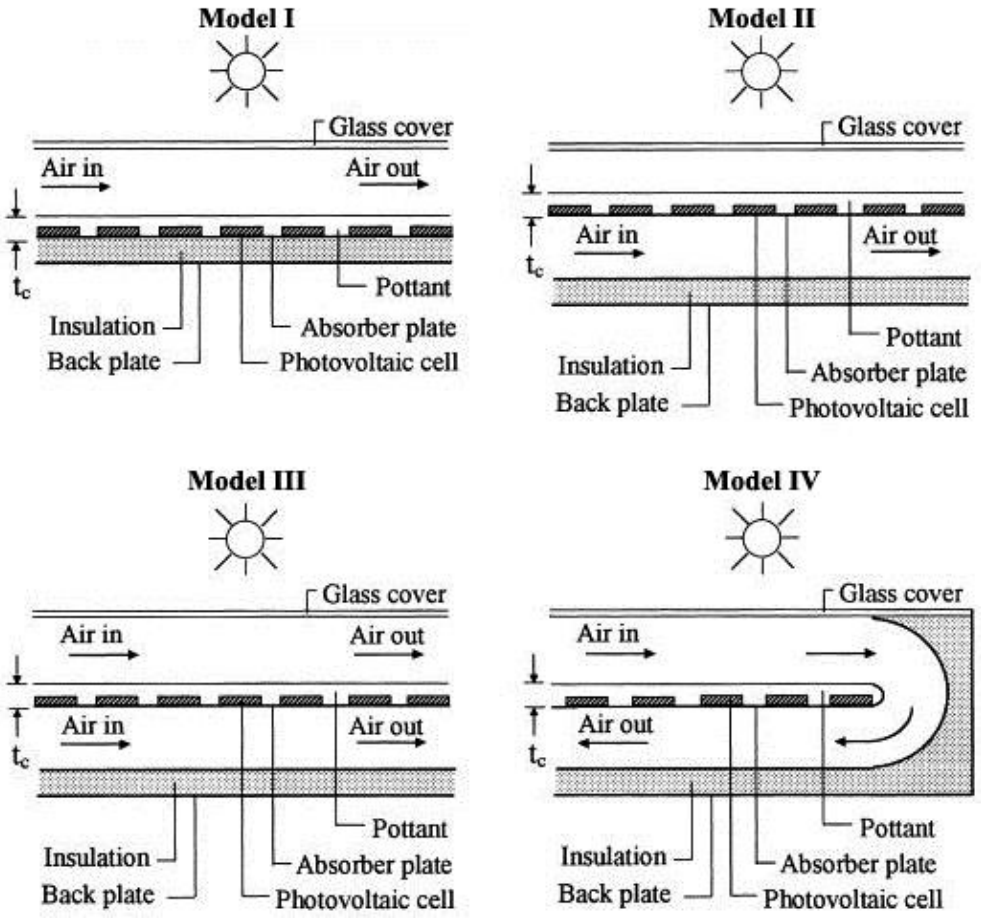

Figure 2.1 – Cross sections of various air based PV/T solar energy systems [21]

Tonui et al. [22] also examined different configurations and parameters of PV/T air collectors with the use of glass cover, thin flat metal absorber suspended at the middle of the air channel, and vertical metal absorber fins attached on the back wall, as shown in Figure 2.2. This study developed numerical models for each configuration and an experimental model was also built and examined to validate against the numerical data.

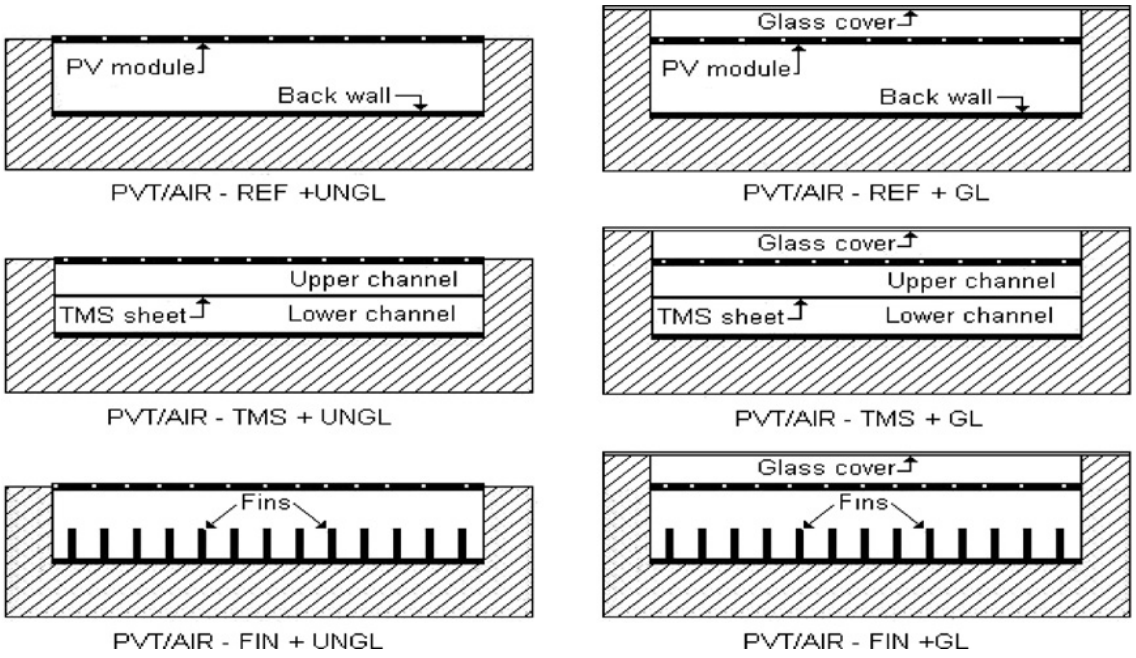

Figure 2.2 – Cross sections of various air based PV/T solar energy systems [22]

Hegazy [21] and Tonui et al. [22] made improvements to achieve a higher collector performance and both findings suggest that the thermal and electrical efficiencies of air based PV/T solar collectors are enhanced with an increase in the air mass flow rate. Based on numerical steady state energy models, Figures 2.3 and 2.4 present comparisons between the various models of air based PV/T solar collectors as a function of the air mass flow rate. As can be seen from both figures, the relationship of the thermal and electrical efficiency to the air mass flow rate is one of diminishing returns. In other words, the increase in air mass flow rate substantially benefits thermal and electrical efficiency at low levels of air mass flow rate and gradually steadies off as air mass flow rate increases.

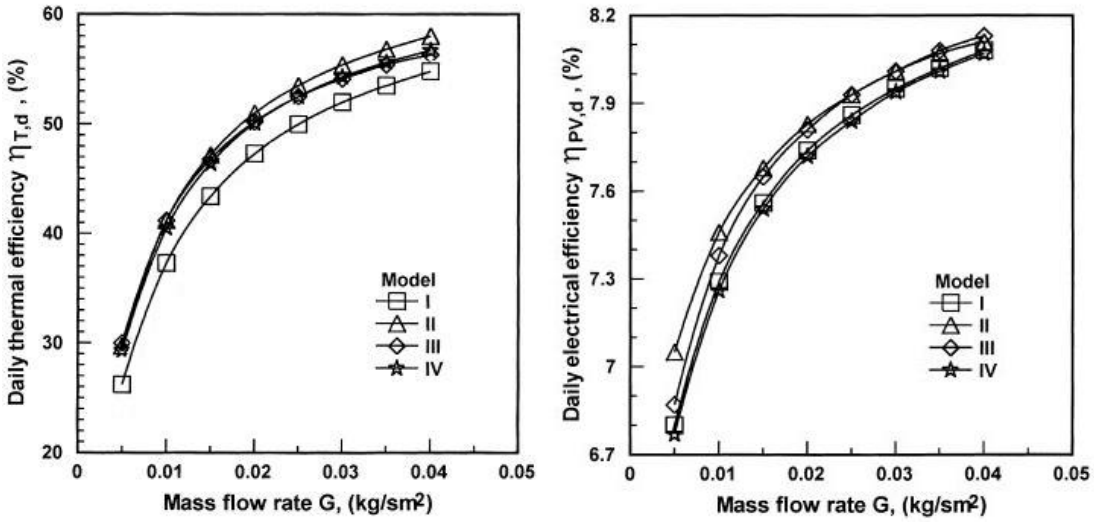

Figure 2.3 –Thermal and electrical efficiency as a function of mass flow rate [21]

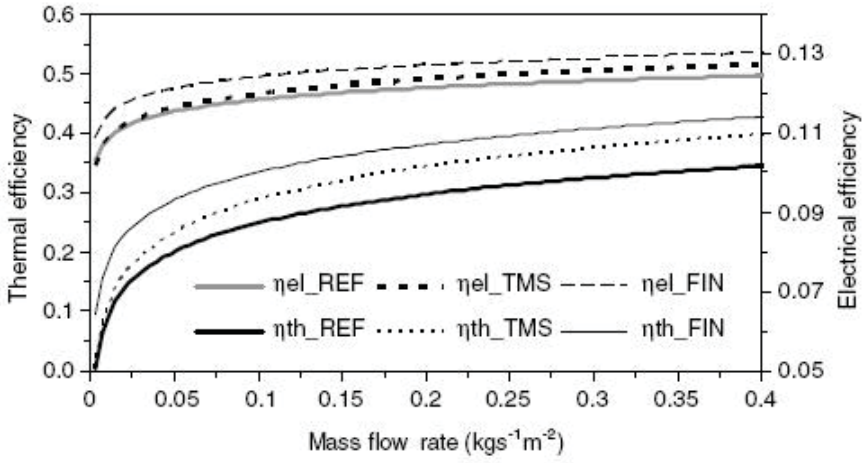

Figure 2.4 – Combined thermal and electrical efficiency as a function of mass flow rate [22]

Garg and Adhikari [20], Hegazy [21], Tonui and Tripanagnostopoulos [22], Prakash, J. [24], and Chen et al. [25] further propose that increasing the air mass flow rate decreases the air temperature within the air channel of an air based PV/T solar collector. This ultimately corresponds to a decrease in the outlet air temperature. The variation in air

temperature rise as a function of the air mass flow rate is illustrated in Figures 2.5 and 2.6. The decrease in air temperature rise is caused by a higher convective heat transfer coefficient resulting at higher air flow rates. However, the higher convective heat transfer coefficient is more dominant and leads to a greater rate of heat removal from the air channel despite the lower air flow rate.

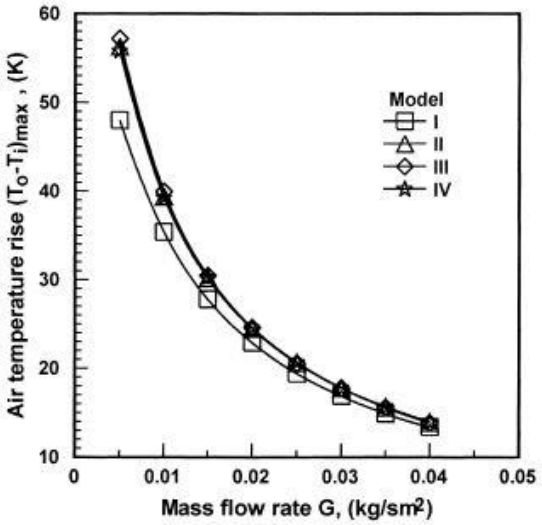

Figure 2.5 – Air temperature rise as a function of air mass flow rate [21]

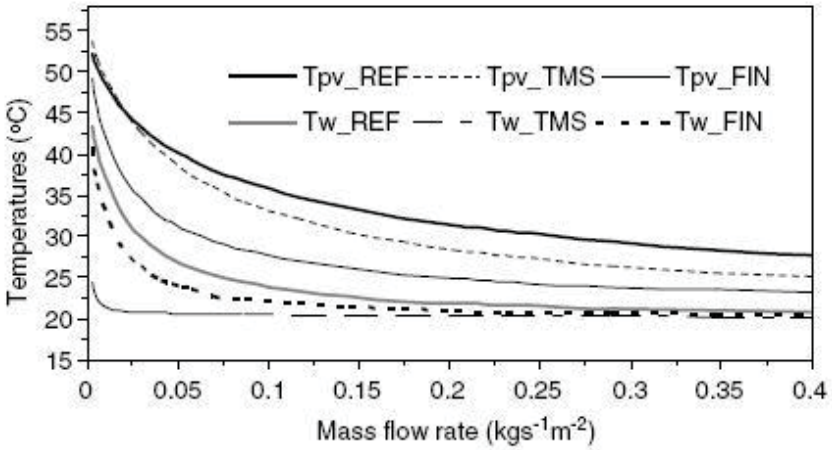

Figure 2.6 – Air temperature rise as a function of air mass flow rate [22]

According to the U.S. DOE [3], it is recommended that the air mass flow rate through a standard solar air collector be in the range of 0.0063 – 0.0189 kg/s·m^2 and the velocity be in the range of 1.5 – 3.1 m/s. The air mass flow rates discussed within the literatures do not all fall in this range and, therefore, require further investigation. CFD analysis will assist in the further investigation of the detailed air fluid flow and heat transfer analysis and enhance our understanding of the optimum air mass flow rate of air based PV/T solar roof systems in various climates.

2.1.2 Air Channel Dimensions

The dimensions of the air channel such as its depth and length are also important in determining the performance and efficiency of air based PV/T solar energy systems. There have been theoretical studies examining the effect of varying the air channel's depth on the operating temperature of the PV unit and the outlet air temperature of an air based PV/T solar collector [22][26]. Tonui and Tripanagnostopoulos [22] state that varying the air channel depth from 0.05m to 0.5m increases the operating temperature of the PV unit from 36℃ to 50℃ and decreases the outlet air temperature from 26℃ to 21℃ using an irradiance of 800 W/m^2, an inlet air temperature of 20℃, and air mass flow rate per unit area of 0.05 kg/s·m^2. Furthermore, thermal efficiency decreased from 30% to 5% and electrical efficiency also dropped from 11.8% to 10.6%. These effects can be attributed to the decrease in air velocity with the increase in channel depth, as the air mass flow rate was kept constant in the study. This is consistent with the air mass flow rate being equal to the mass density of air multiplied by the air velocity and the cross-sectional vector area/surface. Since the cross-sectional area increases with an increase in channel depth, the air velocity

would need to decrease to result in a constant air mass flow rate. This suggests that if air mass flow rate is maintained constant throughout the air channel, the depth of the air channel should be as shallow as possible to increase the air velocity. Hegazy [26] finds further support for such an argument as that study finds that the thermal efficiency and the rise of the air temperature ($T_{out} - T_{in}$, temperature of outlet minus temperature of inlet) of an air based PV/T solar collector decreases as channel depth increases. The findings of the study based on various air mass flow rates are illustrated graphically in Figure 2.7. Overall, prior literature suggests shallow air channels are more beneficial in improving electrical and thermal efficiency of an air based PV/T solar energy system given a constant air mass flow rate since it will increase the air velocity in the channel.

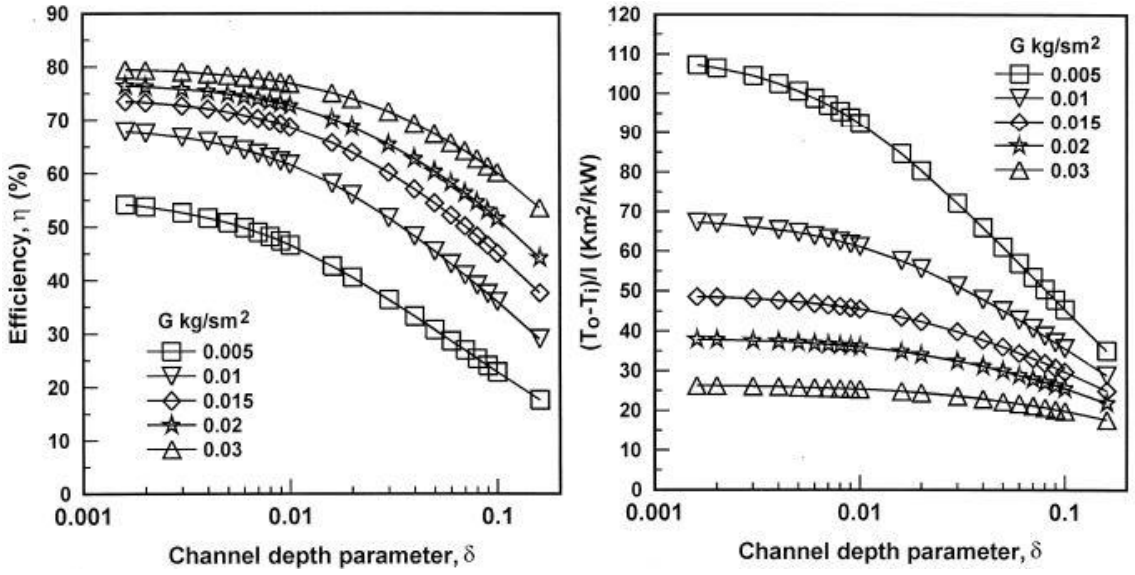

Figure 2.7 – Thermal efficiency and temperature rise as a function of channel depth [26]

The length of the air channel is another parameter that affects the air based PV/T solar energy system's performance. A longer air channel means that the air traveling through the air channel, for a given air mass flow rate, is exposed to solar radiation and the absorber for a longer period of time which results in an increase in the outlet air temperature.

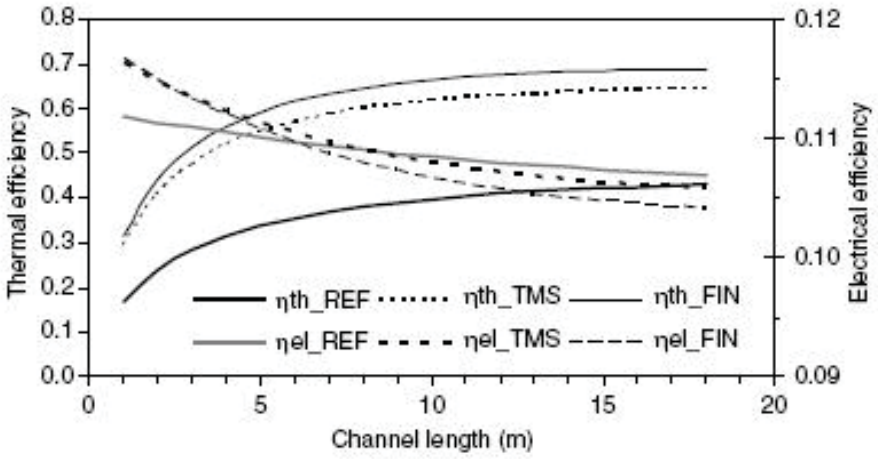

Figure 2.8 – Combined thermal and electrical efficiency as a function of channel length [22]

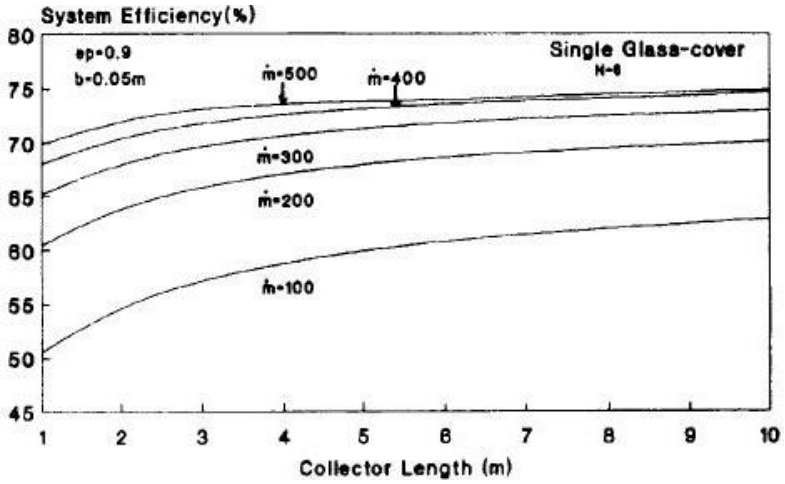

Figure 2.9 – System efficiency as a function of air channel length [27]

Sopian et al. [19] states that an air based PV/T solar collector, with a length of 1m, the outlet air temperature of 44℃ can be reached under the conditions of having an irradiance of 1000 W/m^2, an inlet air temperature of 22℃, and an air mass flow rate of 0.028 kg/s·m^2. If the length of the air channel is increased to 2m, the outlet air temperature is increased to 48℃. Similarly, Tonui and Tripanagnostopoulos [22] and Garg and Adhikari [27] report that an air based PV/T solar collector's system efficiency increases with an increase in air channel length. The results of the variation of performance parameters with collector length are represented in Figures 2.8 and 2.9.

2.1.3 Glazed vs. Unglazed Systems

The function of the glass cover is to permit penetration of shortwave solar irradiation on the PV panel of an active PV/T solar energy system while providing protection from the natural environment. However, having a glass cover reduces the irradiance incident on the PV panels due to the energy that is absorbed in the glass and also reflected from the glass. In addition, the insulating effect of the glass cover causes the PV panels to operate at a higher temperature, thus resulting in a lower electrical efficiency [28][29][30][31][32][33]. All of the studies that examine unglazed vs. glazed systems are in agreement that the thermal performance of unglazed systems is lower than panel glazed systems. However, unglazed systems have been documented to have better electrical performance than glazed systems. Given such findings, whether or not to implement a glass cover over the air based PV/T solar energy system will depend on which of the two – thermal vs. electrical efficiencies is more important. Due to the higher expense of the PV panels, the electrical output is generally favored. Based on an analysis of thermal vs.

electrical energy, Coventry and Lovegrove [34] state that generation of electrical energy is over 4 times more valuable than that of thermal energy due to the higher costs of PV cells according to renewable energy market research.

As seen in the cross sectional diagram of the proposed air based PV/T solar roof system in Figure 1.2, this dissertation investigates only the unglazed system. Even though unglazed systems have lower thermal performances compared to glazed systems, implementing a thick glass roof requires the redesign of structural elements which can lead to a significant increase in the construction costs. Unglazed systems are a much simpler design and can be installed on existing rooftops without replacing the whole structure of the roof. Easier maintenance accessibility of the PV panels is another reason for having unglazed systems. If the PV panel needs maintenance and is placed inside of the air channel with a glass roof on top, the accessibility is more difficult compared to the PV panel being exposed on the outer building envelope.

2.2 Computer Simulation Case Studies

Despite the significant amount of research on active PV/T solar energy systems for the past 30 years, there are only a few computer simulation studies that analyze the energy efficiency when these systems are applied as part of the building envelope. Some of the researchers have used the TRNSYS computer simulation software, which focuses on assessing the performance of thermal and electrical energy systems. The TRNSYS software offers strengths as providing a graphical interface with easy drag and drop components and it has the capability of modeling a variety of energy systems in differing levels of complexity [35].

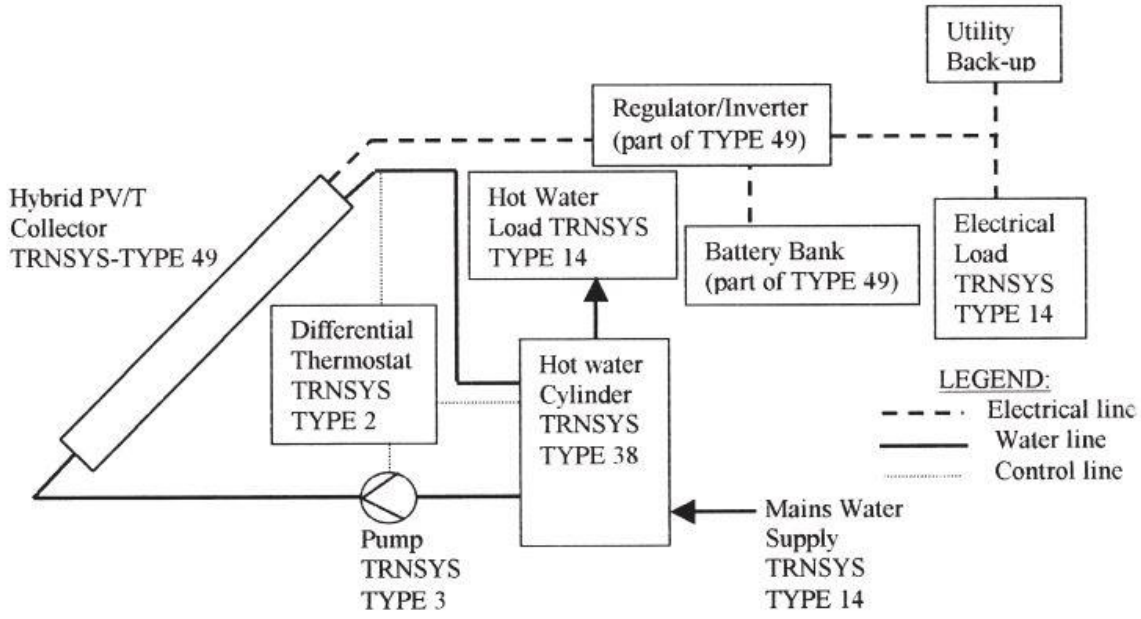

Figure 2.10 – Schematic diagram of liquid based PV/T solar energy system [38]

Bloem [36] and Bosanac et al. [37] both used TRNSYS to determine the annual thermal and electrical efficiency and optimum air mass flow rate. However, both of these studies were in the context of façade integrated and not roof integrated systems. Kalogirou [38] modeled a residential building in Nicosia, Cyprus and ran simulation studies using TRNSYS, but the Kalogirou study was in the context of liquid based PV/T solar energy systems. As shown in the schematic diagram of Figure 2.10, the solar energy system included of a series of PV panels, a battery bank and an inverter, a hot water storage cylinder, a pump, and a differential thermostat. The objective of the study was to quantify the magnitude of the solar energy system's advantages with respect to its output and life cycle savings. The study states that the mean annual thermal and electrical efficiency of the liquid based PV/T solar energy system can be increased by approximately 29% when

compared to a standard PV system. It is also stated that the system's payback time is found to be roughly 4.6 years.

2.3 Summary

This chapter presents a review of the prior research on active PV/T solar energy technology. The review is focused on the important control parameters affecting the performance of the air based PV/T solar energy system such as the air mass flow rate, the dimensions of the air channel, and the use of a glass cover. Numerous researchers have investigated various design configuration and performance improvements of air based PV/T solar energy systems. However, there is a lack of research regarding annual building simulations in the context of roof integrated, air based PVT systems. A summary of the available literature on air based PV/T solar energy systems including the dimensions and air mass flow rates of each study are shown in Table 2.1.

Research findings suggest that the optimum air mass flow rate for an air based PV/T solar energy systems should be in the range of 0.001 – 0.075 kg/s·m^2, whereas the U.S. DOE [3] recommends the range of 0.0063 – 0.0189 kg/s·m^2. Such inconsistency warrants further investigation regarding the optimum air mass flow rate. The CFD analysis studies performed as part of this dissertation will assist further investigations of detailed air fluid flow and heat transfer analysis to obtain better insight on the optimum air mass flow rate in various air channel designs for air based PV/T solar systems.

Authors	Research	Air Mass Flow Rate (kg/s·m^2)	Air Channel Depth (m)	Air Channel Length (m)	Air Channel Width (m)	PV Nominal Power (Watt-peak)
Bhargava et al. [18]	Numerical	0.006 - 0.07	0.05 - 0.15	2.0 - 5.0	-	-
Sopian et al. [19]	Numerical	0.001 - 0.083	0.1	1.0	-	-
Garg et al. [20]	Numerical	0.007 - 0.04	0.05	2.0	1.0	130
Hegazy [21]	Numerical	0.005 - 0.04	0.023	9.0	1.0	1000
Tonui et al. [22]	Numerical and Experimental	0.001 - 0.4	0.05 - 0.5	18.0	0.4	46
Sarhaddi et al. [23]	Analytical	0.05	0.05	1.2	0.45	75
Chen et al. [25]	Experimental	0.001 - 0.0056	0.038	6.2	10.4	2856
Candanedo et al. [28]	Experimental	0.026	0.04	2.84	0.39	66
Dubey et al. [29]	Analytical	0.0058	0.04	1.0	0.605	73
Aste et al. [30]	Experimental	0.018	0.075	2.0	1.2	240
Bloem [36]	Experimental	0.03 - 0.075	0.1	1.2	1.2	100

Table 2.1 – Summary of literature on air mass flow rate and air channel dimensions

Past research also shows that the thermal performance of unglazed systems is lower than glazed systems. However, unglazed systems increases irradiance incident on the PV panels, resulting in higher electrical energy production. As a consequence, the optimal configuration of glazed vs. unglazed is a compromise between the thermal and electrical efficiencies and depends on the operation profile of the PV/T solar energy system and the user's needs. For high temperature operations, increasing the thermal efficiency is generally the priority which tends to point towards a glazed system. Unglazed systems can meet both the thermal and electrical demands and tend to be preferable for low temperature operations. Nevertheless, due to the high costs of PV cells, the generation of electrical energy is generally favored and thus unglazed systems are more commonly chosen. Having a glass cover increases the complexity of the design and also increases its costs. In addition, PV

panels need periodic maintenance inspections and having a glass cover results in increased difficultly of such maintenance.

Currently, the market for air based PV/T solar energy systems is fairly small and only a very limited number of systems have been built. However, the literature shows that these systems are a very promising application of renewable energy technology. The utilization of this environmentally friendly, renewable energy system depends on the climatic region and operation profile of implementation. This dissertation builds on this line of research based on computer simulations and enables a more comprehensive understanding of optimizing the energy efficiency of air based PV/T solar systems in various climates. Specifically, this study generates and utilizes both CFD and annual building energy simulation results for air based PV/T solar energy system in order to make them more energy efficient and economically competitive and thus aid in the application of this environmentally friendly renewable energy system during the critical design development stage of a building. Without this ability, air based PV/T systems will continue to see limited use in buildings and a potential source of significant energy and improved building efficiency will be overlooked and thus wasted.

Chapter 3. Theoretical Background

This chapter presents the concepts of modeling, governing equations for the energy balance, and concepts used for the building simulation of the air based PV/T solar roof system. The model of the air based PV/T solar glass roof system is based on the equations found in a variety of sources including ASHRAE Standard 93 – Methods of Testing to Determine the Thermal Performance of Solar Collectors [7], King et al. [39], Duffie and Beckman [40], Eicker [41], ANSYS Fluent User's Guide [42], the EnergyPlus Engineering Reference Manual [12], and the EnergyPlus Input Output Reference [43].

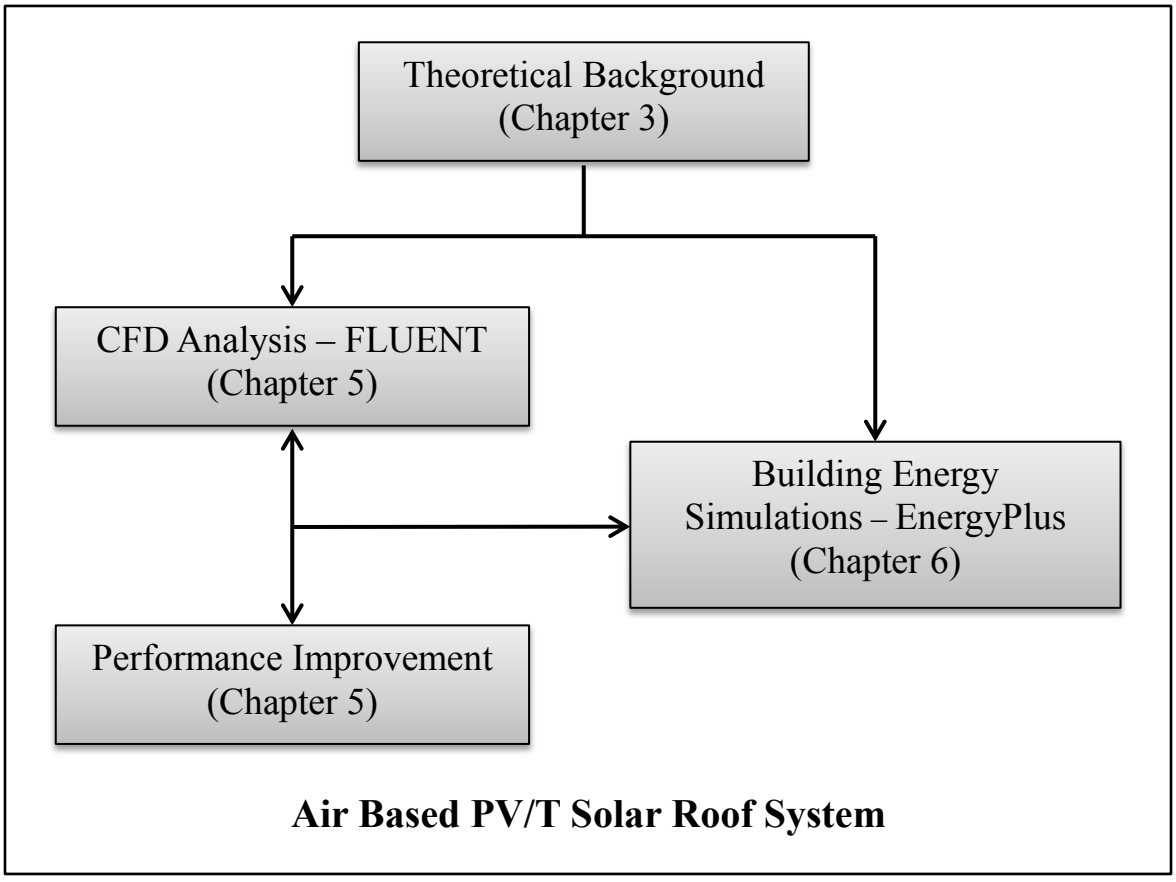

Figure 3.1 – Schematic of research of air based PV/T solar roof system

The concepts of the different models presented below are in forms of mathematical equations which all coexist to determine the performance of the air based PV/T solar glass roof system. The purpose of the *solar and shading model* is to calculate the incident solar radiation on the PV surface of the air based PV/T solar glass roof system. This model is a standard within EnergyPlus and is cohesive with the climate, sky and solar/shading calculations which use weather files, solar position, air temperature, humidity, and solar profile data during building energy simulations. The *PV arrays model* is used to determine the energy produced by solar/electric conversion panels. This model also predicts incident solar radiation and calls other electrical generation components such as gas turbines and diesel engines. The PV arrays model is managed by an electric load center which supplies electrical loads for the rest of the building. The *air based solar thermal model* contains the theoretical concepts behind the solar thermal energy balance calculations within the CFD simulations. The CFD simulations also use a solar ray tracing algorithm which has the capability to calculate the effective radiation load based on the position on the earth's surface (latitude and longitude), the model orientation with respect to North, the time of day, the season, and established conditions for clear or cloudy weather. This analysis will provide thermal conversion efficiency ranges that will be inputted into EnergyPlus. One of the key benefits of using EnergyPlus is that it can handle as many building and HVAC design options either directly or indirectly through links to other programs in order to calculate thermal loads and/or energy consumption for a design day or an extended period of time (up to, including, and beyond a year) under differing climactic conditions [12]. Furthermore, the established algorithms and concepts are considered some of the most

accurate and physically sound models available to the architecture and engineering community for quick design or policy studies as well as in-depth analysis for new building technologies. After computing the building energy demand and thermal environmental parameters, the results provide information on both energy consumption and potential savings characteristics. Such information can be against the capabilities of the air based PV/T solar glass roof system for actual building conditions.

3.1 Solar and Shading Model

The air based PV/T solar roof model presented in this dissertation is based on the standard EnergyPlus surface model in order to take advantage of the detailed solar and shading calculations that already exist in EnergyPlus. The standard EnergyPlus surface model determines the geometry of the roof's area, location, tilt, and azimuth angle as each surface object is configured as a group of up to four vertex coordinates in three-dimensional space. A model developed by Perez et al. [44], calculates solar radiation incident on the surface that includes beam and diffuse radiation as well as radiation reflected from the ground and adjacent surfaces. Shading of the air based PV/T solar roof system by other elements, such as nearby buildings or trees is also be taken into account and is based on the coordinate transformation model of Groth and Lokmanhekim [45] and the shadow overlap model of Walton [46]. The incident solar radiation data are obtained from hourly weather data that is made available for sub-hourly timesteps and carefully distributes and interpolates data between the hours of calculation.

3.2 Photovoltaic (PV) Arrays Model

The mathematical model utilized for predicting the electricity produced by Photovoltaics (PV) within the EnergyPlus program is the Sandia PV model. This model is based on research by King et al. [39] and King [47] with specific implementation details unique to EnergyPlus by Barker and Norton [48]. It uses empirical relationships to predict PV operating performance based on conditions such as incident radiation and cell temperature. Determining the cell temperature is a crucial factor in the performance of a PV system. Hence, this model allows the PV to be integrated with surfaces that form the building envelope of an EnergyPlus model. In other words, the PV interacts with the exterior surface (e.g. roof assembly) heat balance through the use of a source term that accounts for energy exported in the form of electricity. The exterior heat balance models characterize transient heat conduction using Conduction Transfer Functions (CTF) and also account for absorber direct and diffuse solar radiation, net long-wave radiation with air and surroundings, and convective exchange with outside air [47].

There are some limitations with the EnergyPlus model as it does not include models for charge controllers, batteries, or power-point trackers. The entire electrical system is assumed to operate in ideal ways. PV panels are assumed to always operate at the maximum power point. For a variety of reasons, actual installations of PV panels are often observed to exhibit system-level problems that significantly reduce electricity production. Therefore, this modeling should be considered a method of bracketing the upper end of electricity production rather than an accurate prediction of what the PV panels will produce in a real installation [49].

The following presents the basic equations of the Sandia model from King et al. [39] that predict the performance of the PV panel. The equations (3.1) through (3.9) are used when calculating the electricity produced by the PV panel. The solar resource information and weather data required by the model are obtained from tabulated databases of the EnergyPlus weather data files. The three classic points on a panel current-voltage (I-V) curve, the short circuit current point (I_{sc}), the open circuit voltage point (V_{oc}), and the maximum power point (I_{mp}), are presented in equations (3.1) through (3.4). The two additional points on the I-V curve are defined by equations (3.6) and (3.7). The fourth point (I_x), is defined at a voltage equal to one-half of the open circuit voltage, $V = 0.5\ V_{oc}$. The fifth point (I_{xx}), is defined at a voltage midway between V_{mp} and V_{oc}, $V = 0.5\ (V_{mp}+V_{oc})$. The five points provided by the performance model illustrate the basic shape of the I-V curve, Figure 3.2, and can be used to regenerate a close approximation of the entire I-V curve in cases where an operating voltage other than the maximum power voltage is required.

$$I_{sc} = I_{sco} \cdot f_1(AM_a) \cdot \left\{(E_b \cdot f_2(AOI) + f_d \cdot E_{diff})/E_o\right\} \cdot \{1 + \alpha_{Isc} \cdot (T_c - T_o)\} \quad (3.1)$$

$$I_{mp} = I_{mpo} \cdot \{C_0 \cdot E_e + C_1 \cdot E_e^2\} \cdot \{1 + \alpha_{Imp} \cdot (T_c - T_o)\} \quad (3.2)$$

$$V_{oc} = V_{oco} + N_s \cdot \delta(T_c) \cdot \ln(E_e) + \beta_{Voco}(E_e) \cdot (T_c - T_o) \quad (3.3)$$

$$V_{mp} = V_{mpo} + C_2 \cdot N_s \cdot \delta(T_c) \cdot \ln(E_e) + C_3 \cdot N_3 \cdot \{\delta(T_c) \cdot \ln(E_e)\}^2 + \beta_{Vmp}(E_e) \cdot (T_c - T_o) \quad (3.4)$$

$$P_{mp} = I_{mp} \cdot V_{mp} \quad (3.5)$$

$$I_x = I_{xo} \cdot \{C_4 \cdot E_e + C_5 \cdot E_e^2\} \cdot \{1 + \alpha_{Isc} \cdot (T_c - T_o)\} \quad (3.6)$$

$$I_{xx} = I_{xxo} \cdot \{C_6 \cdot E_e + C_7 \cdot E_e^2\} \cdot \{1 + \alpha_{Imp} \cdot (T_c - T_o)\} \quad (3.7)$$

where,

$$E_e = I_{sc}/[I_{sco} \cdot \{1 + \alpha_{Isc} \cdot (T_c - T_o)\}] \quad (3.8)$$

$$\delta(T_c) = n \cdot k \cdot (T_c + 273.15)/q \quad (3.9)$$

$$f_1(AM_a) = a_0 + a_1 AM_a + a_2(AM_a)^2 + a_3(AM_a)^3 + a_4(AM_a)^4 \quad (3.10)$$

$$f_2(AOI) = b_0 + b_1 AOI + b_2(AOI)^2 + b_3(AOI)^3 + b_4(AOI)^4 + b_5(AOI)^5 \quad (3.11)$$

$$\beta_{Voc}(E_e) = \beta_{Voco} + m_{BVoc} \cdot (1 - E_e) \quad (3.12)$$

$$\beta_{Vmp}(E_e) = \beta_{Vmpo} + m_{BVmp} \cdot (1 - E_e) \quad (3.13)$$

$$T_m = E \cdot \{e^{a+b \cdot WS}\} + T_a \quad (3.14)$$

$$T_c = T_m + (\Delta T \cdot E/E_o) \quad (3.15)$$

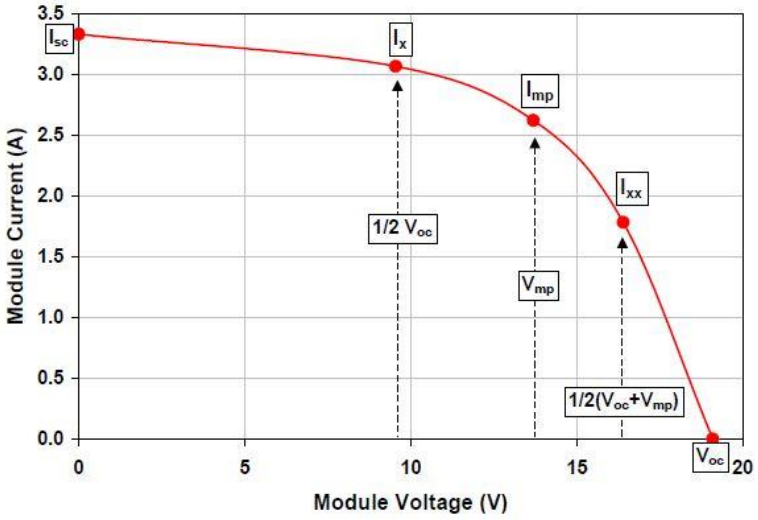

Figure 3.2 – Sandia PV model's I-V curve showing the five points on the curve [39]

Mathematical Variable	Description
I_{sc}	Short circuit current (A)
I_{mp}	Current at the maximum power point (A)
I_x	Current at panel V = 0.5 V_{oc}, defines 4th point on I-V curve
I_{xx}	Current at panel V = 0.5 (V_{oc} + V_{mp}), defines 5th point on I-V curve
V_{oc}	Open circuit voltage (V)
V_{mp}	Voltage at maximum power point (V)
P_{mp}	Power at maximum power point (W)
f_d	Fraction of diffuse irradiance used by PV panel
N_s	Number of cells in series in a PV panel's cell string
N_p	Number of cell strings in parallel in PV panel
k	Boltzmann's constant, 1.38066E-23 (J/k)
q	Elementary charge, 1.60218E-19 (coulomb)
T_c	Cell temperature inside PV panel (°C)
$\delta(T_c)$	'Thermal voltage per cell at temperature T_c, approximately 1 volt for a typical 26 cell crystalline silicon panel
E_e	'Effective' solar irradiance
E_b	Beam solar irradiance
E_{diff}	Diffuse solar irradiance
C_0 , C_1	Empirical coefficients relating I_{mp} to E_e , $C_0 + C_1 = 1$ (both dimensionless)
C_2 , C_3	Empirical coefficients relating V_{mp} to E_e (C_2 dimensionless, C_3 is 1/V)
C_4 , C_5	Empirical coefficients relating I_x to E_e , $C_4 + C_5 = 1$ (both dimensionless)
C_6 , C_7	Empirical coefficients relating I_{xx} to E_e , $C_6 + C_7 = 1$ (both dimensionless)

n	Empirically determined 'diode factor' for individual cells
AM_a	Absolute air mass
AOI	Solar angle of incidence (degrees) from normal
$f_1(AM_a)$	Empirical polynomial function used to relate short circuit current to the solar spectrum via air mass
$f_2(AOI)$	Empirical polynomial function used to relate short circuit current to the solar angle of incidence
a_0 , a_1 , a_2 , a_3 , a_4	Empirical coefficients for $f_1(AM_a)$ polynomial
b_0 , b_1 , b_2 , b_3 , b_4 , b_5	Empirical coefficients for f_2(AOI) polynomial
T_o	Reference cell temperature for rating, typically fixed at 25℃
I_{sco}	Short circuit current at reference conditions
I_{mpo}	Max power point current at reference conditions
V_{mpo}	Voltage at max power at reference conditions
V_{oco}	Open circuit voltage at reference conditions
I_{xo}	Current at V = 0.5 V_{oc} and at reference conditions
I_{xxo}	Current at V = 0.5 (V_{mp} + V_{oc}) and at reference conditions
α_{Isc}	Normalized temperature coefficient for I_{sc} (1/℃)
α_{Imp}	Normalized temperature coefficient for I_{mp} (1/℃)
$\beta_{Voc}(E_e)$	Temperature coefficient for PV panel open circuit voltage as function of E_e
β_{Voco}	Temperature coefficient for PV panel open circuit voltage at reference conditions
m_{BVoc}	Coefficient for irradiance dependence of open circuit voltage temperature coefficient, often zero (V/℃)
T_m	PV panel temperature at back surface (℃)
T_a	Ambient outdoor drybulb temperature (℃)
E	Solar irradiance incident on PV panel surface (W/m^2)
WS	Wind speed at standard 10m height (m/s)

a	Empirical coefficient relating panel temperature at low wind and high solar irradiance
b	Empirical coefficient relating panel temperature decrease with increasing wind speed
T_c	Temperature of solar cell inside panel (℃)
E_o	Reference solar irradiance (1000 W/m^2)
ΔT	Temperature difference between T_c and T_m at E_o (℃)

3.3 Air Based Solar Thermal Model

The energy balance of the air based solar thermal model is based on the assumptions that the roof is a flat surface and the intensity of the incident solar radiation across the surface is uniform. Therefore, the heat transfer process in the air based PV/T solar roof system takes place perpendicular to the absorber direction and is one-dimensional in nature.

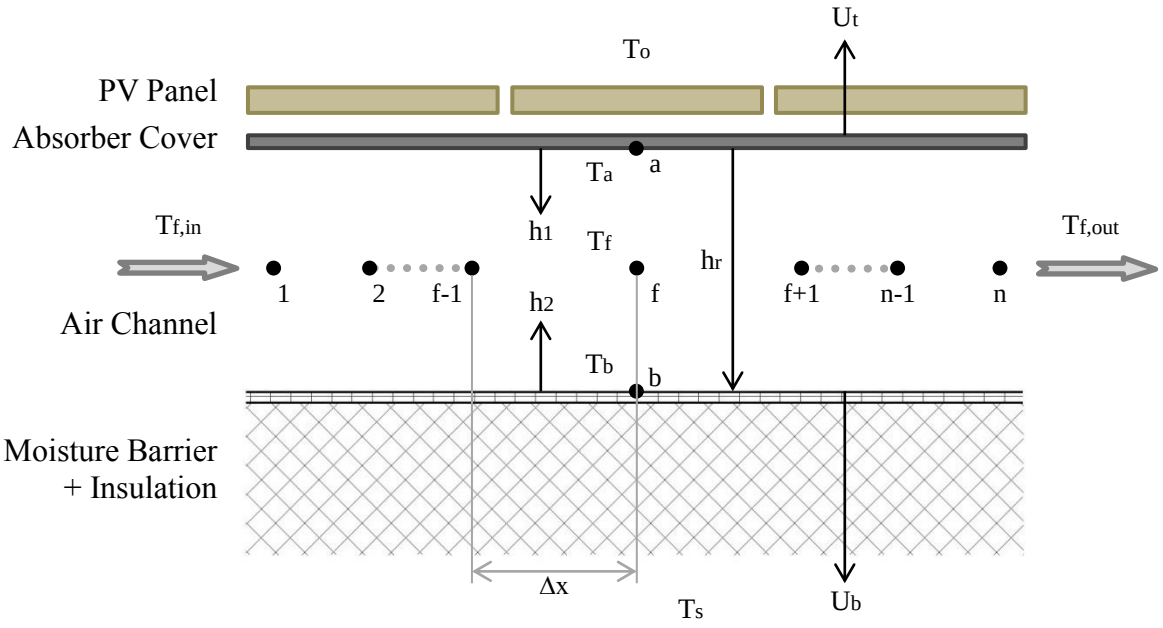

Figure 3.3 – Schematic assembly of the air based PV/T solar roof system with designation of nodes and temperatures

The energy balance of the air based solar thermal model takes into account the various elements of the system including the PV panel and absorber cover, the air fluid, and the moisture barrier and insulation of a building. The following equations are energy balances of nodes, under steady-state conditions (e.g. air is assumed to be a non-participating medium and thus does not absorb any radiation – short or long wavelength), at the PV panel and absorber cover (a), the air flowing within the air channel (f), and the back side of the assembly (b) which consist of the moisture barrier and insulation of a building:

$$Q_{u,f} = \rho \forall c_p \Delta T = \rho \forall c_p (T_f - T_{f-1}) \tag{3.16}$$

$$IA(\tau\alpha) + U_t A(T_a - T_o) + h_1 A\left(T_a - T_f\right) + h_r A(T_a - T_b) = 0 \tag{3.17}$$

$$h_1 B\Delta x\left(T_a - T_f\right) + h_2 B\Delta x\left(T_b - T_f\right) = Q_{u,f} \tag{3.18}$$

$$h_r(T_b - T_a) + h_2\left(T_b - T_f\right) + U_b(T_b - T_s) = 0 \tag{3.19}$$

As the energy balance equations above can be complex, a simplified energy balance over the air based PV/T solar roof system may be written as

$$Q_u = AI(\tau\alpha) - U_L \tag{3.20}$$

Where, U_L can be written as a function of the overall top and bottom heat loss coefficients U_t and U_b

$$U_L = U_t(T_a - T_o) + U_b(T_b - T_s) \tag{3.21}$$

If measuring the fluid outlet and inlet temperatures and the fluid flow rate, the energy balance over the air based PV/T solar roof system may also be written as

$$Q_u = \rho \forall c_p(T_{out} - T_{in}) \tag{3.22}$$

Equations (3.20), (3.21), and (3.22) then becomes

$$Q_u = AI(\tau\alpha) - U_t(T_a - T_o) - U_b(T_b - T_s) = \rho \forall c_p(T_{out} - T_{in}) \tag{3.23}$$

Mathematical Variable	Description
A	Area of absorber [m^2]
I	Incident solar radiation [W/m^2]
τ	Transmittance coefficient [dimensionless]
α	Absorption coefficient [dimensionless]
ρ	Density of air [kg/m^3]
$\forall$	Volumetric flow rate [m^3/s]
c_p	Specific heat of air at constant pressure [$J/kg \cdot ℃$]
U_b	Bottom loss coefficient [$W/m \cdot ℃$]
U_t	Top loss coefficient [$W/m \cdot ℃$]
U_L	Overall heat loss coefficient [$W/m \cdot ℃$]
T_a	Temperature of absorber [℃]
T_b	Temperature of moisture barrier [℃]
T_f	Temperature of fluid [℃]
T_o	Temperature of ambient air [℃]
T_s	Temperature of interior space [℃]
h_1	Heat transfer coefficient between absorber and fluid [$W/m^2 \cdot ℃$]

h_2	Heat transfer coefficient between moisture barrier and fluid [W/m^2·°C]
h_r	Heat transfer coefficient between absorber and moisture barrier [W/m^2·°C]
$Q_{u,f}$	Heat gain of fluid at generic node f [W]
Q_u	Heat gain of fluid [W]
B	Width of absorber [m]
Δx	Distance of direction of airflow for a single node [m]

3.4 EnergyPlus – Heat and Mass Balance Model

The building energy simulation program that will be used for this dissertation is EnergyPlus. EnergyPlus, the official program of and funded by the U.S. Department of Energy, is a whole building annual energy simulation program which models "heating, cooling, lighting, ventilation, other energy flows, and water use" in buildings [51]. The program calculates the heating and cooling loads necessary to maintain thermal control setpoints, conditions throughout a secondary HVAC system and coil loads, and the energy consumption of primary plant equipment. EnergyPlus also enables integrated energy performance analysis of other low-energy technologies in commercial and residential buildings including on-site generation and renewable energy sources.

The inside and outside transient surface heat balance concepts and features of the EnergyPlus program are utilized during the complex heat balance calculations. Figure 3.4 presents the schematic structure of the EnergyPlus integrated solution manager which manages the surface/air heat balance and building systems simulation manager. The surface heat balance manager is connected with the sky model, shading, daylighting, window glass, and conduction modules. It simulates inside/outside surface heat balances and convection,

radiation, and mass transfer effects. The air heat balance manager acts as an interconnector between surface heat balance manager and building systems simulation manager and simulates conditioned and/or unconditioned ventilation air, exhaust air, and infiltration. The building systems simulation manager controls and simulates the HVAC and electrical systems, equipment, and components. These established algorithms and concepts are considered some of the most accurate and physically sound models available and full discussions of how this is modeled in EnergyPlus can be found in the EnergyPlus Engineering Reference manual [12].

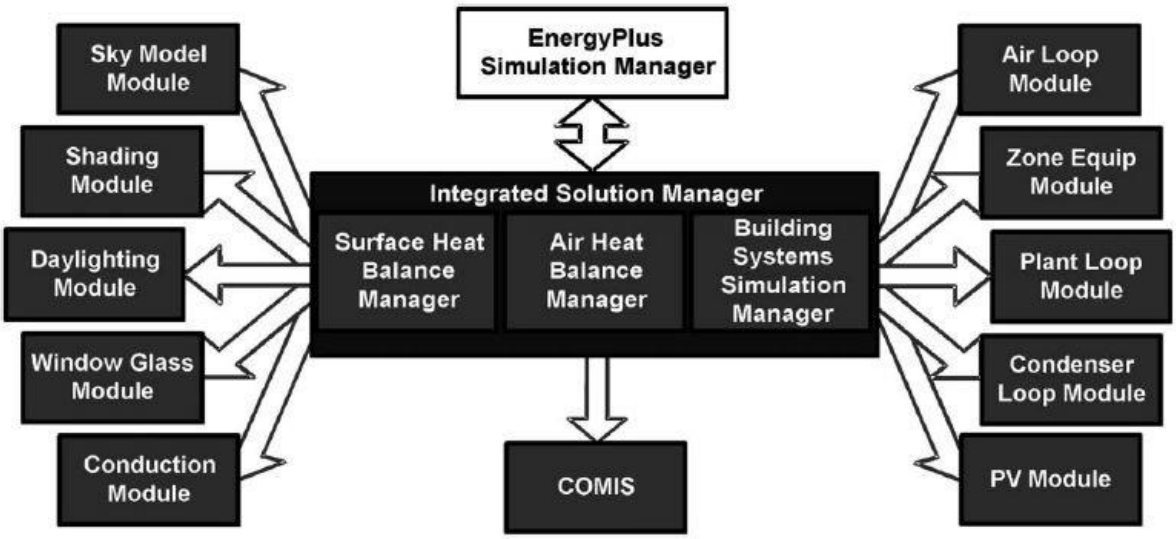

Figure 3.4 – Integrated solution manager of EnergyPlus [12]

3.5 EnergyPlus – Air Based Solar PV/T Model

The air based solar PV/T model within the EnergyPlus program is provided for design and policy studies. The user provides values for the thermal efficiency and the incident solar radiation heats the air within the air channel. The system is part of the HVAC

air system loop with air nodes connecting the building air system. The model requires a drybulb air temperature setpoint be placed on the outlet node. If the solar incident on the roof surface is greater than 0.3 W/m^2, the model assumes it is intended and available for heating. To determine if heating is beneficial, the inlet temperature is compared to the setpoint on the outlet node. If the outlet temperature is greater than the inlet temperature and there is a need for heating within the building air system, the air based PV/T solar thermal models are applied to condition the air stream. A modulating bypass damper is also included within the air based PV/T solar thermal model to better meet setpoint temperatures. If heating is not required the inlet node is passed directly to the outlet node to model a completely bypassed damper arrangement.

The air based solar thermal model calculates the outlet temperature based on the inlet temperature and the collected heat using the following equations:

$$Q_{therm} = A_{surf} \cdot f_{activ} \cdot I \cdot \eta_{thermal} \tag{3.24}$$

Mathematical Variable	Description
Q_{therm}	Thermal energy collected [W]
A_{surf}	Net area of the surface [m^2]
f_{activ}	Fraction of surface air with air based PV/T solar roof system
I	Incident solar radiation [W/m^2]
$\eta_{thermal}$	Thermal conversion efficiency

$$T_{out} = T_{in} + \frac{Q_{therm}}{m \cdot c_p} \tag{3.25}$$

Mathematical Variable	Description
T_{out}	Outlet node temperature [℃]
T_{in}	Inlet node temperature [℃]
m	Mass flow rate of air [kg/s]
c_p	Specific heat of air [J/kg·℃]

The value of T_{out} is then compared to the temperature setpoint on the outlet node. If T_{out} exceeds the desired outlet temperature, $T_{set,out}$, then a bypass fraction is calculated to model a modulating bypass damper using following equation:

$$f_{bypass} = \frac{T_{set,out} - T_{out}}{T_{in} - T_{out}} \tag{3.26}$$

When the air based PV/T solar roof system is controlled to be 'on', the air is flowing and the model calculates the outlet temperature based on the inlet temperature and the heat radiated and convected to the ambient air using a heat balance on the outside face of the collector:

$$mc_p(T_{out} - T_{in}) = Q_{LWR} + Q_{conv} + Q_{cond} \tag{3.27}$$

This equation is based on EnergyPlus's Outside Surface Heat Balance model where Q_{LWR}, is the net rate of long wavelength (thermal) radiation exchange with the air, night sky, and ground, Q_{conv}, is the net rate of convective flux exchange with outdoor air, and Q_{cond} is

the net rate of conduction flux exchange with assembly of the air based PV/T solar roof system. The radiation heat flux is calculated from the surface absorptivity, surface temperature, sky and ground temperatures, and sky and ground view factors. The longwave radiation heat exchange between surfaces is dependent on surface temperatures, spatial relationships between surface and surroundings, and material properties of the surfaces. The relevant material properties of the surface, emissivity ε and absorptivity α, are complex functions of temperature, angle, and wavelength for each participating surface. However, it is generally agreed that reasonable assumptions for building loads calculations are [52][53]:

- Each surface emits or reflects diffusely and is gray and opaque ($\alpha = \varepsilon$, $\tau = 0$, $\rho = 1 - \varepsilon$)
- Each surface is at a uniform temperature
- Energy flux leaving a surface is evenly distributed across the surface
- The medium within the enclosure is non-participating

These assumptions are frequently used in all but the most critical engineering applications and we can express the long wavelength (thermal) radiation as the sum of components due to radiation exchange with the ground, sky, and air [46][49].

$$Q_{LWR} = Q_{gnd} + Q_{sky} + Q_{air} \tag{3.28}$$

Appling the Stefan-Boltzmann Law to each component yields:

$$Q_{LWR} = \varepsilon\sigma F_{gnd}\left(T_{gnd}^4 - T_{surf}^4\right) + \varepsilon\sigma F_{gnd}\left(T_{gnd}^4 - T_{surf}^4\right) + \varepsilon\sigma F_{gnd}\left(T_{gnd}^4 - T_{surf}^4\right) \tag{3.29}$$

Linearized radiative heat transfer coefficients are introduced to render the above equation more compatible with the heat balance formulation,

$$Q_{LWR} = h_{r,gnd}\left(T_{gnd} - T_{surf}\right) + h_{r,sky}\left(T_{sky} - T_{surf}\right) + h_{r,air}\left(T_{air} - T_{surf}\right) \quad (3.30)$$

where,

$$h_{r,gnd} = \frac{\varepsilon\sigma F_{gnd}(T_{surf}^4 - T_{gnd}^4)}{T_{surf} - T_{gnd}} \quad (3.31)$$

$$h_{r,sky} = \frac{\varepsilon\sigma F_{sky}(T_{surf}^4 - T_{sky}^4)}{T_{surf} - T_{sky}} \quad (3.32)$$

$$h_{r,air} = \frac{\varepsilon\sigma F_{air}(T_{surf}^4 - T_{air}^4)}{T_{surf} - T_{air}} \quad (3.33)$$

The longwave view factors to ground and sky are calculated with the following expressions [46]:

$$F_{gnd} = 0.5(1 - cos\phi) \quad (3.34)$$

$$F_{sky} = 0.5(1 + cos\phi) \quad (3.35)$$

where ϕ is the tilt angle of the surface. The view factor to the sky is further split between sky and air radiation by:

$$\beta = \sqrt{0.5(1 + cos\phi)} \quad (3.36)$$

The ground surface temperature is assumed to be the same as the air temperature. The final forms of the radiative heat transfer coefficients are shown as:

$$h_{r,gnd} = \frac{\varepsilon\sigma F_{gnd}(T_{surf}^4 - T_{air}^4)}{T_{surf} - T_{air}} \tag{3.37}$$

$$h_{r,sky} = \frac{\varepsilon\sigma F_{sky}\beta(T_{surf}^4 - T_{sky}^4)}{T_{surf} - T_{sky}} \tag{3.38}$$

$$h_{r,air} = \frac{\varepsilon\sigma F_{sky}(1-\beta)(T_{surf}^4 - T_{air}^4)}{T_{surf} - T_{air}} \tag{3.39}$$

The air based solar thermal model assumes that the effective system temperature, T_{sys}, is the average of the air inlet and outlet temperatures and the following substitution can be made:

$$T_{out} = 2T_{sys} - T_{in} \tag{3.40}$$

Substituting and solving for T_{sys}, the following equation can be obtained for the system temperatures during a (possible) cooling process:

$$T_{sys} = \frac{2\dot{m}c_p T_{in} + A_{surf} f_{activ}(h_{r,gnd}T_{gnd} + h_{r,sky}T_{sky} + h_{r,air}T_{air} + h_{c,ext}T_{air})}{2\dot{m}c_p + A_{surf} f_{activ}(h_{r,gnd} + h_{r,sky} + h_{r,air} + h_{c,ext})} \tag{3.41}$$

Consequently, the outlet temperature, T_{out}, can be calculated and the heat losses can be determined. In addition, this model allows for sensible cooling of the air stream and limits the outlet temperature to not go below the dew point temperature of the inlet.

3.6 Summary

This chapter presents the theoretical background of the concepts used for the CFD and building simulations that together are used to determine the performance of the air based PV/T solar roof system. The *air based solar thermal model* presents the theoretical concepts behind the solar thermal energy balance calculations within the CFD simulations. The *solar and shading model* and the *PV arrays model* are concepts incorporated into the EnergyPlus program which calculates the incident solar radiation on the PV surface and determines the electrical energy produced by the PV unit. The *heat and mass balance model* presents the schematic structure of the EnergyPlus integrated solution manager which is considered the 'engine' behind the complex building energy simulations. The *air based solar PV/T model* within the EnergyPlus calculates how the incident solar radiation heats the air within the air channel.

Chapter 4 presents an overview of the computational case study models which includes dimensions, construction properties, HVAC systems, and schedules for different types of occupancy and equipment. The dimensions and construction properties of the roof of the small commercial office building will be incorporated into the CFD case study model. The CFD simulations in Chapter 5 will determine and provide values for the thermal efficiency which then will be incorporated into EnergyPlus air based solar PV/T model to run the whole annual building energy simulations in Chapter 6.

Chapter 4. Overview of Computational Case Study Models

This chapter presents the overview of computational case study models which is used in the CFD simulations (Chapter 5) and building energy simulations (Chapter 6). The CFD study model is a replica of the roof assembly of the computational case study models with the same construction material specifications. The CFD analysis in this chapter will provide thermal conversion efficiency ranges which will be input into the building energy simulations in Chapter 6. Building energy simulations using the building's thermal zone internal loads, schedules, and other key modeling input information provides investigation of the performance of the air based PV/T solar roof system for various building types under differing climacteric conditions.

The U.S. DOE in collaboration with the National Renewable Energy Laboratory (NREL), Pacific Northwest National Laboratory (PNNL), and Lawrence Berkeley National Laboratory (LBNL) have developed building energy simulation reference models for the most common *commercial buildings*[1] [54]. They consist of 16 building types including restaurants, health care, schools, offices, supermarkets, retail, lodging, and warehouses. EnergyPlus and OpenStudio were used to develop the reference models and serve as starting points for energy efficiency research as well as represent realistic building and typical construction practices within the United States [55]. Moreover, the building models are in compliance with ASHRAE 90.1 (Energy Standard for Buildings except Low-Rise Residential Buildings) which provides minimum requirements for energy efficient designs

[1] U.S. DOE classifies *commercial buildings* as all buildings other than low-rise residential building, including multi-family high-rise residential buildings over three stories in height above grade [54].

for buildings except for low-rise residential buildings. Each commercial reference building type has a different form or shape. The shape, total area, floor height, and thermal zoning of each building are determined from the 2003 Commercial Buildings Energy Consumption Survey (CBECS) dataset [56].

This study will focus on two building energy simulation reference buildings, a quick-service restaurant and a small commercial office building, to investigate the energy efficiency of the air based PV/T solar roof system under various climates. These were chosen because they are both designed with a Gable roof which can potentially expose half of the roof area to the sun depending on the roof configuration and orientation. Gable roof is one of the most popular choices of building roofs and the simple design allows for economical and feasible construction. Moreover, the slope of the Gable roof allows for effective water drainage and provides reasonable ceiling space for insulation to be installed. The following summarizes the building descriptions, construction material specifications, thermal zone internal loads, schedules, and other key modeling input information which is used in the CFD simulations and building energy simulations. The CFD simulations provide thermal conversion efficiency ranges, and the building energy simulations using the building's thermal zone internal loads, schedules, and other key modeling input information provide information on the energy efficiency of the air based PV/T solar roof system. This two stage process will be used to obtain a comprehensive insight towards understanding the performance of the air based PV/T solar roof system for various climates. Furthermore, overall impacts or benefits of the air based PV/T solar roof system will be presented in terms of energy consumptions/savings and CO_2 emissions.

4.1 Small Commercial Office Building

The small commercial office building is a single story building with six thermal zones – four perimeter zones, one core zone, and an attic zone. The thermal zones are controlled by a thermostat except for the attic zone, which is unconditioned. Figure 4.1 depicts the perspective of a small commercial office building while Figure 4.2 illustrates the elevations. Figure 4.3 further illustrates a diagram of the thermal zone plan for a small commercial office building. The perimeter accounts for 70% of the floor area and the core accounts 30% of the floor area. Tables 4.1 – 4.3 describe the building's basic input data of geometry, construction, HVAC, internal load conditions, and zone summary.

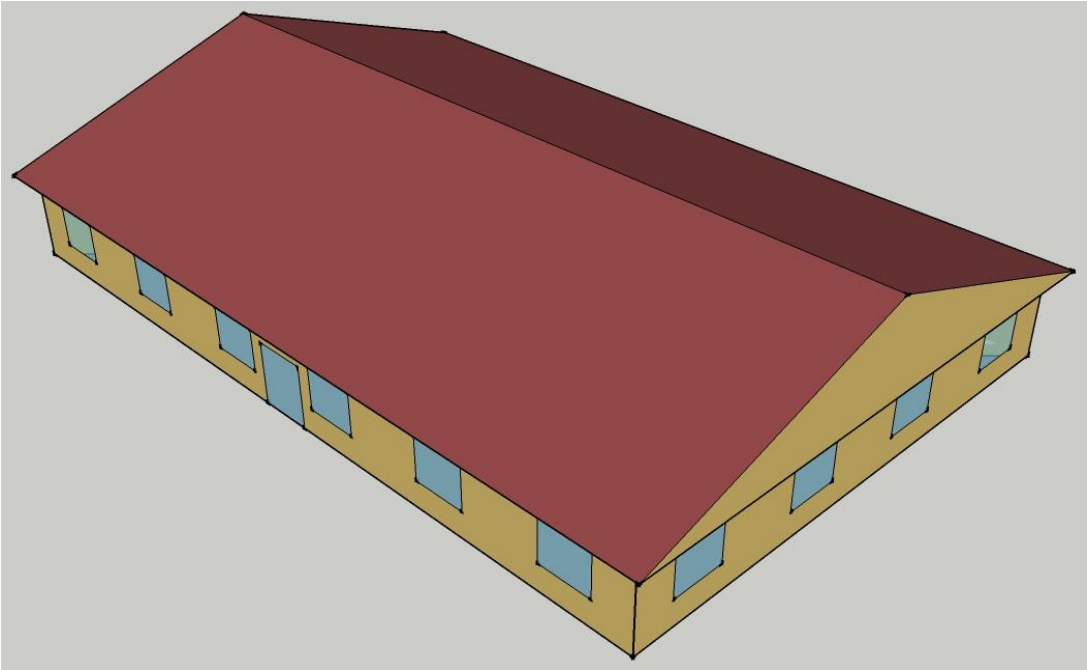

Figure 4.1 – Perspective view of small commercial office building

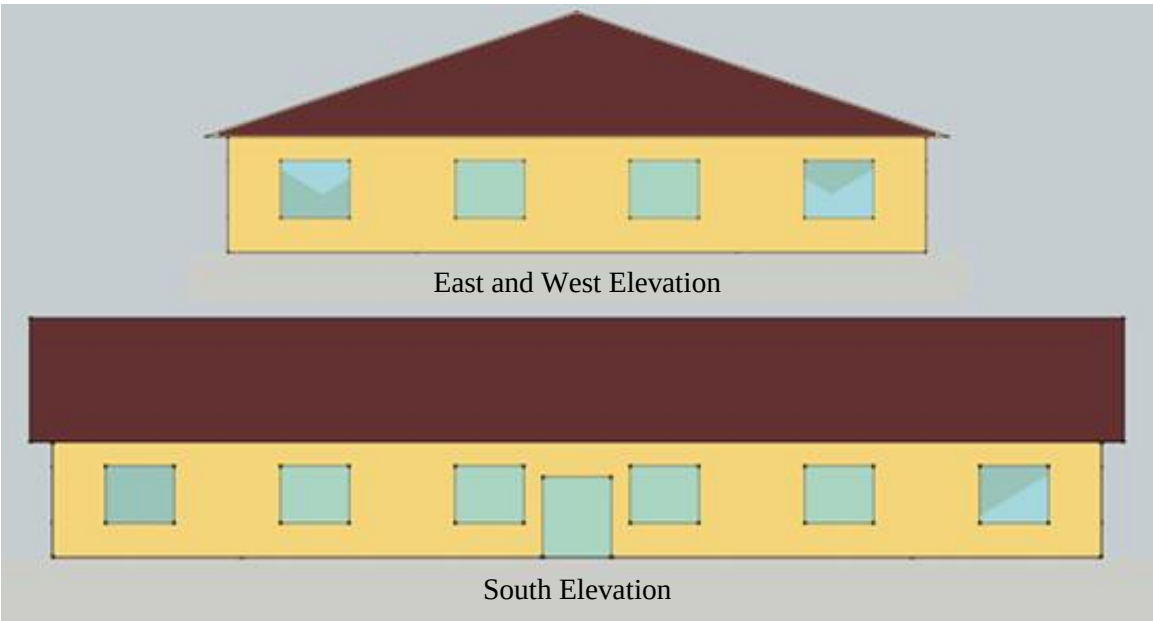

Figure 4.2 – Elevations of small commercial office building

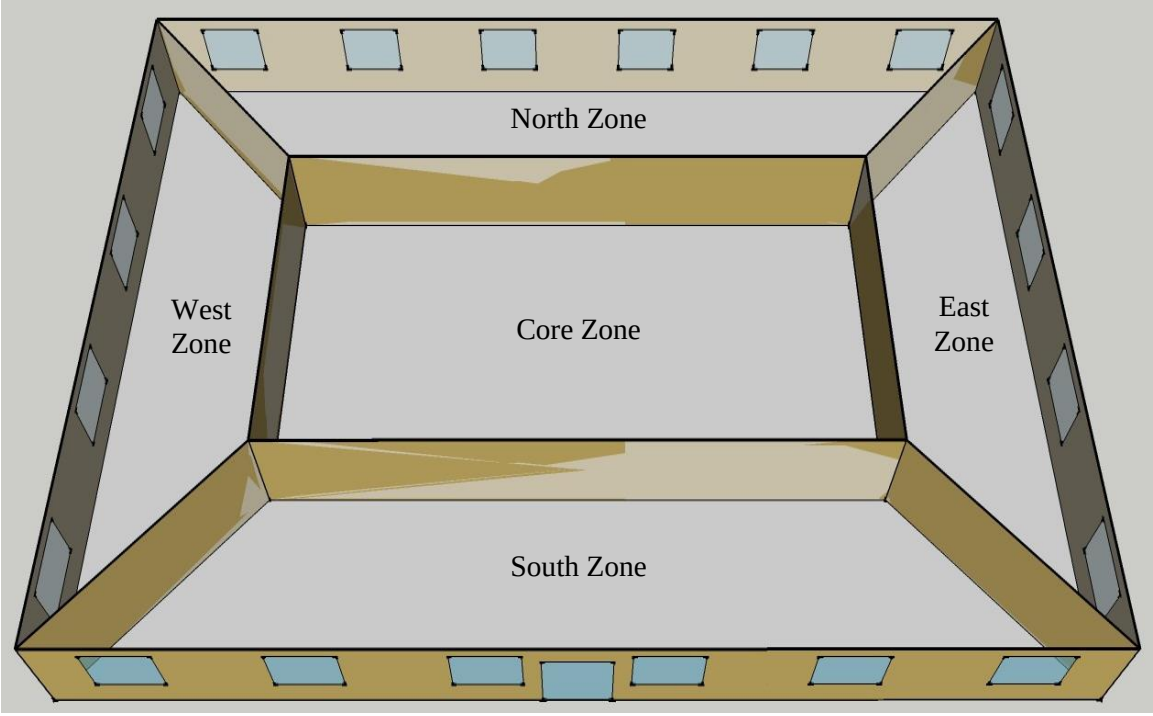

Figure 4.3 – Thermal zones of small commercial office building

Parameter	Data / Descriptions
Total Floor Area (m^2)	511 (27.68 m × 18.44 m)
Building shape	Rectangular
Aspect Ratio	1.5
Number of Floors	1
Window Fraction	24.4% for South and 19.8% for the other three orientations
Window Locations	Evenly distributed along four façades
Thermal Zoning	Four perimeter zones, one core zone, and unconditioned attic zone Percentages of floor area: perimeter 70%, core 30%
Floor to Ceiling Height (m)	3.05
Glazing Sill Height (m)	0.91 (Top of the window is 2.44 m high with 1.52 m high glass)
Exterior Walls	
Construction	2 × 4 Wood-frame walls 1" stucco + 5/8" gypsum board + wall insulation + 5/8" gypsum board
R-value	ASHRAE 90.1 requirements Nonresidential; walls, above-grade, wood-framed
Roof	
Construction	Attic roof with wood joist Roof insulation + 5/8" gypsum board
R-value	ASHRAE 90.1 requirements Nonresidential; roofs, attic
Windows	
Dimensions	Punch window, each 1.52 m high by 1.83 m wide
U-factor	ASHRAE 90.1 requirements Nonresidential; vertical glazing, 20-30%, U fixed
Foundation	
Foundation Type	Slab-on-grade floors (unheated)
Construction	20.32 cm concrete slab poured directly on to the earth
R-value	ASHRAE 90.1 requirements Nonresidential; Slab-on-grade floors, unheated
Interior Partitions	
Construction	2 x 4 uninsulated stud wall
Internal Mass	6" standard wood

Table 4.1 – Building description of small commercial office building

System Type	
Heating type	Air-source heat pump with gas furnace as back up
Cooling type	Air-source heat pump
Distribution and terminal units	Single zone, constant air volume air distribution, one unit per occupied thermal zone
HVAC Sizing	
Air Conditioning	Auto-sized to design day
Heating	Auto-sized to design day
HVAC Efficiency	
Air Conditioning	ASHRAE 90.1 requirements
Heating	ASHRAE 90.1 requirements
HVAC Control	
Thermostat Setpoint	23.9℃ Cooling / 21.1℃ Heating
Thermostat Setback	29.4℃ Cooling / 15.6℃ Heating
Supply air temperature	Maximum 40℃, Minimum 12.8℃
Economizers	Various by climate location and cooling capacity Control type: differential dry bulb
Ventilation	ASHRAE Ventilation Standard 62.1
Demand Control Ventilation	ASHRAE 90.1 requirements
Energy Recovery	ASHRAE 90.1 requirements
Supply Fan	
Supply Fan Total Efficiency (%)	Depending on the fan motor size
Supply Fan Pressure Drop	Various depending on the fan supply air
Pump	
Pump Power	Auto-sized
Service Water Heating	
SWH type	Storage tank
Fuel type	Natural gas
Thermal efficiency (%)	ASHRAE 90.1 requirements
Tank Volume (Liter)	150
Water temperature setpoint	49℃

Table 4.2 – HVAC summary of small office commercial building

Parameter	Core Zone	North Zone	South Zone	East Zone	West Zone
Area (m^2)	150	113	113	67	67
Volume (m^3)	456	346	346	205	205
Gross Exterior Wall Area (m^2)	0	84	56	84	56
Window Glass Area (m^2)	0.00	20.64	11.16	16.73	11.16
Occupancy Density (m^2/person)	18.58	18.58	18.58	18.58	18.58
Lighting Power (W/m^2)	10.76	10.76	10.76	10.76	10.76
Equipment Power (W/m^2)	10.76	10.76	10.76	10.76	10.76

Table 4.3 – Zone summary of small commercial office building

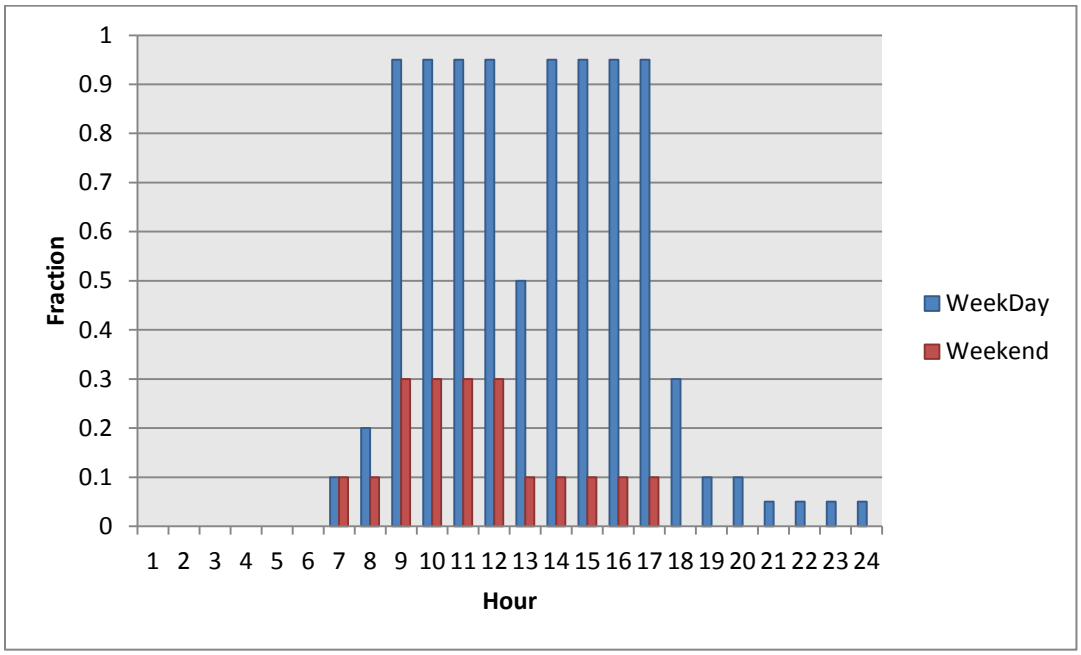

Figure 4.4 – Hourly occupancy schedule of small commercial office building

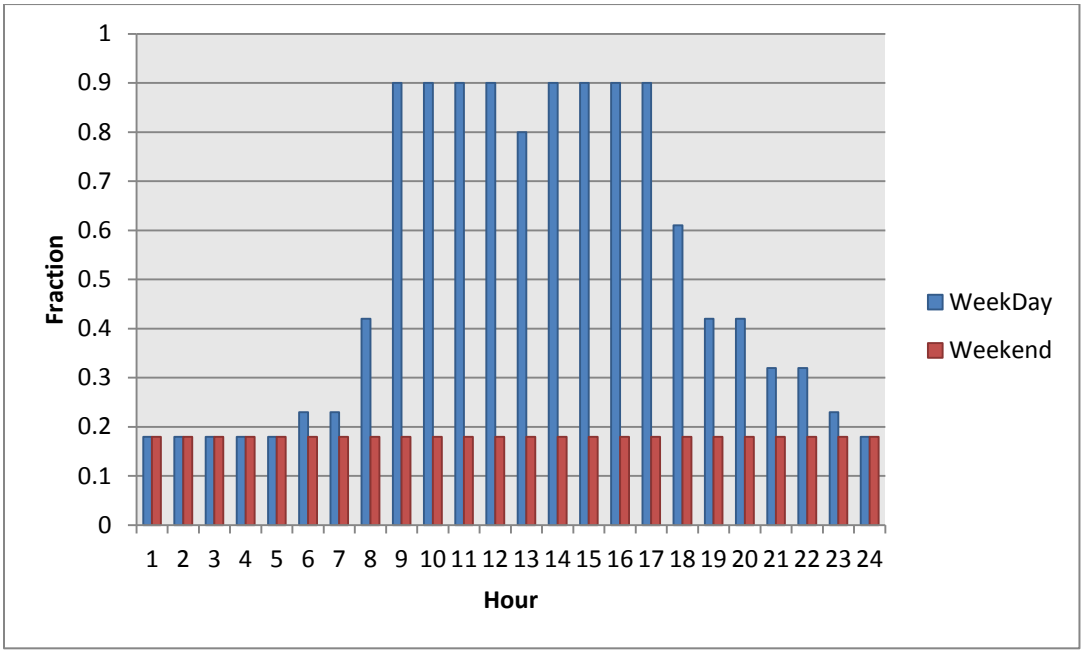

Figure 4.5 – Hourly lighting schedule of small commercial office building

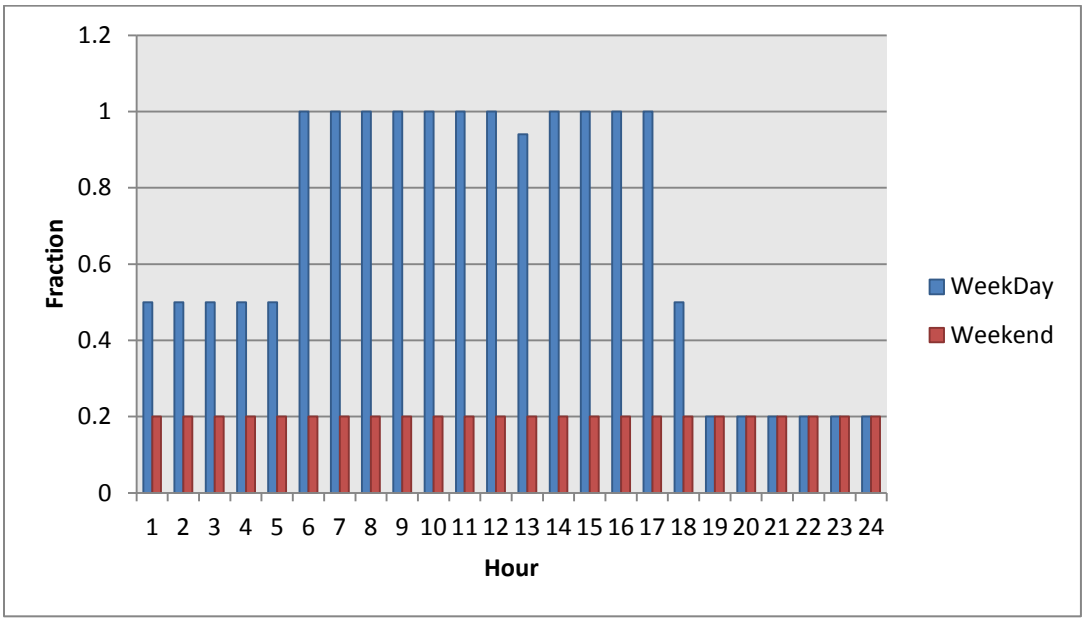

Figure 4.6 – Hourly equipment schedule of small commercial office building

The hourly occupancy, lighting, and equipment schedules are illustrated in Figures 4.4 – 4.6. These schedules including the building data inputs (Tables 4.1 – 4.3) are used to calculate the hourly, daily, weekly, and annual energy consumptions of the small office building. The schedules show that the internal load conditions are quite different between typical weekdays and weekends.

Figures 4.7 and 4.8 show the heating and cooling setpoint temperature schedules of the small commercial office building. These schedules are used to generate both the heating/cooling availability schedule and the temperature setpoint schedules used in the building energy simulations. The heating setpoint temperature is set to 21.1℃ and the cooling setpoint temperature is set to 23.9℃ during the occupied hours. When the building is unoccupied the heating setpoint temperature is dropped to 15.6℃ and the cooling setpoint temperature is raised to 29.4℃.

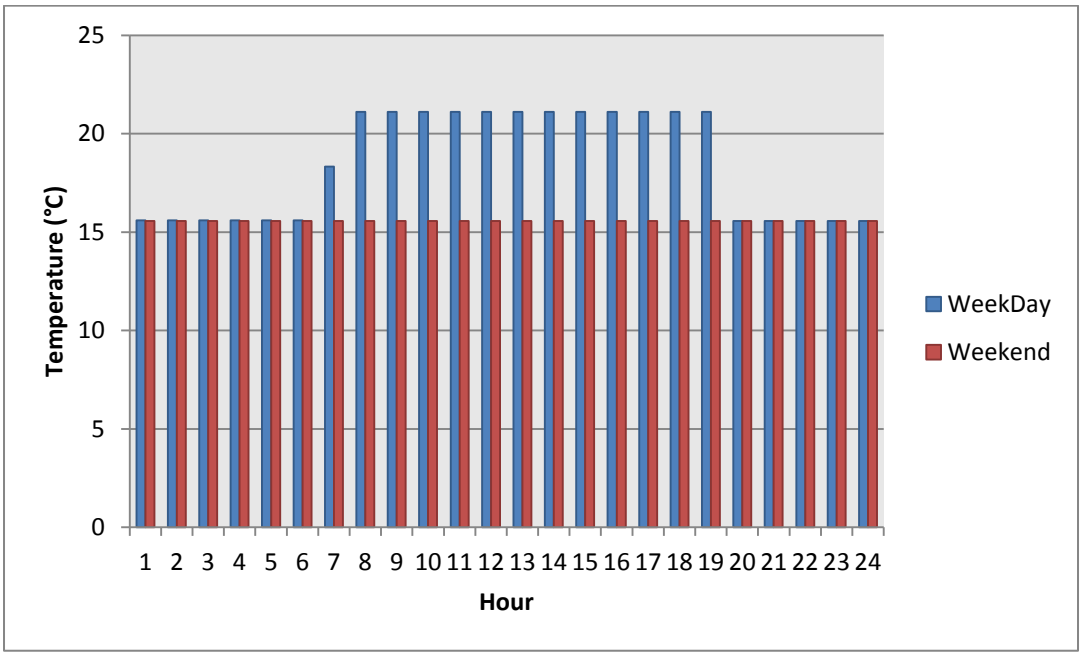

Figure 4.7 – Heating setpoint temperature schedule of small commercial office building

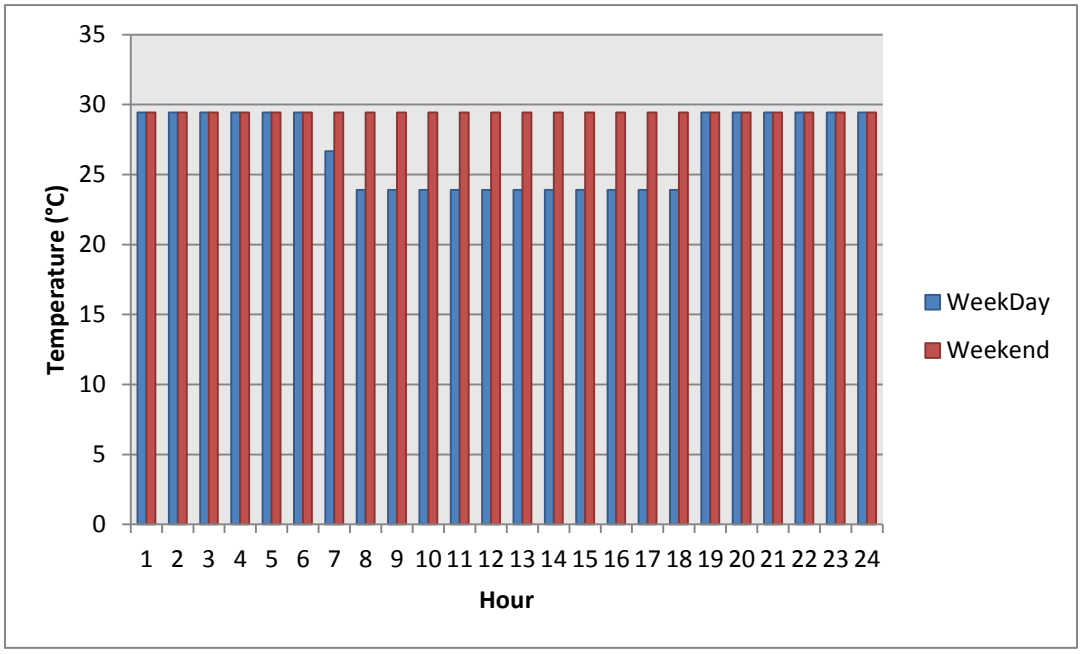

Figure 4.8 – Cooling setpoint temperature schedule of small commercial office building

4.2 Quick-Service Restaurant

The quick-service restaurant is also a single story building but with three thermal zones – dinning zone, kitchen zone, and an attic zone. The dining and kitchen zones are controlled by a thermostat while the attic zone remains unconditioned. The kitchen and the dining zones are equally spaced, each having an area of 116 m^2. Figure 4.9 depicts the perspective view and thermal zones of the quick-service restaurant. Tables 4.4 – 4.6 describe the building's basic input data of geometry, construction, HVAC, internal load conditions, and zone summary.

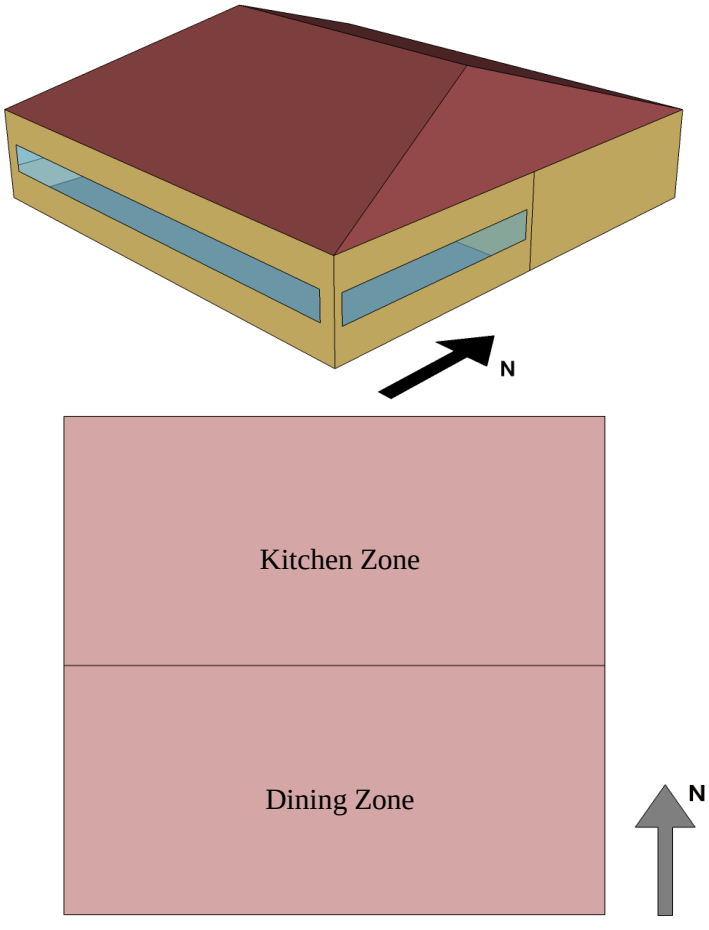

Figure 4.9 – Perspective view and thermal zones of quick-service restaurant

Parameter	Data / Descriptions
Total Floor Area (m²)	232 (15.24 m × 15.24 m)
Building shape	Square
Aspect Ratio	1
Number of Floors	1
Window Fraction	North: 0%, South: 28%, East and West: 14%
Window Locations	East and West (7.1m × 0.91m), South (14.2m × 0.91m) of the dining zone façades
Thermal Zoning	One dining zone, one kitchen zone, and unconditioned attic zone Percentages of floor area: dining 50%, kitchen 50%
Floor to Ceiling Height (m)	3.05
Glazing Sill Height (m)	1.07 (Top of the window is 1.98 m high with 0.91 m high glass)
Exterior Walls	
Construction	Wood-frame walls 1” stucco + 5/8” gypsum board + wall insulation + 5/8” gypsum board
R-value	ASHRAE 90.1 requirements Nonresidential; walls, above-grade, wood-framed
Roof	
Construction	Attic roof with wood joist Roof insulation + 5/8” gypsum board
R-value	ASHRAE 90.1 requirements Nonresidential; roofs, attic
Windows	
Dimensions	Based on window fraction, location, glazing sill height, floor area and aspect ratio
U-factor	ASHRAE 90.1 requirements Nonresidential; vertical glazing, 20-30%, U fixed
Foundation	
Foundation Type	Slab-on-grade floors (unheated)
Construction	15.24 cm concrete slab poured directly on to the earth
R-value	ASHRAE 90.1 requirements Nonresidential; slab-on-grade floors, unheated
Interior Partitions	
Construction	0.5” gypsum board + 0.5” gypsum board
Internal Mass	6” standard wood

Table 4.4 – Building description of quick-service restaurant

System Type	
Heating type	Gas furnace inside the packaged air conditioning unit
Cooling type	Packaged air conditioning unit
Distribution and terminal units	Single zone, constant air volume air distribution
HVAC Sizing	
Air Conditioning	Auto-sized to design day
Heating	Auto-sized to design day
HVAC Efficiency	
Air Conditioning	ASHRAE 90.1 requirements
Heating	ASHRAE 90.1 requirements
HVAC Control	
Thermostat Setpoint	Dining: 23.9℃ Cooling / 21.1℃ Heating Kitchen: 26.1℃ Cooling / 18.9℃ Heating
Thermostat Setback	30℃ Cooling / 15.6℃ Heating
Supply air temperature	Maximum 40℃, Minimum 12.8℃
Economizers	Various by climate location and cooling capacity Control type: differential dry bulb
Ventilation	ASHRAE Ventilation Standard 62.1
Demand Control Ventilation	ASHRAE 90.1 requirements
Energy Recovery	ASHRAE 90.1 requirements
Supply Fan	
Supply Fan Total Efficiency (%)	Depending on the fan motor size
Supply Fan Pressure Drop	Various depending on the fan supply air
Pump	
Pump Type	Service hot water
Pump Power	100% efficient motor. Negligible power consumption
Service Water Heating	
SWH type	Storage tank
Fuel type	Natural gas
Thermal efficiency (%)	ASHRAE 90.1 requirements
Tank Volume (Liter)	200
Water temperature setpoint	60℃

Table 4.5 – HVAC summary of quick-service restaurant

Parameter	Dining Zone	Kitchen Zone
Area (m^2)	116	116
Volume (m^3)	354	354
Gross Exterior Wall Area (m^2)	93	93
Window Glass Area (m^2)	26	0
Occupancy Density (m^2/person)	1.33	18.52
Lighting Power (W/m^2)	22.60	12.92
Equipment Power (W/m^2)	116.79	1063.81

Table 4.6 – Zone summary of quick-service restaurant

The hourly occupancy, lighting, and equipment schedules of the quick-service restaurant are illustrated in Figures 4.10 – 4.13. These schedules including the building's internal loads and the ventilation requirements (Tables 4.4 – 4.6) are used to calculate the installed capacity, actual peak demand, and total energy consumptions.

The quick-service restaurant's kitchen has high electric and gas equipment densities for refrigeration, food preparation, and dishwashing, and often has high ventilation requirements. The internal loads in the kitchen can vary tremendously depending on the types and amounts of food served. It is estimated that about 800 meals are served per day, according to Brown [58], California Energy Commission [59], Fisher [60], and Smith et al. [61], which reviewed actual kitchen designs and examined annual utility data from more than hundred operating commercial kitchens. Table 4.7 shows the energy distribution of the kitchen loads within the EnergyPlus program's zone energy balance. All gas appliances are assumed to be under exhaust hoods, so a high fraction of the energy is 'lost' out the exhaust hood and not added to the space internal load.

Fraction	Gas Equipment	Electrical Equipment	Exhaust Hoods
Lost	0.7	0.20	1.0
Latent	0.1	0.25	0.0
Radiant	0.2	0.30	0.0
Convective	0.0	0.25	0.0

Table 4.7 – Distribution of quick-service kitchen loads in zone energy balance

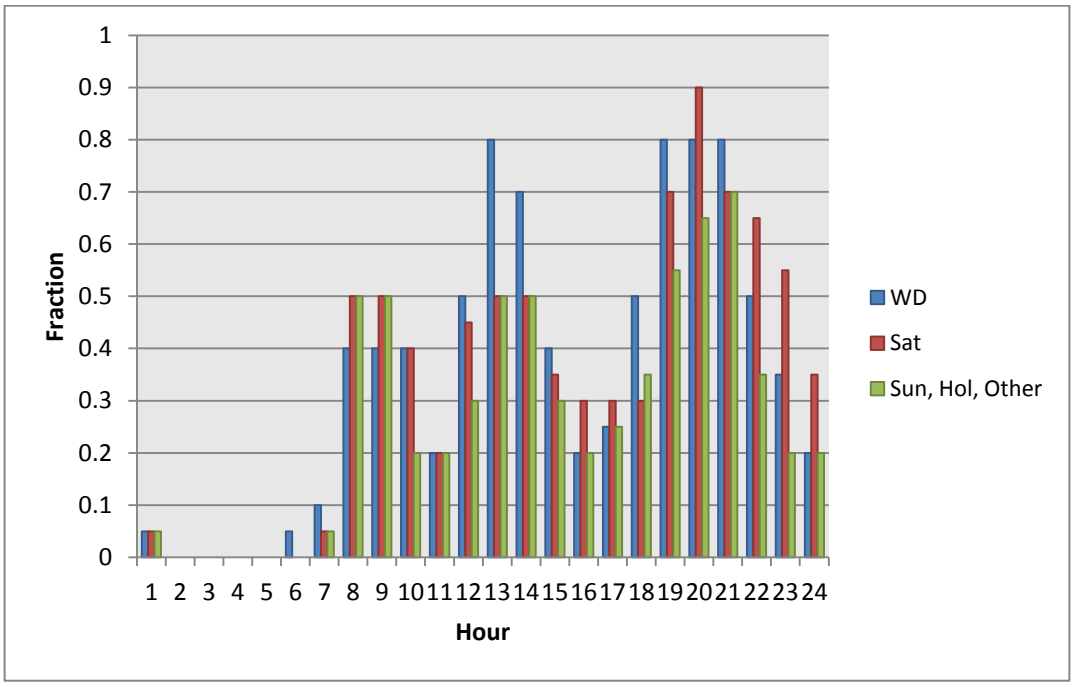

Figure 4.10 – Hourly occupancy schedule of quick-service restaurant

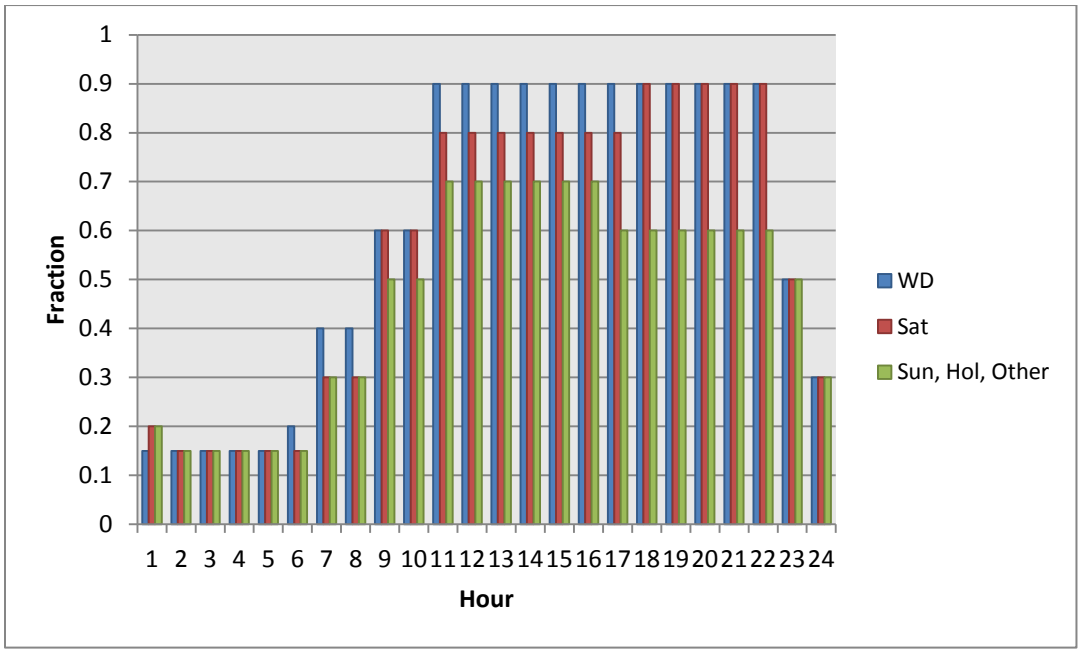

Figure 4.11 – Hourly lighting schedule of quick-service restaurant

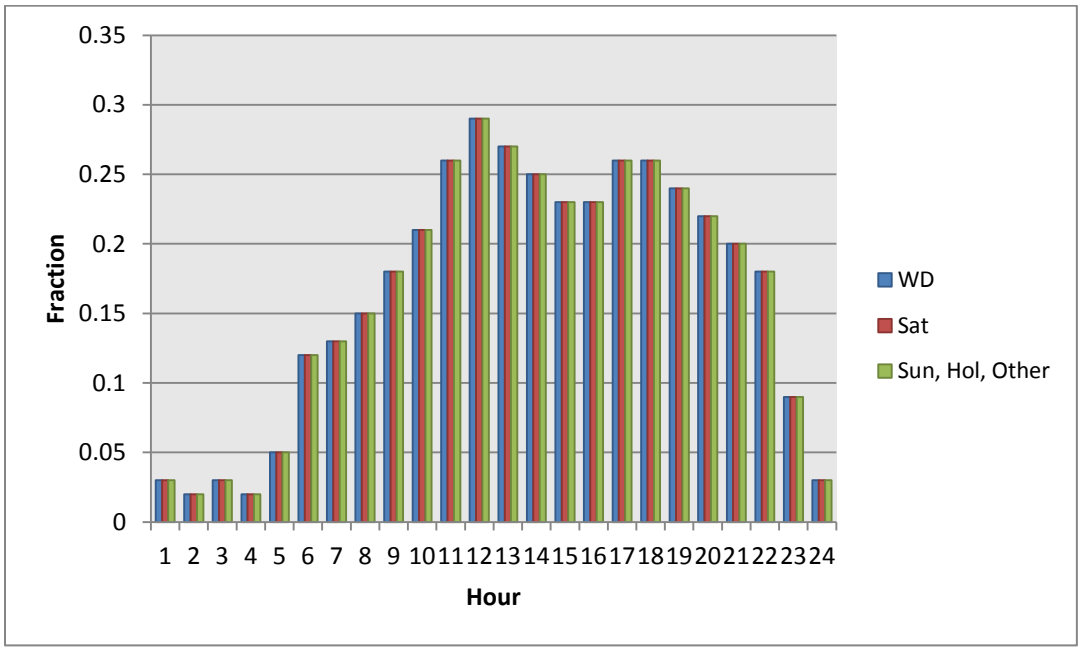

Figure 4.12 – Hourly equipment schedule of quick-service restaurant

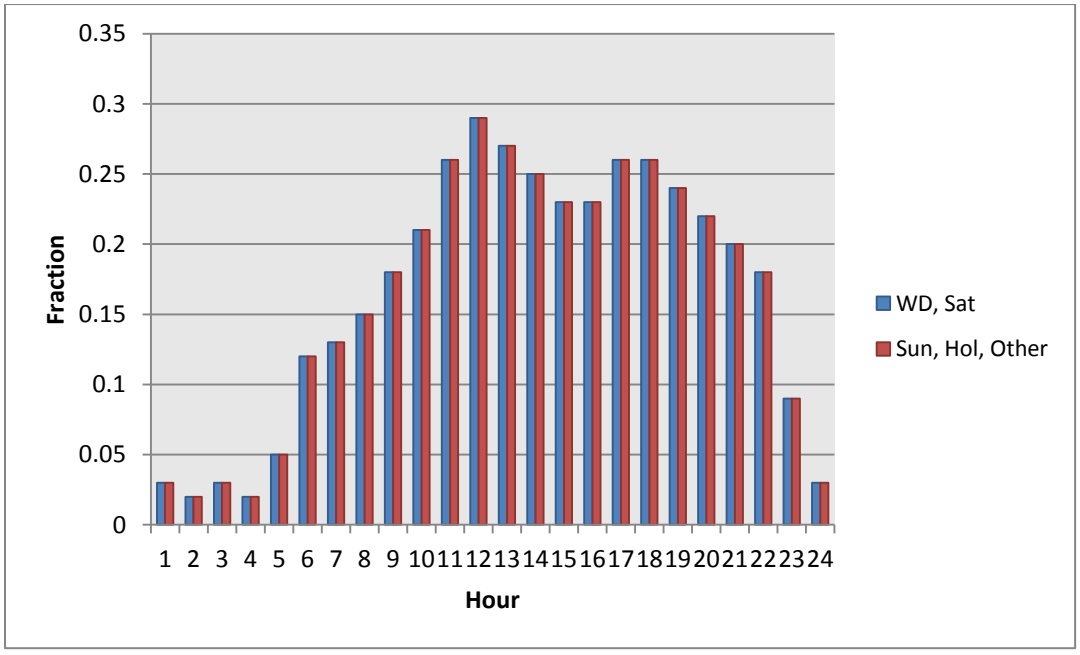

Figure 4.13 – Hourly gas equipment schedule of quick-service restaurant

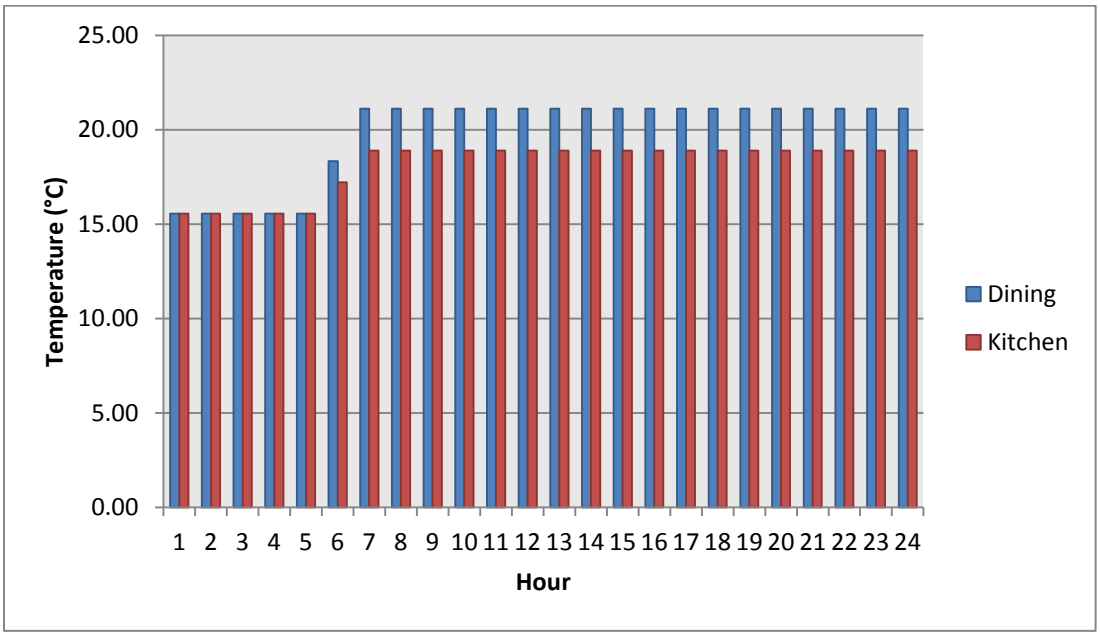

Figure 4.14 – Hourly heating setpoint temperature schedule of quick-service restaurant

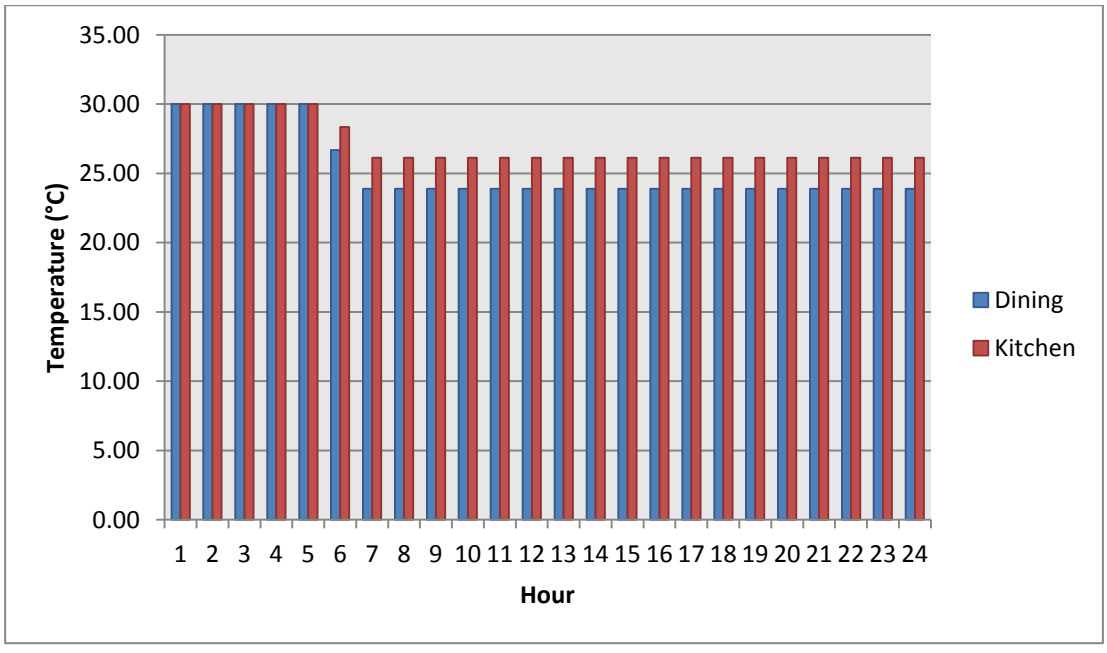

Figure 4.15 – Hourly cooling setpoint temperature schedule of quick-service restaurant

Figures 4.14 and 4.15 show the heating and cooling setpoint temperature schedules of the quick-service restaurant. These schedules are used to generate both the heating/cooling availability schedule and the temperature setpoint schedules used in the building energy simulations. The heating setpoint temperatures of the dining and kitchen zones are to 21.1°C and 18.9°C, respectively, during the restaurant's open hours (8am to 12am). The cooling setpoint temperatures of the dining and kitchen zones are set to 23.9°C and 26.1°C, respectively, during the restaurant's open hours (8am to 12am). When the restaurant is closed (1am to 7am) the heating setback temperature is dropped to 15.6°C and the cooling setpoint temperature is raised to 30°C.

4.3 Summary

This chapter presents an overview of computational case study models for a small commercial office building and a quick-service restaurant, which will be used to investigate the energy efficiency of the proposed air based PV/T solar roof system. The overview includes building data and descriptions, construction specifications, HVAC specifications, zone summary, various schedules, and heating and cooling setpoint schedules of the two buildings. The roofs of the two case study models are designed as a Gable roof and both buildings include an unconditioned attic and are constructed with wood joists and insulations. The Gable roof design allows for the installation of the air based PV/T solar roof system which can expose half of the roof area when facing south. This is the main reason why these two buildings were chosen for the study. In the next two chapters, these two building descriptions will be used as the basis for CFD studies (Chapter 5) and annual building energy simulation studies in various climates (Chapter 6).

Chapter 5. Computational Fluid Dynamics (CFD) Simulations

The developments in computer hardware and software have affected the practice of architecture in many ways. Computer technology and computational modeling allows for exploration of alternative conceptual and material strategies in a wide range of areas of engineering, architectural design, and natural environmental analysis. One approach for designing and conducting numerical analysis of emerged architectural designs is simulating thermal heat transfer through computational fluid dynamics (CFD) analysis. CFD is a tool widely used for wind/airflow analysis, HVAC design, and indoor thermal environment analysis in the concept phase of architectural design. This technique has the potential to assist investigations of detailed fluid flow and heat transfer analysis and allows the incorporation of realistic boundary conditions and obstructions.

Until recently, CFD and building energy simulations were often restricted to projects with high budgets by employing energy experts. However, with advancements in computer engineering, significant developments have been made towards integrating CFD and building energy simulation tools in the conceptual phase of architectural design. CFD also offers many advantages such as time, cost, and ease of visualizing results. This enables architects and engineers to consider the energy performance of a building during the early design stages.

The fluid dynamics program used for this study is the commercial CFD code FLUENT (version 12.1.2) by ANSYS, Inc. FLUENT's source code uses a finite-volume discretization method to solve the governing equations, which means the region of interest

(domain) is divided into a finite number of cells or control volumes (mesh or grid). During CFD simulations, the variables are solved at the center of the cell. The values at other locations are determined by interpolating those values. In other words, the accuracy of the numerical solution will usually improve with an increased number of grid points. Consequently, the creation of the mesh or grid is one of the most critical elements when considering a successful CFD simulation. FLUENT also includes three main components: a pre-processor, a solver, and a post-processor. The pre-processor is where the domain, geometry and mesh are created, and the fluid flow properties and the type of boundaries are specified. The solver is where boundary conditions are created or modified and the convergence criterion is applied. The post-processor is where the simulation results are analyzed both numerically and graphically. Thus, CFD simulations can give both quantitative and qualitative data throughout the whole model.

One of the features of FLUENT is the availability of the solar load model within the program and this model is a combination of a solar ray tracing algorithm and a radiation model called surface to surface (S2S). The solar ray tracing algorithm works as the source of the solar radiation absorbed on the outside surface and the S2S radiation model accounts for the internal heat transfer. Another feature of FLUENT is that the program has the capability to allow flow to enter and exit the solution domain. One of the condition options of the inlet and outlet boundaries is that the velocity and scalar properties of the air flow at the inlet boundary can be defined. This also means that the total (or stagnation) pressure is not fixed but will rise (in response to the computed static pressure) to whatever value is necessary to provide the prescribed velocity distribution. When the velocity inlet boundary

condition defines flow entering the physical domain of the CFD model, FLUENT uses both the velocity components and the scalar quantities that are defined as boundary conditions to compute the inlet mass flow rate, momentum fluxes, and fluxes of energy. The mass flow rate entering the air fluid cell adjacent to a velocity inlet boundary is computed as

$$\dot{m} = p\,\vec{v}\,A_{inlet} \tag{5.1}$$

Mathematical Variable	Description
$\dot{m}$	Mass flow rate [kg/s]
p	Density of air [kg/m^3]
$\vec{v}$	Inlet velocity [m/s]
A_{inlet}	Inlet flow area [m^2]

The CFD study model is restricted to the roof assembly of the building energy simulation reference models with same construction material specifications as defined in Chapter 4. Instead of building the entire building energy simulation reference models, the computational domain needs only to extend over a representative element, which is the southern exposed portion of the gable roof. The CFD simulations are carried out over a wide range of conditions, and the thermal effectiveness is determined and results are incorporated into a correlation model. The thermal efficiency can be defined as the ratio of the useful heat gain of the entire air system versus the total incident solar radiation on the gross surface area of the PV/T roof:

$$\eta_{thermal} = \frac{(Q_{therm} / A_{surf})}{I} = \frac{\dot{m} c_p (T_{out} - T_{in})}{I\, A_{surf}} \quad (5.2)$$

Mathematical Variable	Description
$\eta_{thermal}$	Thermal conversion efficiency
Q_{therm}	Thermal energy collected [W]
A_{surf}	Net area of the surface [m^2]
I	Incident solar radiation [W/m^2]
$\dot{m}$	Mass flow rate [kg/s]
c_p	Specific heat of air [J/kg·℃]
T_{out}	Outlet node temperature [℃]
T_{in}	Inlet node temperature [℃]

5.1 CDF Studies of Air Channel Depth and Inlet Velocity

The air channel depth of the air based PV/T solar roof system is an important parameter affecting the system's thermal efficiency. According to findings documented in the academic literature and the Solar Rating and Certification Corporation's 'Directory of SRCC Certified Solar Collector Ratings' handbook [8], the air channel depth of previous studies and various manufacture's specifications are in the range of 3.81 cm and 15.24 cm. The CFD studies in this dissertation incorporates the specification ranges of the air channel depth as mentioned above and simulations are tested while increasing the depth in increments of 1.27 cm.

According to the U.S. DOE [3], it is recommended that the inlet velocity through a standard solar air collector be in the range of 1.5 – 3.1 m/s. Along with increasing the air channel depth, three different inlet velocities of 1.5 m/s (low), 2.3 m/s (mid), and 3.1 m/s

(high) are incorporated into the simulations for further evaluations. Furthermore, the solar radiation absorbed on the PV panel surface (top) will be set to 200 W/m^2, 400 W/m^2, and 600 W/m^2 and the inlet temperature is set to 20℃ as it is the base point temperature which is in the range of the heating thermostat setpoint and setback temperatures of the two computational case study models. Changing the parameters of inlet velocity, solar radiation absorbed on the PV panel surface, and increasing the air channel depth shows a comprehensive correlation between the system's thermal efficiency and the air channel depth.

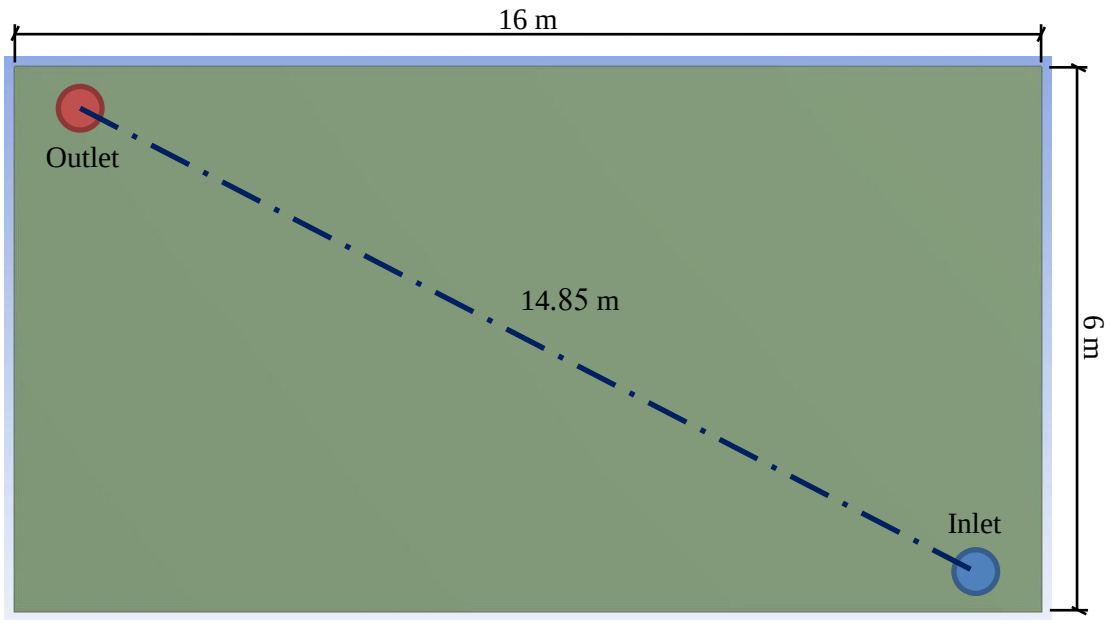

Figure 5.1 – Bottom view of pre-meshing CFD model

Figure 5.1 illustrates the bottom view of the CFD simulation study model before the meshing process. The CFD model is 16 m (width) by 6 m (length) and has an area of 96 m^2.

The inlet and outlet are circular shapes with a radius of 0.5 m and the shortest distance from the inlet to the outlet is 14.85 m.

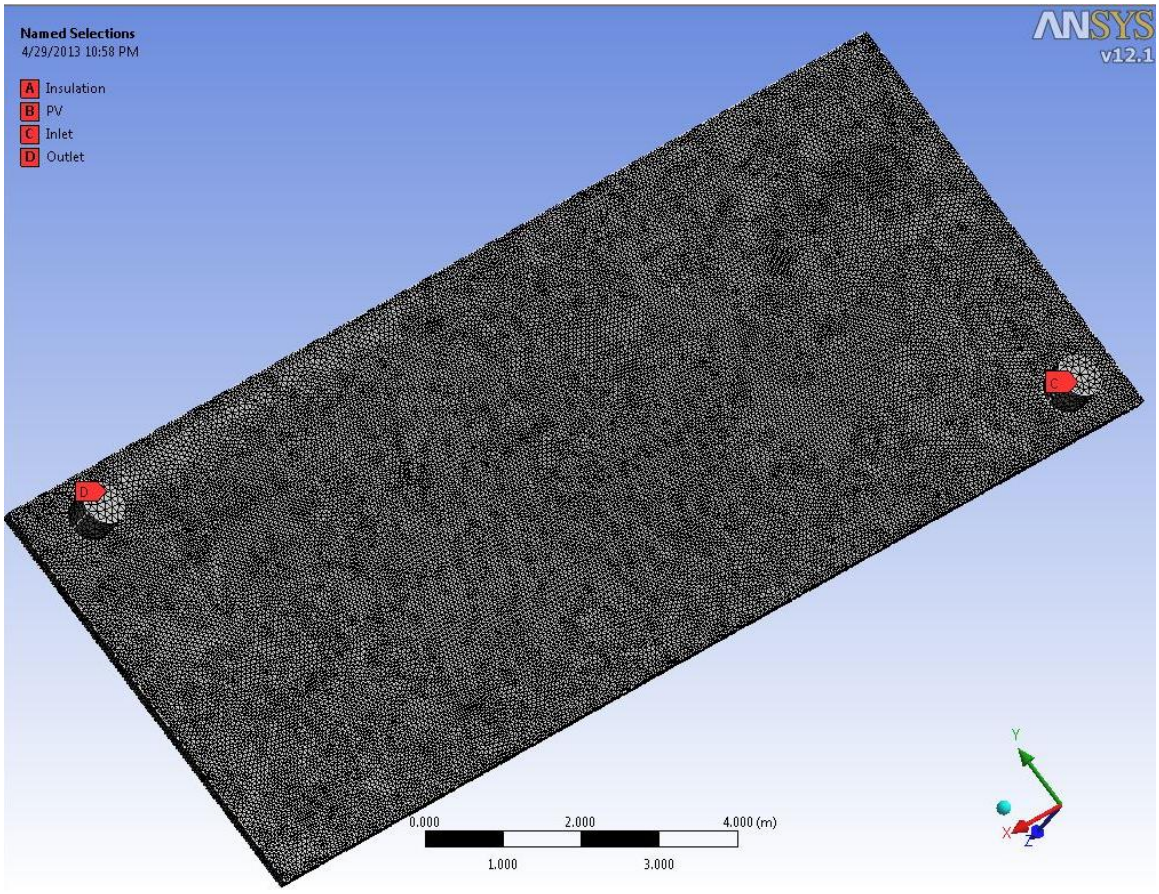

Figure 5.2 – Perspective view of meshed CFD model

Figure 5.2 shows the perspective view of the CFD model after the meshing process, and Figure 5.3 presents the details of the mesh used for the CFD model. In order to analyze the fluid flow and heat transfer, the domains are split into smaller subdomains (made up of geometric primitives like hexahedra) and discretized governing equations are solved inside each of these portions of the domain.

Details of "Mesh"	
Defaults	
Physics Preference	CFD
Solver Preference	Fluent
Relevance	0
Sizing	
Use Advanced Si...	On: Proximity and Curvature
Relevance Center	Coarse
Initial Size Seed	Active Assembly
Smoothing	Medium
Transition	Slow
Span Angle Center	Fine
Curvature Norma...	Default (18.0 °)
Proximity Accuracy	0.5
Num Cells Across...	Default (3)
Min Size	5.e-002 m
Max Face Size	0.20 m
Max Tet Size	0.50 m
Growth Rate	Default (1.20)
Minimum Edge L...	0.1110 m
Inflation	
Use Automatic Te...	None
Inflation Option	Smooth Transition
Transition Ratio	0.272
Maximum Layers	5
Growth Rate	1.2
Inflation Algorit...	Pre
View Advanced ...	No
Advanced	
Shape Checking	CFD
Element Midside ...	Dropped
Straight Sided El...	
Number of Retries	0
Rigid Body Beha...	Dimensionally Reduced
Mesh Morphing	Disabled
Pinch	
Pinch Tolerance	Default (4.5e-002 m)
Generate on Refr...	No
Statistics	
Nodes	243450
Elements	222137
Mesh Metric	None

Figure 5.3 – Cell sizing and statistical details of the meshed CFD model

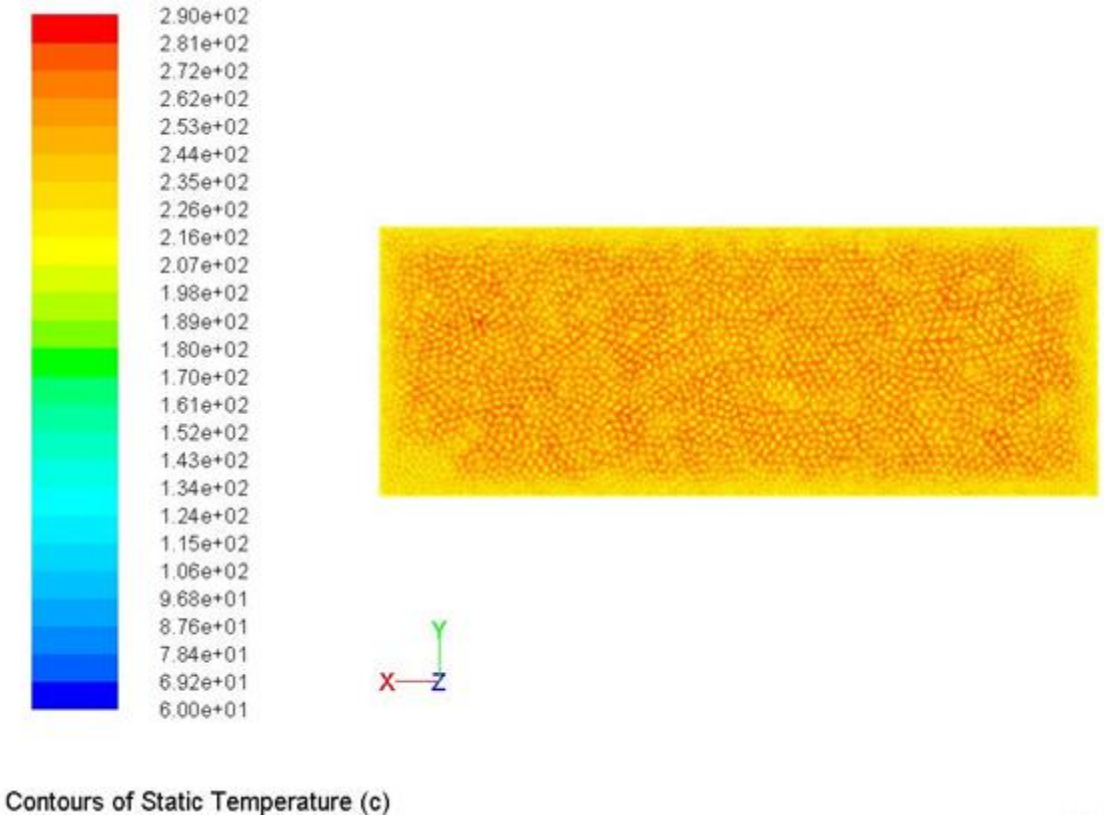

Figure 5.4 – PV panel surface temperature distribution of simulated CFD model

Figure 5.4 shows an example of the temperature distribution on the surface of the PV panel after solar radiation is absorbed which range between 235℃ (yellow) and 272℃ (orange).

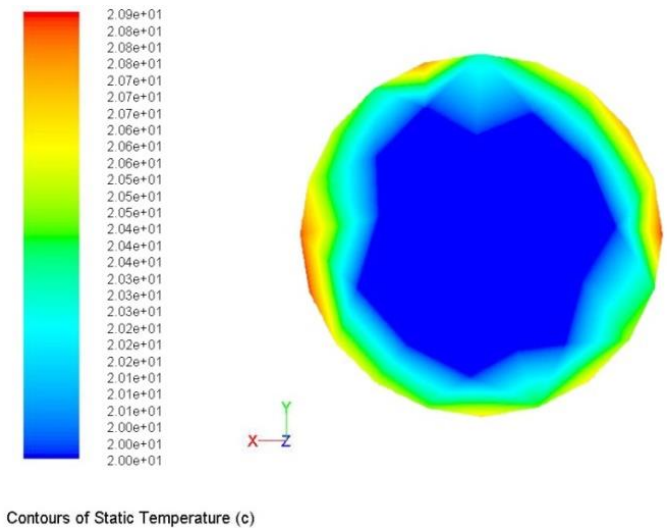

Figure 5.5 – Inlet temperature distribution of simulated CFD model

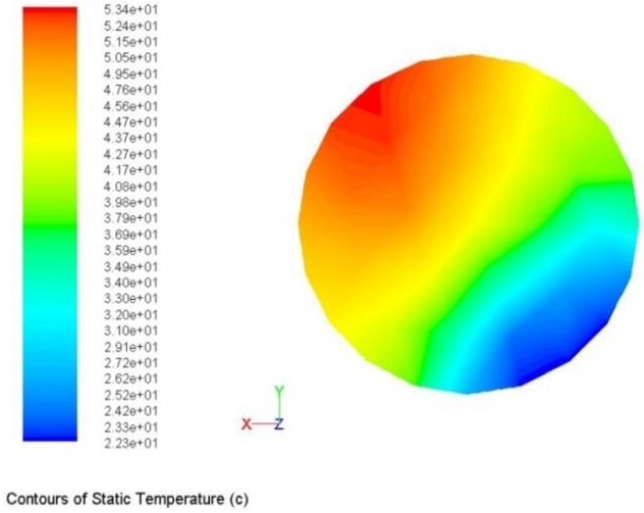

Figure 5.6 – Outlet temperature distribution of simulated CFD model

Figures 5.5 – 5.6 show examples of inlet and outlet temperatures of the simulated CFD model. The temperature distribution of the inlet illustrates the initial set temperature of 20℃ (blue). The outlet illustrates the temperature distribution after the thermal heat transfer simulation within the air channel. The temperatures shown in the outlet are in the

range between 22.3℃ (blue) – 53.4℃ (red), which calculates to an average outlet temperature of 37.9℃.

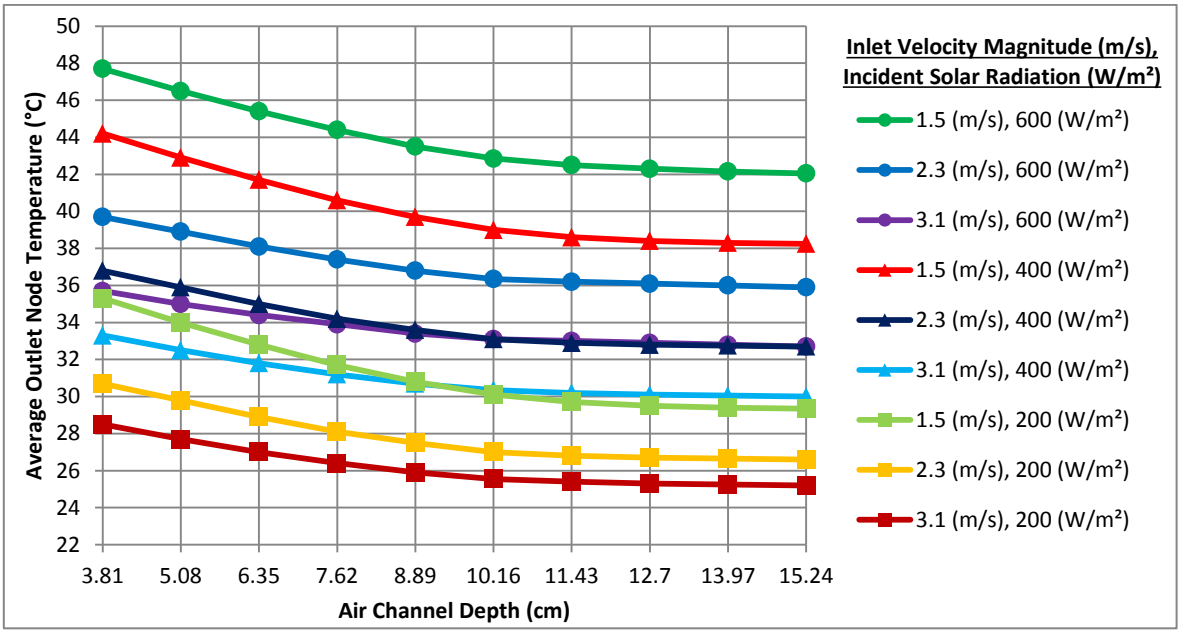

Figure 5.7 – Average outlet node temperature as a function of air channel depth

Figure 5.7 presents the variation of system's outlet temperature as a function of air channel depth. It is observed that the outlet temperature decreases with increasing air channel depth. An inlet velocity of 1.5 m/s with an incident solar radiation of 600 W/m^2 showed the highest outlet temperatures, and an inlet velocity of 3.1 m/s with an incident solar radiation of 200 W/m^2 showed the lowest outlet temperatures. The air channel depth of 3.81 cm, an inlet velocity of 1.5 m/s, and a solar radiation of 600 W/m^2 resulted in an outlet temperature of 47.7℃ which is the highest among all the different cases. The air channel depth of 15.24 cm, an inlet velocity of 3.1 m/s, and a solar radiation of 200 W/m^2 resulted in the lowest outlet temperature of 25.2℃. This simulation results indicates that

having the shallowest air channel depth of 3.81 cm results in the highest outlet temperature and that once the air channel depth reaches 10.16 cm, the outlet temperatures converges to a constant value.

The finding that shallower depth of the air channel leads to higher temperature can be primarily attributed to the higher velocity that results from having a shallower air channel depth. Higher velocity, in turn, causes the convective heat transfer coefficient of air to increase. Such effect will level off with increase in depth and serve as the most likely reason for the outlet temperature profile.

Another potential explanation is the greater total volume of air that results from having greater air channel depth. The greater volume of air will lead to a decrease in the PV panel surface area to air volume rate within the air channel. This leads to the effect of the exterior solar radiation absorbed by the PV panel being spread among the greater volume of air within the air channel and ultimately reducing the outlet node temperature. Simultaneously, however, the effect of the solar radiation absorbed by the PV panel will start to decrease with the increased air volume within the air channel, making the outlet node temperature to decrease at a diminishing rate and ultimately converging to a constant value.

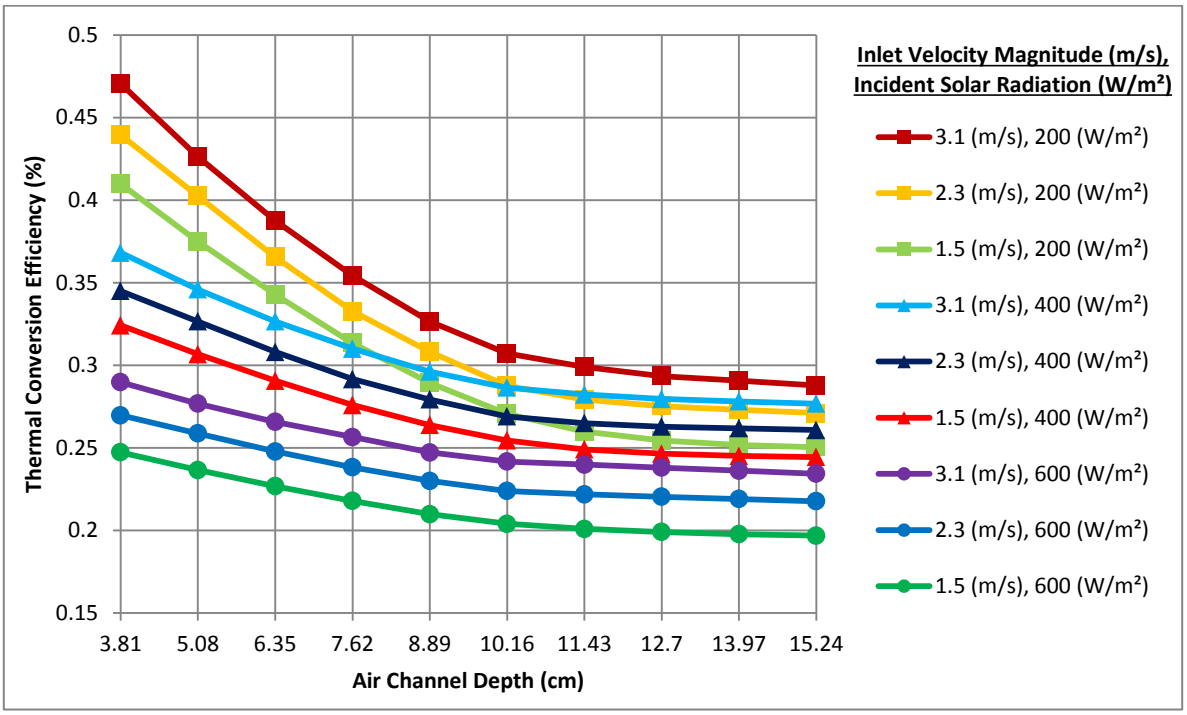

Figure 5.8 – Thermal conversion efficiency as a function of air channel depth

Figure 5.8 presents the variation of the system's thermal efficiency as a function of air channel depth. Similar to Figure 5.7, the system's thermal efficiency is observed to decrease with increasing air channel depth. Such observation is consistent with what can be predicted under Equation 5.2 where thermal efficiency is positively associated with the outlet temperature. However, while higher velocities were shown to result in lower outlet temperatures (Figure 5.7), they were shown to result in higher thermal efficiency (Figure 5.8). This may seem inconsistent with Equation 5.2 where thermal efficiency is positively associated with the outlet temperature as well as the mass flow rate. However, changes in velocities not only affect the outlet temperature, but also affect the mass flow rate which is a critical component in computing thermal efficiency. An increase in velocity from 1.5 m/s

to 3.1 m/s nearly doubles the mass flow rate from 0.511 kg/s to 1.056 kg/s. The same increase in velocity, however, only results in a temperature reduction of approximately 8 degrees given different combinations of air channel depth and solar radiation. In other words, the increase in air mass flow rate is significantly greater compared to the decrease in outlet temperature caused by an increase in velocity. This is the reason why higher thermal efficiency is observed with higher velocity despite the decrease in outlet temperature due to the higher velocity. The figure also illustrates that the 'group' of incident solar radiation of 200 W/m^2 showed the system's highest thermal efficiency. This is consistent with Equation 5.2 where thermal efficiency is inversely related to solar radiation. This implies that the air based PV/T solar roof system can be effective even with a relatively low amount of incident solar radiation on the PV panel's surface.

5.2 CFD Studies of Air Mass Flow Rate

The air mass flow rate is another important parameter affecting the system's thermal efficiency. According to the U.S. DOE [3], it is recommended that the air mass flow rate through a standard solar air collector be between 0.0063 – 0.0189 $kg/s \cdot m^2$ and the velocity be between 1.5 – 3.1 m/s. Figure 5.9 presents the variation of the CFD model's air mass flow rate as a function of velocity. The horizontal red line across the graph is the recommended air mass flow rate specified by the U.S. DOE. The blue line results from applying the base cases discussed in section 5.1 in computing the air mass flow rate[2] for different velocity magnitudes. Velocities below the horizontal red line, 1.5 – 1.7 m/s, are

[2] Air mass flow rate ($kg/s \cdot m^2$) = mass flow rate (kg/s) / absorber heat exchange surface area (m^2)

not in the specified range and therefore were neglected when determining the system's air mass flow rates. Hence, only velocities in the range of 1.8 – 3.1 m/s were used to calculate the air mass flow rates for this system. An analysis of Figure 5.9 show that the highest velocity of 3.1 m/s resulted in an air mass flow rate of 0.0110 kg/s·m^2 which is within the recommended range of the U.S. DOE.

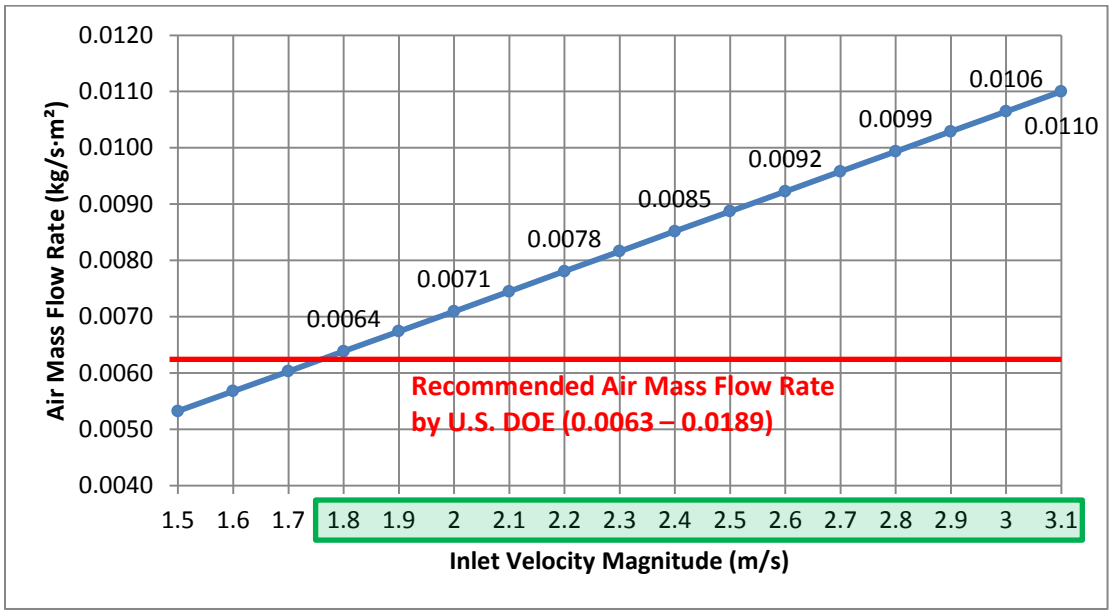

Figure 5.9 – Air mass flow rate as a function of velocity magnitude

The findings from the CFD studies further show significant differences in the thermal conversion efficiency depending on the air mass flow rate of the air based PV/T solar roof system. As shown in Figure 5.10 – 5.12, the thermal conversion efficiency ranged from 16.7% to 47.1% (incident solar radiation of 200 W/m²), 16.1% to 36.8% (incident solar radiation of 400 W/m²), and 13.6% to 29.0% (incident solar radiation of 600 W/m²) where higher air mass flow rates resulted in higher thermal efficiency. This is

consistent with Equation 5.2 where thermal efficiency is shown to be positively associated with the air mass flow rate. The findings are also consistent with the discussion provided in the previous section regarding the effect of air channel depth on thermal efficiency where shallower air channels lead to greater thermal efficiency. Specifically, the air channel depth of 3.81 cm with a flow rate of 0.011 kg/s·m^2 had the highest thermal efficiency of 47.1% (incident solar radiation of 200 W/m²), 36.8% (incident solar radiation of 400 W/m²), and 29.0% (incident solar radiation of 600 W/m²) an increase of 19.7%, 15.4%, and 12.2%, respectively, when compared to initial flow rate of 0.0064 kg/s·m^2. The air channel depth of 15.24 cm had a thermal efficiency range between 16.7% – 28.8% (incident solar radiation of 200 W/m²), 16.1% – 27.7% (c), 13.6% – 23.4% (incident solar radiation of 600 W/m²), which is the lowest rate of increase at 12.1%, 11.6, and 9.8%, respectively. This indicates that the rate of increase is highest when the air channel depth is most shallow at 3.81 cm and decreases as the air channel depth gets deeper. Such findings confirm the findings from the previous section.

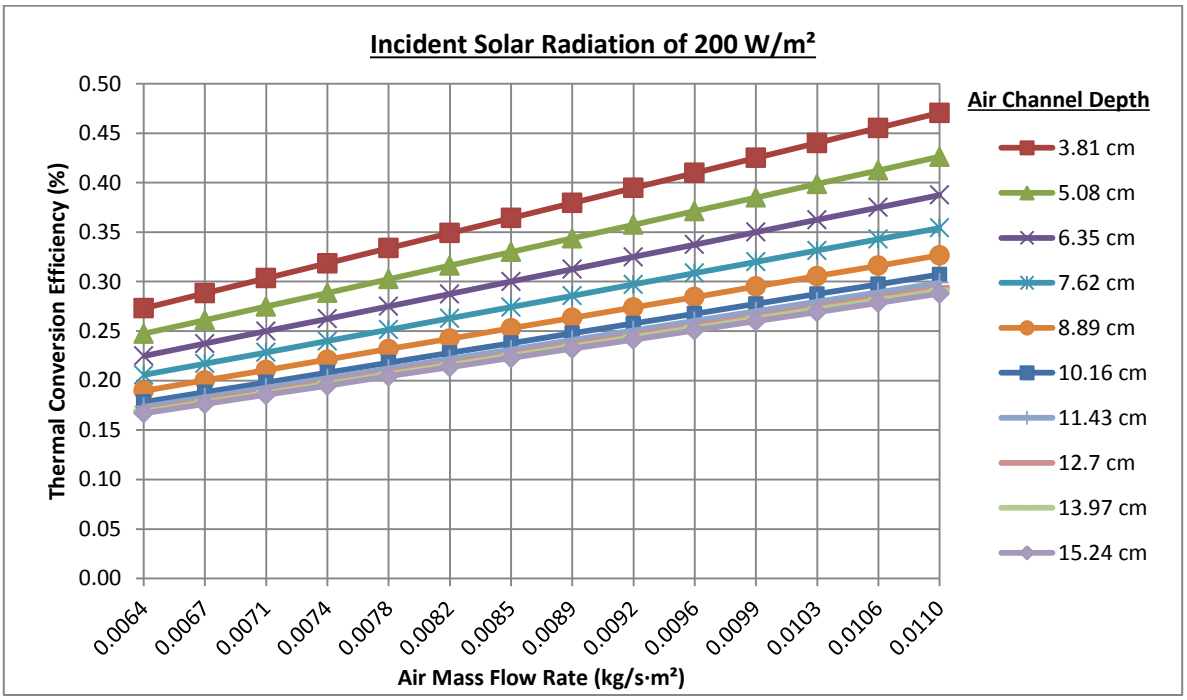

Figure 5.10 – Thermal efficiency as a function of air mass flow rate [200 (W/m²)]

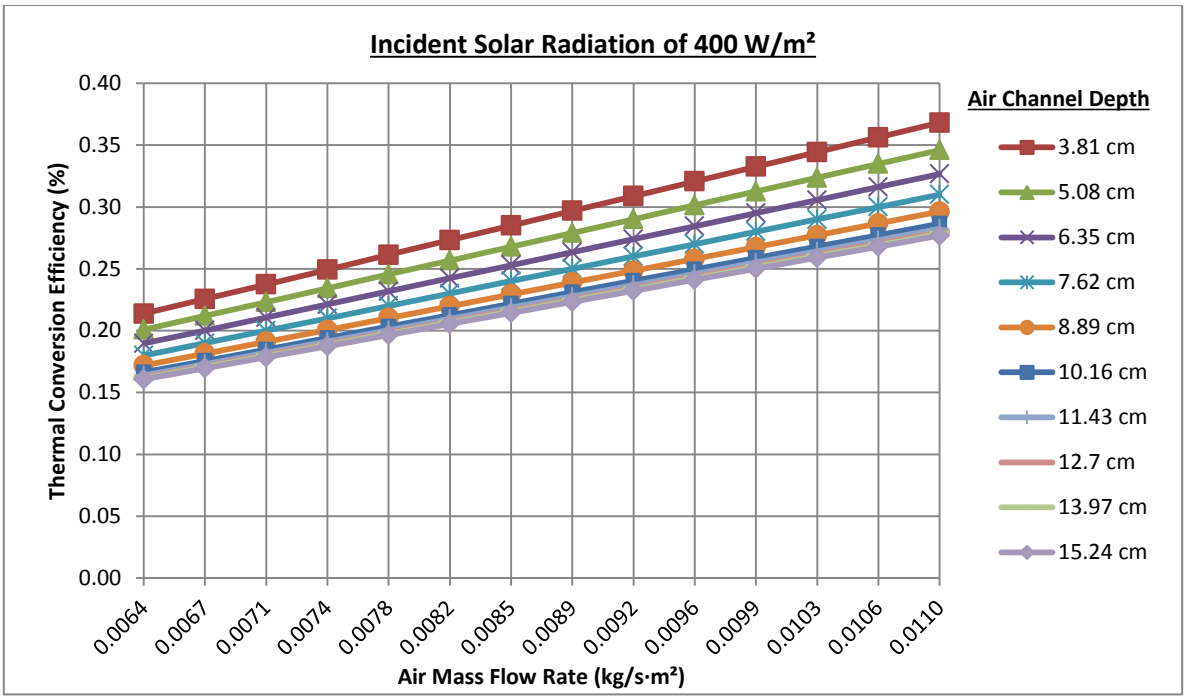

Figure 5.11 – Thermal efficiency as a function of air mass flow rate [400 (W/m²)]

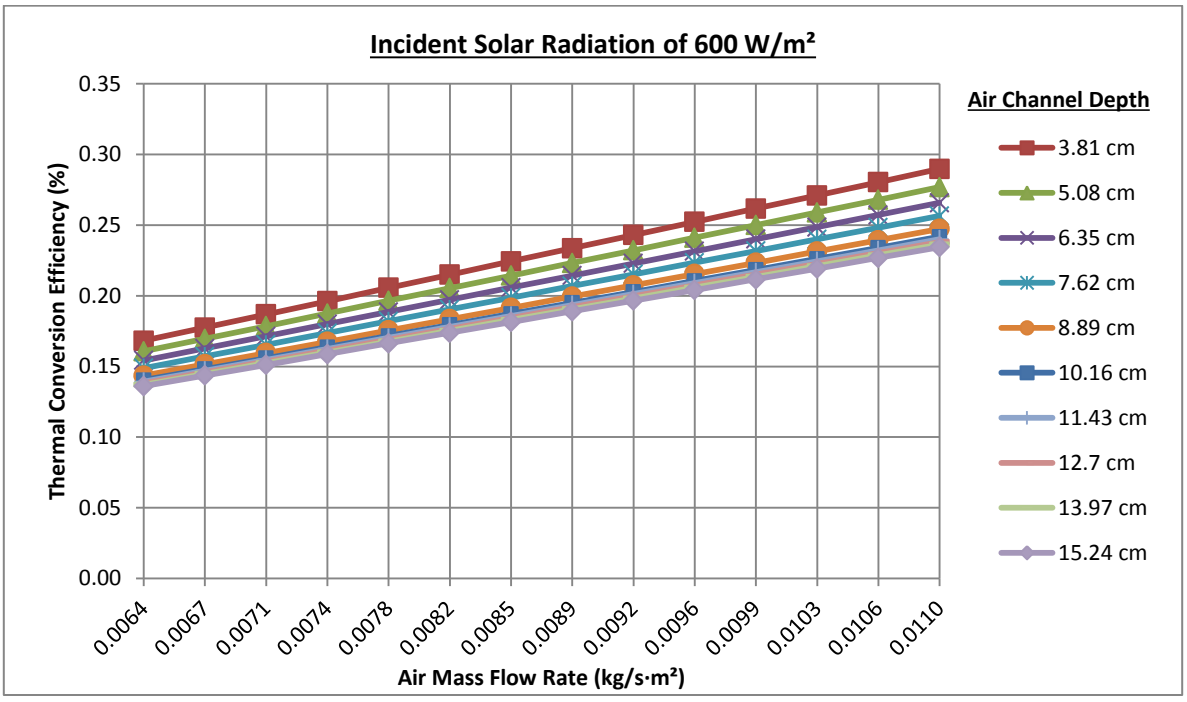

Figure 5.12 – Thermal efficiency as a function of air mass flow rate [600 (W/m²)]

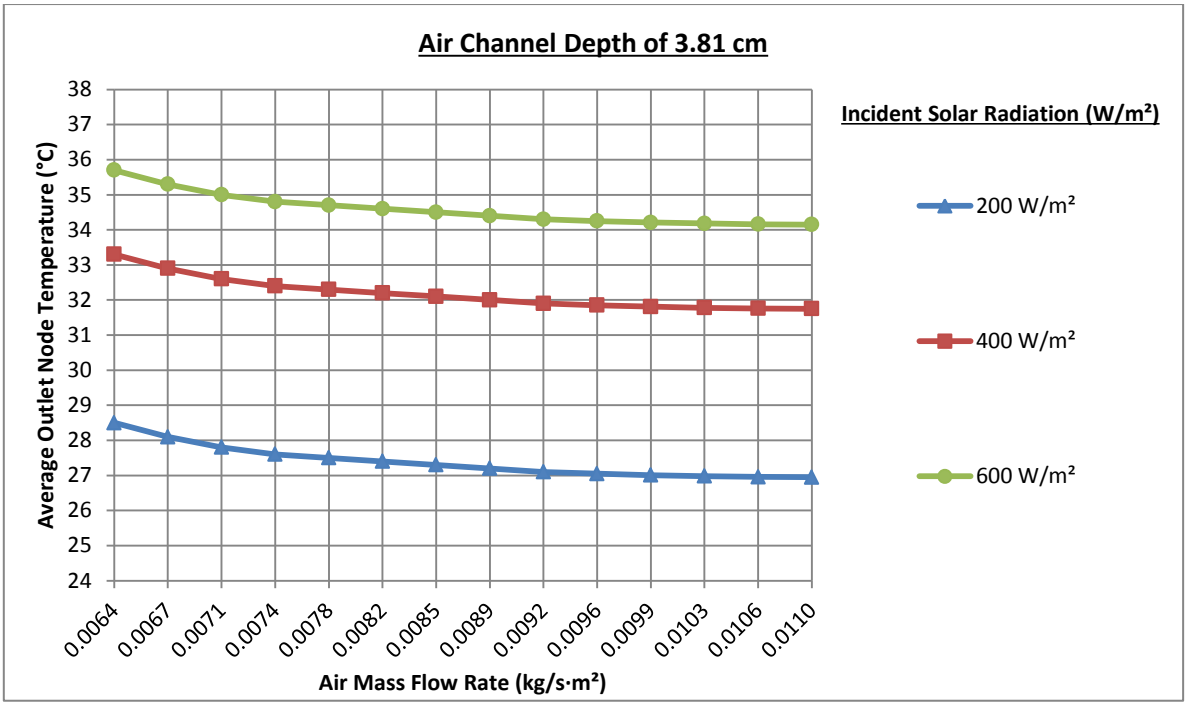

Figure 5.13 – Average outlet node temperature as a function of air mass flow rate

Figure 5.13 shows that higher air mass flow rates lead to a decrease in outlet temperatures. This is attributable to more air volume being available to take away more thermal heat from the air channel and air having less time inside the air channel to attain higher outlet temperatures. Equation 5.2 suggests that lower outlet temperatures would lead to lower thermal efficiency. However, the effect of increased air mass flow rate on outlet temperature change appears to be at a minimal level with the biggest change being approximately two degrees. In other words, the effect of increased air mass flow rate on outlet temperature is not significant enough to decrease the overall level of thermal efficiency. Figure 5.13 also shows that as the air mass flow rate increases over 0.0096 $kg/s \cdot m^2$, the outlet temperatures start to converge to a constant value. Overall, the findings suggest that incorporating a higher air mass flow rate will enable greater thermal efficiency of the air based PV/T solar roof system despite the slight decrease in outlet temperatures that result from increased air mass flow rates.

5.3 CFD Studies of Air Channel Design Configurations

Previous CFD studies show that an air based PV/T solar roof system with the shallowest air channel depth along with the highest air mass flow rate within the recommendations provided by the U.S. DOE, led to the highest system thermal efficiency of the cases studied in this dissertation so far. In order to see if a higher thermal efficiency could be reached, different design configurations of the air channel were examined. This section presents the results of the design configurations of the air channel within the air based PV/T solar roof system and how the design configuration influences the amount of heat extraction.

As mentioned previously in Chapter 2 as part of the literature review, the length of the air channel is a critical parameter that affects the air based PV/T solar energy system's performance. A longer air channel means that the air traveling through the air channel, for a given air mass flow rate, is exposed to solar radiation and absorbs it for a longer period of time which leads to an increase in the outlet air temperature. The initial CFD study model, Figures 5.1, show the shortest distance from the system's inlet to the outlet to be 14.85 m. In order to increase the distance from the inlet to the outlet, vertical baffles which allow the air to move up and down vertically within the air channel and horizontal baffles which allows the air to move side to side horizontally within the air channel were installed, Figures 5.14 – 5.15. Adding vertical and horizontal baffles can increases the distance from the inlet to outlet over 125 m and accordingly, it is predicted that installation of these baffles will lead to a higher average outlet node temperature as well as a higher thermal efficiency compared to the initial CFD studies in this dissertation that had no baffles.

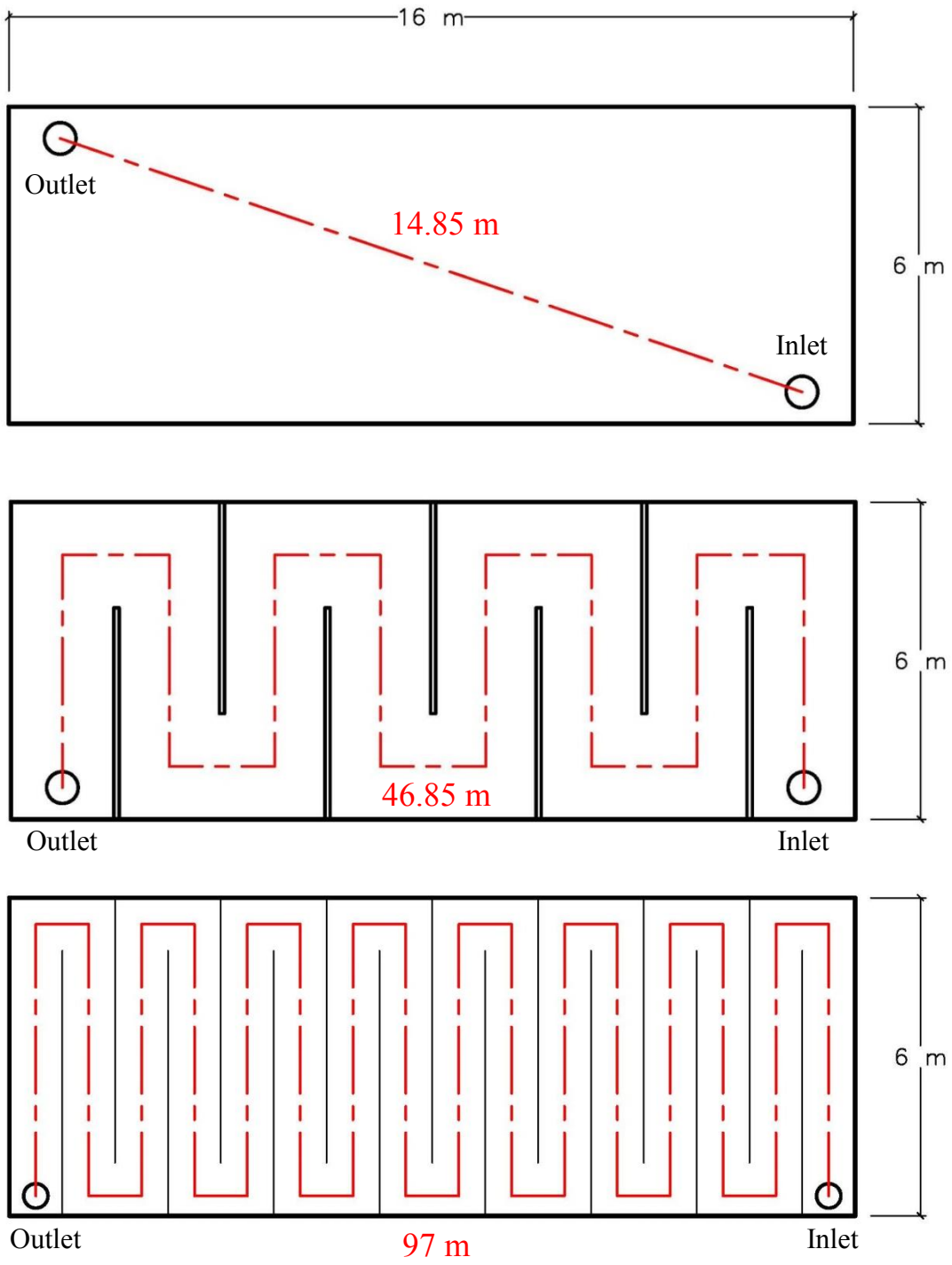

Figure 5.14 – Air channel with addition of vertical baffles

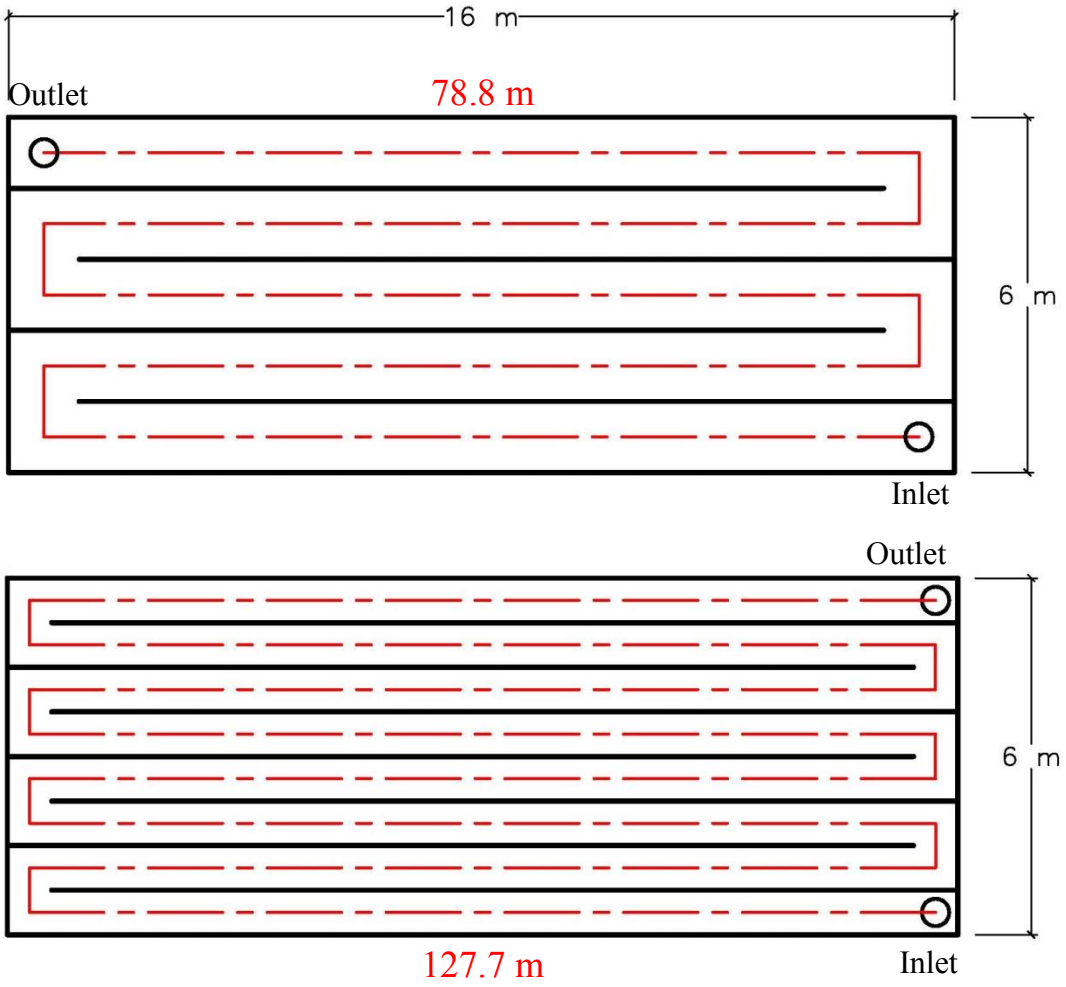

Figure 5.15 – Air channel with addition of horizontal baffles

After numerous CFD simulations under different configurations to increase the distance from the inlet to the outlet, the calculated thermal efficiency converged to a constant value of 73.2% (incident solar radiation of 200 W/m²), 72.1% (incident solar radiation of 400 W/m²), and 71.0% (incident solar radiation of 600 W/m²). Figure 5.16 further implies that an increase in the air channel length leads to greater thermal conversion efficiency regardless of whether the horizontal or vertical baffles are used to create greater

distance. Moreover, as the air channel length increases, the difference between the thermal conversion efficiency based on three different levels of incident solar radiations decreases and ultimately converges to a thermal conversion efficiency that is greater than 70%. This is also an indication that the performance of the proposed air based PV/T solar roof system eventually hits a maximum level and that the level of incident solar radiation does not play a significant role once the system's thermal efficiency is near the maximum range. As the thermal conversion efficiency was shown to reach a level higher than 70%, this value will be used in the next chapter for the whole building annual energy simulations using the EnergyPlus program as the simulations are targeted to bracket the upper end of performance.

The CFD simulations suggest that a longer air channel length increases thermal efficiency and eventually hits a maximum level. However, increasing the length of the air channel also increases the friction loss of the air moving through the air based PV/T solar roof system which presumably leads to an increase in fan energy consumption. Thus, increasing the channel length does not come without a potential drawback. The current EnergyPlus model of the air based PV/T solar roof system does not model the presence of vertical or horizontal baffles within the air channel, so the fan energy is set in this study to bracket the upper end of performance. The EnergyPlus model is based on user-defined efficiencies and a detailed model based on first-principles. A more detailed model that includes the impact of length on fan energy consumption is one of the potential future improvements of this study and could thus answer questions regarding the potential increase in fan energy as channel length increases.

Furthermore, future studies that implement additional CFD simulations of different inlet velocities for differing air channel length to determine the length requirement for various inlet velocities as well as the performance ceiling will help strengthen the results of this study. Additional studies will also help in predicting potential performance as a function of inlet velocity, air channel depth, and air channel length.

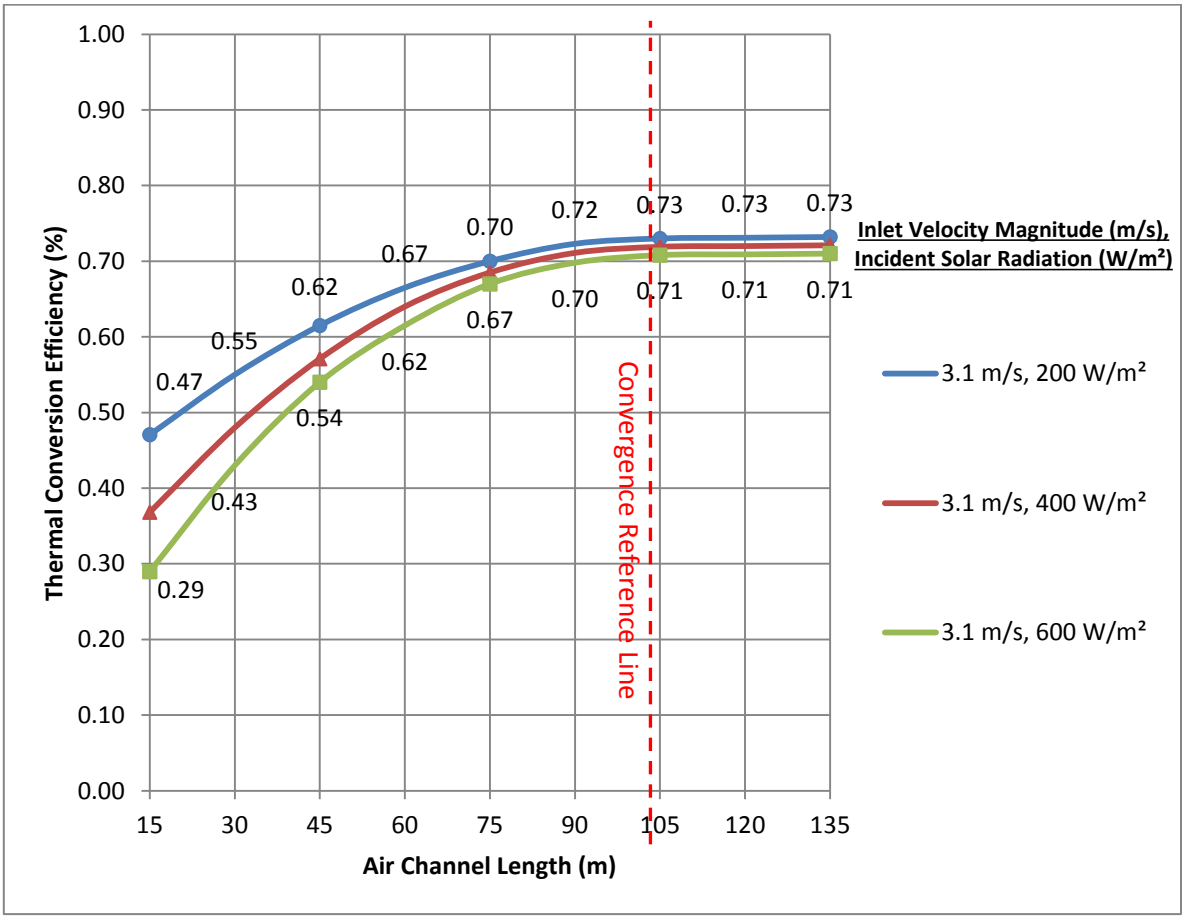

Figure 5.16 – Thermal conversion efficiency as a function of air channel length

5.4 Summary

The computer fluid dynamics solution used for this study is the commercial CFD code FLUENT (version 12.1.2) by ANSYS, Inc., and the CFD study model is a representation of the roof assembly of the case study models with identical construction material specifications. With FLUENT having the capability to allow air flow simulations, the air can enter through the inlet of the CFD model, absorb heat transfer from solar radiation while traveling through the air channel, and exit through the outlet with various velocity inlet boundary conditions. The CFD simulations were carried out over a wide range of conditions to compute the inlet mass flow rate, momentum fluxes, and fluxes of energy and ultimately calculate the thermal effectiveness of the solar roof system. In other words, the parametric CFD studies used similar input variables for all the configurations so that the results would provide further insight regarding the performance comparison. Moreover, the thermal efficiency, defined as the ratio of the useful heat gain of the entire air system versus the total incident solar radiation on the gross surface area of the PV/T roof was computed.

The first set of the CFD studies examined how the air channel depth and inlet velocity of the air based PV/T solar roof system affects thermal efficiency. Findings show that having the shallowest air channel depth, within the range provided by the Solar Rating and Certification Corporation (SRCC), lead to the highest system thermal efficiency. The findings also showed that an increase in air channel depth resulted in a lower outlet temperature which converges to a constant value once the air channel reaches 10.16 cm. The increase in outlet node temperature due to shallower air channel depth can be attributed

to the increase in velocity that follows from having a shallower air channel depth, which in turn, increases the convective heat transfer coefficient. Such effect will tend to level off with an increase in depth and serve as the most likely reason for the outlet temperature profile observed in this study. Another potential consideration would be the greater total volume of air caused by the increase in air channel depth which leads to a decrease in the PV panel surface area to air volume within the air channel. This leads to the effect of the exterior solar radiation absorbed by the PV panel being spread among the greater volume of air within the air channel and ultimately reducing the outlet node temperature. Also, as the air channel depth increases, the effect of the solar radiation absorbed by the PV panel will start to decrease with the increased air volume within the air channel. This will lead to the outlet node temperature decreasing at a diminishing rate with increases in air channel depth and ultimately converging to a constant value.

The first set of the CFD studies also showed that higher velocities lead to higher thermal efficiency. However, higher velocities were also shown to lower outlet temperatures at the same time. The finding that higher thermal efficiency is observed with higher velocity despite the decrease in outlet temperature can be attributed to the fact that higher velocities result in higher air mass flow rates and that such increase is significantly greater compared to the decrease in outlet temperature caused by an increase in velocity.

The second set of the CFD studies analyzed the effect of air mass flow rate on the system's thermal efficiency. Findings show that having the highest air mass flow rate, within the range provided by the U.S. DOE, led to the highest system thermal efficiency. However, the study further shows that higher air mass flow rates lead to a decrease in outlet

temperatures. This is attributable to more air volume being available to take away more thermal heat from the air channel and air having less time inside the air channel to attain higher outlet temperatures. Nevertheless, the effect of increased air mass flow rate on outlet temperature change appeared to be minimal with the biggest change being approximately two degrees. In other words, the effect of increased air mass flow rate on outlet temperature was not significant enough to decrease the overall level of thermal efficiency.

The third set of the CFD studies examined how design configurations of the air channel within the air based PV/T solar roof system affects thermal efficiency. Study results using vertical and horizontal baffles to increase the distance between the inlet and the outlet show that thermal efficiency is positively related with the length of the air channel. Further analysis using air channel lengths ranging from 14.85 m to 127.7 m based on an air channel depth of 3.81 cm and air mass flow rate of 0.011 $kg/s \cdot m^2$ show that thermal efficiency increases as the air channel length increases and eventually converges to a constant value of 73.2% (incident solar radiation of 200 W/m^2), 72.1% (incident solar radiation of 400 W/m^2), and 71.0% (incident solar radiation of 600 W/m^2) which are the highest percentage among the CFD study simulations. This suggests a thermal conversion efficiency that is greater than 70% can be reached using the proposed air based PV/T solar energy system. This is also an indication that the performance of the proposed air based PV/T solar roof system eventually hits a maximum and that the level of incident solar radiation does not play a significant role once the system's thermal efficiency is near the maximum range. While the CFD studies showed that increasing the air channel length using vertical and horizontal baffles leads to an increase in thermal efficiency, such

increase in air channel length also increases the friction loss of the air moving through the air channel of the air based PV/T solar roof system which presumably will lead to an increase in fan energy consumption. This study of the air based PV/T solar roof system did not account for this in the EnergyPlus model and an investigation of this is one of the potential improvements which will provide a better understanding of the potential impact of increasing the channel length on overall energy efficiency.

Overall, the CFD studies conducted in this chapter provide evidence that higher thermal efficiency can be reached by a design that incorporates a shallower air channel depth, lower air mass flow rate, and a longer air channel depth. With these findings, the next chapter will examine various case studies and conduct analysis of the performance of the air based PV/T solar roof system in different climates and verify its potential capability as a building integrated solar system.

Chapter 6. Building Energy Simulations

6.1 Introduction to EnergyPlus

The building energy simulation program that will be used for this dissertation is the EnergyPlus program. EnergyPlus, supported by the U.S. DOE, is a whole building annual energy simulation program which models heating, cooling, lighting, ventilation, other energy flows, and water use in buildings [13]. The main purpose of EnergyPlus is to determine the energy consumption of a building during the early design stages or aid in retrofitting an existing building. This can result in a better system selection and potentially an energy optimization of the building design. The program calculates heating and cooling loads necessary to maintain thermal control setpoints, conditions throughout a secondary HVAC system and coil loads, and the energy consumption of primary plant equipment. EnergyPlus also enables integrated energy performance analysis of other low-energy technologies in commercial and residential buildings including on-site generation and renewable energy sources. The key features of EnergyPlus [12][63] are that it:

- Serves as a manager interface protocol that supports multiple solution techniques within the overall context of the simulation.

- Integrates building and HVAC systems and performs the simultaneous simulation where the building response and the primary and secondary HVAC systems are tightly coupled. It can also perform iteration when necessary.

- Investigates the effect of under-sizing fans and other equipment and what impact that might have on the thermal comfort of occupants within the building.

- Investigates high/low temperature radiant heating and cooling systems.

- Performs simulations on sub-hourly or user-definable time steps. The variable HVAC time steps improve the interactions between the thermal zones and the HVAC systems.

- Performs a heat balance based solution technique for building thermal loads that allows for simultaneous calculation of radiant and convective effects at interior and exterior surfaces during each time step.

- Performs transient heat conduction through building elements such as walls, roofs, floors, etc. using conduction transfer functions.

- Models combined heat and mass transfer and can account for moisture adsorption/desorption either as a layer-by-layer integration into the conduction transfer functions or as an Effective Moisture Penetration Depth model (EMPD).

- Performs human thermal comfort calculations based on activity, inside dry bulb temperature, humidity, and radiation.

- Performs anisotropic sky model calculations where the sky radiance depends on sun position for better calculation of diffuse solar on tilted surfaces.

- Performs advanced fenestration calculations including controllable window blinds, electro-chromic glazing, layer-by-layer heat balances that allow proper assignment of solar energy absorbed by window panes, and has a performance library for commercially available windows and shading.

- Performs daylighting illumination and controls calculations that include the interior illuminance from windows and skylights, step, dimming, on/off luminaire controls, glare simulation and control, and the effects of dimming on heating and cooling.

- Performs atmospheric pollution calculations (CO_2, SO_x, NO_x, CO, particulate matter and hydrocarbon production).

- Builds loop based configurable HVAC systems that allow users to model typical systems and slightly modified systems without recompiling the program source code.

- Accepts ASCII text based weather, input, and output files that include hourly or sub-hourly environmental conditions. This feature is significant to build the evaluation model since multi-simulation is required.

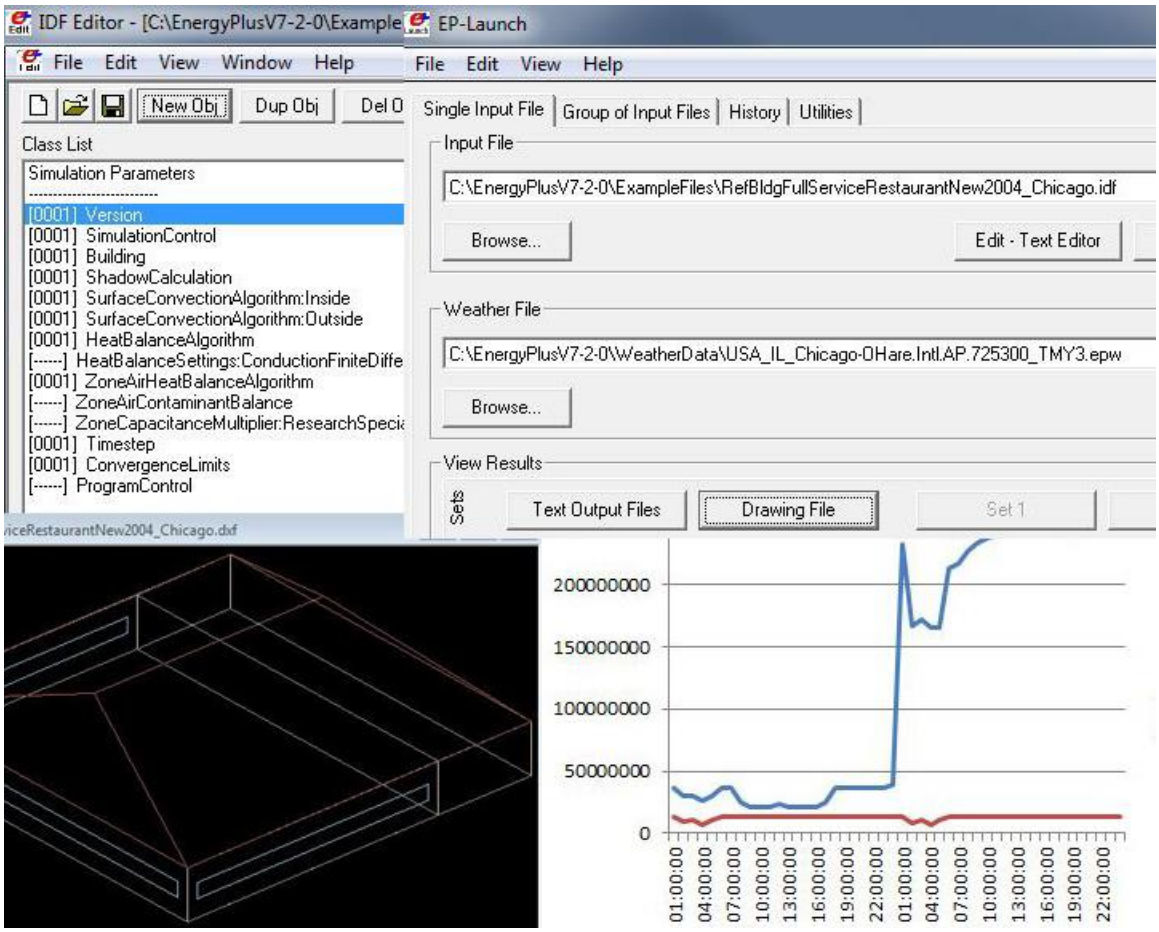

Figure 6.1 – Screen Captures of EnergyPlus Utilities and Results

The current EnergyPlus source code is written in Fortran 90, and it is used as a simulation engine without a graphical interface. Figure 6.1 shows screen images of EnergyPlus utilities and example results. The building information modeling inputs and building energy simulation outputs are simple comma-separated ASCII text files.

6.2 Climatic Zones and Weather of Selected Cites

Local climatic patterns greatly influence heating and cooling needs, and the amount of insolation received is an important factor in determining how much heat a solar energy system can provide. Figure 6.2 shows a map and description of six regional climatic zones of the United States regarding the amount of insolation and the need for space heating which is adapted from Jones [64] and Kornher and Zaugg [65]. The diagonal lines shown in the southern regions of the United States denote a climatic zone where the heating demand is too low to justify the implementation of an air based solar energy system.

Zones 1 and 2 have plenty of sunshine and a substantial need for space heating and therefore a properly designed solar energy system is a sensible choice for these climatic zones. Zones 3 and 4 also have moderate sunshine so it would also be reasonable to have a solar energy system in these zones. Zones 5 and 6 have poor sunshine throughout the year and therefore, careful consideration of whether or not it is reasonable to have a solar energy system is needed. The whole building annual energy simulations presented later in this chapter show if a solar energy system would be reasonable in these climatic zones.

Table 6.1 lists the 28 different cities chosen for this study. The 28 cities are also shown as dots in Figure 6.2. Cities with significantly large populations were selected for analysis and an effort was made to cover a wide variety of different climates within the United States. Tables 6.2 – 6.5 list the maximum, minimum, and daily average values for the monthly dry bulb temperatures (°C) and Tables 6.6 – 6.9 list the direct average, direct maximum, and diffuse average values for monthly solar radiation (W/m^2) of the selected cities [66].

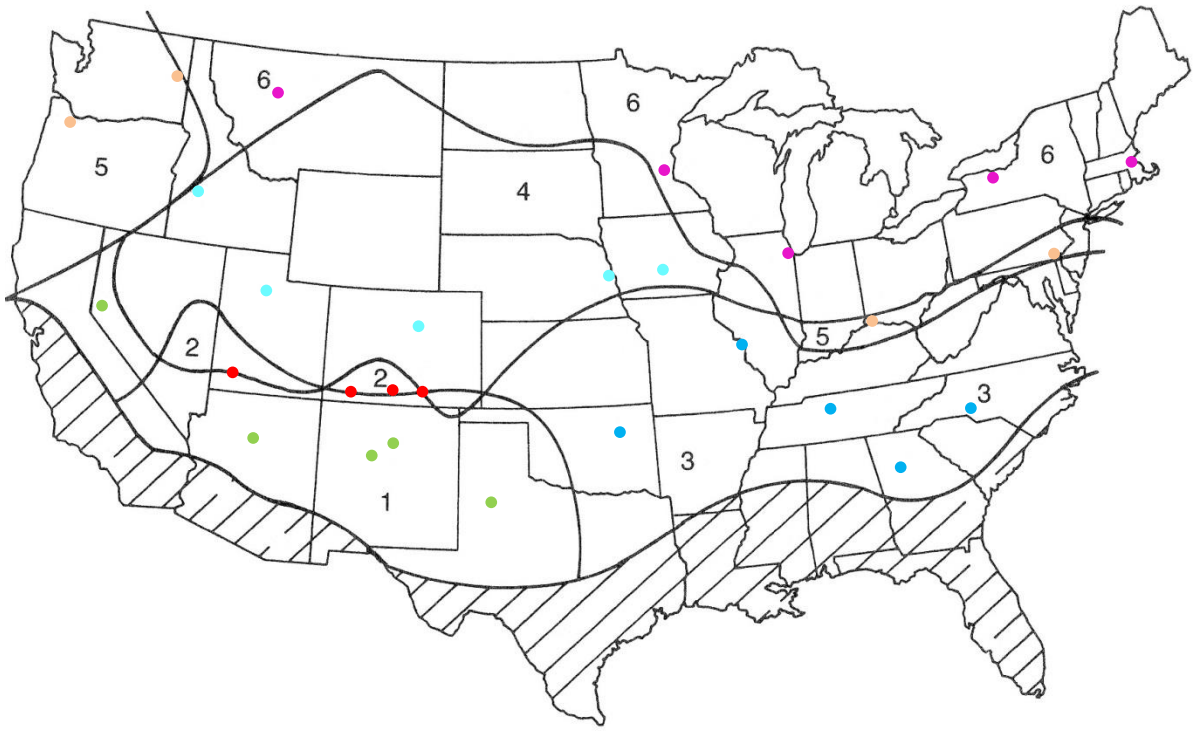

Zones	Sun Availability	Mean Daily Solar Radiation (Langley)	Heating Degree Days (HDD)	Heating Needs
Zone 1	Great Sun	350 ~ 450	2500 ~ 5000	Moderate Heating Need
Zone 2	Great Sun	350 ~ 450	5000 ~ 9000	High Heating Need
Zone 3	Good Sun	250 ~ 350	2500 ~ 5000	Moderate Heating Need
Zone 4	Good Sun	250 ~ 350	5000 ~ 9000	High Heating Need
Zone 5	Poor Sun	175 ~ 250	2500 ~ 5000	Moderate Heating Need
Zone 6	Poor Sun	175 ~ 250	5000 ~ 9000	High Heating Need

Figure 6.2 – Map and description of six climatic zones of the United States [64][65]

Zone	City, State	Köppen Climate Classification
Zone 1	Reno, NV	Hot, semi-arid climate (BSh)
	Flagstaff, AZ	Semi-arid climate (BSk)
	Albuquerque, NM	Hot, desert climate (BWh)
	Santa Fe, NM	Semi-arid climate (BSk)
	Lubbock, TX	Hot, semi-arid climate (BSh)
Zone 2	St. George, UT	Hot, desert Climate (BWh)
	Durango, CO	Semi-arid climate (BSk)
	Alamosa, CO	Semi-arid climate (BSk)
	Trinidad, CO	Semi-arid climate (BSk)
Zone 3	Tulsa, OK	Humid subtropical climate (Cfa)
	St. Louis, MO	Humid subtropical/Humid continental climate (Cfa/Dfa)
	Nashville, TN	Humid subtropical climate (Cfa)
	Atlanta, GA	Humid subtropical climate (Cfa)
	Charlotte, NC	Humid subtropical climate (Cfa)
Zone 4	Boise, ID	Semi-arid climate (BSk)
	Salt Lake City, UT	Dry-summer continental climate (Dsa)
	Denver, CO	Semi-arid climate (BSk)
	Omaha, NE	Humid continental climate (Dfa)
	Des Moines, IA	Humid continental climate (Dfa)
Zone 5	Portland, OR	Oceanic/Dry-summer subtropical Mediterranean climate (Csb)
	Spokane, WA	Dry-summer, humid continental climate (Dsb)
	Cincinnati, OH	Humid subtropical climate (Cfa)
	Philadelphia, PA	Humid subtropical climate (Cfa)
Zone 6	Great Falls, MT	Semi-arid climate (BSk)
	Minneapolis, MN	Humid continental climate (Dfa)
	Chicago, IL	Humid continental climate (Dfa)
	Rochester, NY	Humid continental climate (Dfb)
	Boston, MA	Humid continental climate with a maritime influence (Dfa/Cfa)

Table 6.1 – Zones and Köppen climate classifications for 28 selected cities

	Jan	Feb	Mar	Apr	May	Jun	Jul	Aug	Sep	Oct	Nov	Dec
Reno, NV (Zone 1)												
Maximum	20	20.6	23	28	29	34	37	36	34	27	22.8	15.6
Minimum	-12	-12	-7.8	-3.9	-2.8	3.3	6.1	2.2	-2.2	-5	-11	-22
Daily Avg	0.7	2.5	6	9.8	12	19	23	20	16	9.3	4.6	-0.8
Flagstaff, AZ (Zone 1)												
Maximum	16.1	13.9	16.7	20.6	24.4	34.4	31.1	29.4	26.7	23.3	18.9	11.7
Minimum	-18.3	-18.3	-15	-9.4	-6.7	0	6.7	3.9	-0.6	-10	-12.2	-26.1
Daily Avg	-1.9	-1.9	1.6	6.1	10	16.6	18.5	16.9	13.8	8.1	2.3	-3
Albuquerque, NM (Zone 1)												
Maximum	16.7	22.2	23	31	32	36	37	36	33	28	20.6	15.6
Minimum	-11	-6.7	-7.2	-2.2	2.8	11	16	13	11	-3.3	-7.8	-9.4
Daily Avg	2	4.3	7.1	13	19	23	26	23	21	13	6.3	1.5
Santa Fe, NM (Zone 1)												
Maximum	16	14	26	24	32	34	36	32	30	28	14	13
Minimum	-16	-13	-5	-4	-1	5	11	11	0	-5	-10	-12
Daily Avg	-0.5	2.2	8.4	11	16	21	22	21	16	11	3.3	-1.3
Lubbock, TX (Zone 1)												
Maximum	24.4	23.3	26	31	36	37	36	36	34	33	26.1	24.4
Minimum	-15	-16	-12	-2.8	6.7	13	16	16	5	5.6	-7.2	-11
Daily Avg	2.8	4.7	11	16	20	25	25	26	21	17	8.4	5.5
St. George, UT (Zone 2)												
Maximum	19	17	27	35	41	41	44	41	39	34	22	17
Minimum	-3.5	1	1.9	6	9	16	23	19	8.4	3.4	-4	-6
Daily Avg	7.3	8.4	14	20	23	29	33	31	24	18	8.9	5.6
Durango, CO (Zone 2)												
Maximum	21	10	18	22	25	31	33	33	30	25	14	12
Minimum	-23	-16	-11	-7	-4	2	8	10	3	-4	-9	-19
Daily Avg	-4.6	-2.9	2.9	7.7	11	18	21	20	16	9.6	1.3	-4.1

Table 6.2 – Monthly statistics for dry bulb temperatures (°C) of climatic Zones 1-2

	Jan	Feb	Mar	Apr	May	Jun	Jul	Aug	Sep	Oct	Nov	Dec
Alamosa, CO (Zone 2)												
Maximum	10	8.9	16	20	24	31	32	31	26	24	13.9	5
Minimum	-32	-19	-14	-12	-5.6	0	3.9	0.6	-2.2	-18	-19	-23
Daily Avg	-9.5	-5.8	1.4	5.8	11	15	18	17	12	5.7	-2.1	-9.7
Trinidad, CO (Zone 2)												
Maximum	17.2	17.8	22	26	31	36	36	36	33	28	22.2	21
Minimum	-18	-10	-8.9	-6.2	-2.7	6.1	12	9.2	1.1	-3	-16	-21
Daily Avg	0.2	2.3	5.6	8.5	17	20	23	22	18	12	6.2	-0.4
Tulsa, OK (Zone 3)												
Maximum	18.3	26.7	28	32	33	36	39	39	37	31	25	20.6
Minimum	-18	-13	-6.1	-1.1	7.2	12	17	16	7.8	1.7	-5.6	-16
Daily Avg	0.2	4.6	11	16	21	25	28	27	21	16	9.3	4
St. Louis, MO (Zone 3)												
Maximum	17.8	18.3	27	33	32	34	38	38	33	27	24.4	14.4
Minimum	-16	-17	-9.4	-1.1	5	10	13	14	7.8	1.1	-6.7	-18
Daily Avg	-2.7	0.4	7.2	14	20	24	26	25	21	13	7	-0.9
Nashville, TN (Zone 3)												
Maximum	20.6	23.9	24.4	30.6	32.2	36.7	35.6	37.8	38.3	29.4	27.2	21.1
Minimum	-19.4	-14.4	-8.9	-2.2	8.3	11.1	13.3	12.2	6.1	-2.8	-3.9	-11.1
Daily Avg	0.3	2.5	8.9	14.9	20.3	24.5	25.8	25	23.3	15.5	9.8	5.9
Atlanta, GA (Zone 3)												
Maximum	19.4	21.7	25	30	31	34	36	33	30	32	22.8	21.1
Minimum	-9.4	-11	-1.1	-1.1	12	15	14	16	14	3.3	-3.3	-8.3
Daily Avg	4.7	6.6	12	16	21	24	25	25	23	17	10.5	6.6
Charlotte, NC (Zone 3)												
Maximum	18.3	23.9	23.9	32.8	31.1	32.8	35.6	33.3	31.1	28.9	23.3	22.8
Minimum	-6.7	-11.7	-1.7	0.6	5.6	14.4	16.7	14.4	12.1	1.1	-5.6	-8.9
Daily Avg	4.4	5.4	10.5	14.9	20.1	23.5	25.8	24.5	22.6	15.5	11.5	5.1

Table 6.3 – Monthly statistics for dry bulb temperatures (℃) of climatic Zones 2-3

	Jan	Feb	Mar	Apr	May	Jun	Jul	Aug	Sep	Oct	Nov	Dec
Boise, ID (Zone 4)												
Maximum	11.7	15	15	25	33.3	34.4	38.9	37.8	33.9	27.2	17.2	10.6
Minimum	-16.1	-6.7	-3.3	-5	-1.1	3.9	9.2	4.4	3.9	-8.9	-9.4	-15
Daily Avg	-1.7	2.8	5.2	9.1	14.5	18.4	24.7	21	17.1	9.3	4.6	-2.4
Salt Lake City, UT (Zone 4)												
Maximum	8.3	14.4	20.6	23.9	31.7	37.2	38.3	37.2	31.7	27.2	18.9	11.1
Minimum	-17.8	-10	-6.7	-1.7	1.7	4.4	13.3	11.1	2.8	-2.8	-7.8	-12.2
Daily Avg	-2.1	1.5	6.5	9.6	15.7	19.8	26.3	24.7	17.5	11	4.8	-1.1
Denver, CO (Zone 4)												
Maximum	16.7	18.3	21.1	22.8	30.6	40	36.1	34.4	33.9	28.3	21.1	21.1
Minimum	-18	-15.6	-6.1	-8.9	0	7.2	11.7	11.7	3.9	-1.9	-16.1	-19.4
Daily Avg	0.8	-0.1	6.1	5.8	15.5	23.1	22.3	22.6	19.2	10	2.9	1.4
Omaha, NE (Zone 4)												
Maximum	11.7	13.9	28.9	27.8	28.3	35.6	36.7	35.6	30.6	27.2	17.8	14.4
Minimum	-25	-26.1	-12.2	-0.6	5	9.4	13.9	13.3	6.7	0	-10.6	-25
Daily Avg	-5.7	-3.5	4.8	12.2	17.2	22.5	24.8	23.7	18.4	13	4.4	-4.6
Des Moines, IA (Zone 4)												
Maximum	11.7	13.3	25	29.4	30	32.8	36.1	36.7	32.2	28.9	18.9	11.7
Minimum	-27.8	-18.3	-10	-6.1	1.7	8.9	12.2	10.6	3.3	-3.3	-7.8	-22.2
Daily Avg	-8.1	-4.4	4.2	10.6	17	21.5	24.8	22.3	17.3	11.9	4	-3.7
Portland, OR (Zone 5)												
Maximum	13.3	15.6	21.1	25	30.6	33.3	32.2	33.3	33.3	26.7	17.8	16.1
Minimum	-6.7	-2.2	-1.7	1.1	5	7.8	11.1	10.6	7.2	1.1	-0.6	-1.7
Daily Avg	3.8	6.1	8.3	9.9	13.6	16.6	18.6	20.2	17.2	11.8	8.5	5.8
Spokane, WA (Zone 5)												
Maximum	6.7	11.1	17.8	22.8	27.8	33.3	37.8	35	36.1	23.3	11.1	11.7
Minimum	-25	-10.6	-5	-2.2	0	3.3	5.6	7.2	1.7	-4.4	-11.7	-11.7
Daily Avg	-2.8	0.6	4.3	7.2	11.7	16.3	21.8	19.3	14.9	8	1.7	-1

Table 6.4 – Monthly statistics for dry bulb temperatures (℃) of climatic Zones 4-5

	Jan	Feb	Mar	Apr	May	Jun	Jul	Aug	Sep	Oct	Nov	Dec
Cincinnati, OH (Zone 5)												
Maximum	13.3	19.4	22.2	26.7	30.5	31.1	36.6	34	32.2	28.9	22.2	18.3
Minimum	-16.1	-16.7	-11.7	1.1	4.4	6.1	12.2	14	5	1.1	-3.9	-14.4
Daily Avg	-0.2	0	6	13.6	17.4	20	25.2	23.3	18.4	12	8.9	2.4
Philadelphia, PA (Zone 5)												
Maximum	8.9	11.7	18.3	27.8	29.4	33.9	35	33.9	30	27.2	26.1	15.6
Minimum	-11.7	-11.7	-5.6	-0.6	4.4	9.4	15	14.4	7.2	-3.9	-6.1	-9.4
Daily Avg	-1.2	-0.2	5.3	10.6	17.1	21.7	24.9	23.1	20.1	13	7.7	1.4
Great Falls, MT (Zone 6)												
Maximum	16.1	16.1	17.2	22.8	31.7	33.9	35	34.4	28.9	25	14.4	6.7
Minimum	-27.2	-28.9	-15	-5.6	1.1	1.1	8.3	5	0	-6.1	-26.1	-32.8
Daily Avg	-5.5	-6	0.9	7.2	12.9	17.9	21.1	19.4	13.6	8.6	-1	-3.2
Minneapolis, MN (Zone 6)												
Maximum	3.9	4.4	18.3	25	35	33.9	32.2	31.7	28.9	28.3	20	4.4
Minimum	-27.8	-28.9	-18.3	-4.4	0.6	9.4	11.1	11.7	4.4	-3.9	-12.8	-29.4
Daily Avg	-11.8	-8.1	0.3	8.7	16	20.5	22	21.6	16.1	8.7	0.7	-8.2
Chicago, IL (Zone 6)												
Maximum	12.2	11.7	23.3	22.8	30.6	33.3	35.6	31.7	31.7	25.6	24.4	11.7
Minimum	-22.8	-16.7	-8.9	-2.2	1.7	6.7	11.7	11.7	5	-2.2	-5	-22.8
Daily Avg	-4.6	-2.2	1.6	8.4	15.3	21.1	23.5	21.8	18.1	11.7	4.2	-2.6
Rochester, NY (Zone 6)												
Maximum	10	13.9	21.1	28.9	31.1	32.2	32.8	30.6	33.9	26.7	16.7	18.3
Minimum	-16.1	-19.4	-12.8	-6.1	-2.8	7.2	10.6	11.7	2.2	0	-6.7	-19.4
Daily Avg	-3.5	-5	0.8	9.4	13.7	20	21.5	20.9	16.7	10.8	3.8	-0.5
Boston, MA (Zone 6)												
Maximum	13.9	8.3	17.8	27.8	30	32.2	33.3	30.6	31.1	22.2	21.7	18.3
Minimum	-11.1	-12.8	-8.9	-3.3	3.1	11.1	14.4	12.2	7.8	3.3	-7.2	-15
Daily Avg	-1.5	-0.5	2.5	7.4	14.9	19.3	22.6	21.5	18.1	12.3	5.7	1.2

Table 6.5 – Monthly statistics for dry bulb temperatures (℃) of climatic Zones 5-6

	Jan	Feb	Mar	Apr	May	Jun	Jul	Aug	Sep	Oct	Nov	Dec
Reno, NV (Zone 1)												
Direct Avg	3398	4514	5326	6705	6963	8478	9336	8658	8384	6280	4636	3939
Direct Max	7927	9239	10333	11086	11695	12193	12179	11340	10653	9627	8613	7573
Diffuse Avg	1000	1228	1687	1839	2117	1938	1628	1475	1150	1041	908	782
Flagstaff, AZ (Zone 1)												
Direct Avg	5137	5546	6158	7037	7798	8578	6374	5574	6978	6677	5628	5371
Direct Max	8926	10063	11185	11727	12390	12376	12010	11072	10585	9837	8394	8737
Diffuse Avg	998	1350	1573	1682	1766	1654	2128	1789	1394	1011	938	769
Albuquerque, NM (Zone 1)												
Direct Avg	5546	6001	6158	7459	8362	8513	7569	7040	6630	6876	5869	5374
Direct Max	9104	9356	11331	11847	12284	12903	10677	10421	10034	10521	8160	8498
Diffuse Avg	918	1168	1769	1942	2084	2033	2169	2121	1615	1183	953	847
Santa Fe, NM (Zone 1)												
Direct Avg	5626	7227	7720	7541	8287	8738	7078	7158	7799	7272	5855	5987
Direct Max	8541	10146	10450	11322	11094	11646	10737	10928	10228	10235	9029	8181
Diffuse Avg	667	832	1276	1694	1780	1646	2011	1838	1297	904	871	590
Lubbock, TX (Zone 1)												
Direct Avg	4623	5218	6151	6401	6674	7060	6191	5770	5461	6504	5439	4891
Direct Max	8555	9320	10208	10698	11351	11115	11438	9117	9214	9388	8370	8098
Diffuse Avg	1057	1240	1605	1876	2133	2138	2212	2169	1808	1105	1009	894
St. George, UT (Zone 2)												
Direct Avg	5526	4622	7584	7852	9197	10090	8330	7856	9596	5644	5767	4639
Direct Max	7981	8488	9804	10141	10973	11339	11124	10316	10799	8901	8007	7815
Diffuse Avg	837	1149	1371	1813	1848	1712	1818	1739	790	1159	831	774
Durango, CO (Zone 2)												
Direct Avg	4729	6445	5173	7322	7992	9813	6986	6395	7110	6639	5768	5770
Direct Max	8936	9652	10829	11043	11229	12058	11748	10452	10440	10261	8941	7950
Diffuse Avg	687	852	1564	1721	1810	1695	2115	1921	1234	1067	894	730

Table 6.6 – Monthly statistics for solar radiation (W/m^2) of climatic Zones 1-2

	Jan	Feb	Mar	Apr	May	Jun	Jul	Aug	Sep	Oct	Nov	Dec
Alamosa, CO (Zone 2)												
Direct Avg	6068	6132	6660	7761	7670	8676	7068	7183	7049	7353	5936	5600
Direct Max	9112	9932	10735	11738	12609	12896	11438	11281	10866	10624	9103	8459
Diffuse Avg	757	1085	1502	1759	2026	1901	2116	1880	1457	956	866	700
Trinidad, CO (Zone 2)												
Direct Avg	5375	6839	6112	5643	7038	7728	7558	6594	7152	6636	5238	4917
Direct Max	8469	9872	10150	9694	11312	11570	11309	10415	10234	8906	9141	7821
Diffuse Avg	741	881	1429	1814	2067	2054	1807	1840	1357	1001	876	678
Tulsa, OK (Zone 3)												
Direct Avg	3537	3572	4537	5374	4589	5195	5783	5346	4194	4919	3764	3339
Direct Max	7089	8580	9012	10572	9895	10088	9977	9370	8697	8747	7695	7697
Diffuse Avg	1073	1513	1749	2119	2750	2667	2468	2306	1970	1423	1037	982
St. Louis, MO (Zone 3)												
Direct Avg	3067	3495	4123	4410	4828	5235	5647	4963	4441	4355	2841	2354
Direct Max	7666	8442	9098	10229	10248	10303	9146	9928	9690	8697	7570	7182
Diffuse Avg	998	1341	1795	2224	2567	2706	2538	2217	1937	1243	1116	1006
Nashville, TN (Zone 3)												
Direct Avg	2844	3183	4216	4475	4489	5014	4916	4121	3667	4123	2925	2736
Direct Max	8797	9114	9542	9763	9972	11062	9792	8505	8520	8242	7885	7632
Diffuse Avg	1214	1659	1949	2274	2849	2972	2858	2798	2422	1562	1202	969
Atlanta, GA (Zone 3)												
Direct Avg	3363	4174	4269	5531	4917	4869	4795	4590	3737	4969	3886	3261
Direct Max	8257	9109	9932	10259	9664	9838	8721	7894	7745	8423	8227	8331
Diffuse Avg	1142	1369	1915	2244	2780	2920	2791	2628	2323	1479	1239	1089
Charlotte, NC (Zone 3)												
Direct Avg	3518	3890	4428	5481	5051	5092	4245	4038	4185	4583	3841	3360
Direct Max	8521	8887	9600	10190	10234	9566	8386	8828	8754	8632	7975	7576
Diffuse Avg	1115	1387	1782	2052	2531	2650	2917	2654	1990	1485	1075	975

Table 6.7 – Monthly statistics for solar radiation (W/m^2) of climatic Zones 2-3

	Jan	Feb	Mar	Apr	May	Jun	Jul	Aug	Sep	Oct	Nov	Dec
Boise, ID (Zone 4)												
Direct Avg	2003	3477	4280	5399	6513	7325	9137	8155	6992	5176	2979	2266
Direct Max	6992	8956	10313	10841	12068	12114	12595	11614	10728	9109	8147	6888
Diffuse Avg	1037	1205	1661	2054	2156	2305	1585	1527	1276	1117	921	790
Salt Lake City, UT (Zone 4)												
Direct Avg	2502	3752	4285	5022	6045	7665	8200	7957	6543	5251	3528	1880
Direct Max	7107	8433	9403	11653	10904	12367	12036	11331	10212	8820	7983	5519
Diffuse Avg	1099	1283	1789	2151	2654	2093	1911	1642	1501	1229	982	1005
Denver, CO (Zone 4)												
Direct Avg	4827	4599	5915	4459	5804	7329	6550	6113	6158	5182	3943	4066
Direct Max	8300	8650	10874	9918	12067	11119	12109	10621	10041	8390	7547	7546
Diffuse Avg	738	1108	1373	2018	2358	2099	2199	1974	1617	1123	972	695
Omaha, NE (Zone 4)												
Direct Avg	3600	3786	3947	4318	5577	5993	5387	5007	4870	4017	2665	2335
Direct Max	7032	8638	9330	10590	10650	10944	9846	9203	8775	8373	6965	6725
Diffuse Avg	874	1430	1800	2154	2400	2654	2586	2366	1824	1318	972	944
Des Moines, IA (Zone 4)												
Direct Avg	3106	4079	3948	4453	5378	5659	6140	5184	4527	3936	2891	2649
Direct Max	7588	8699	9334	10145	10850	9912	10855	9502	9497	8578	7360	6877
Diffuse Avg	920	1157	1657	2195	2253	2647	2434	2224	1799	1291	939	845
Portland, OR (Zone 5)												
Direct Avg	1301	1444	2713	2872	3922	4369	6034	5833	4496	2923	1102	793
Direct Max	6562	5505	8994	8846	9134	10421	11593	10160	8240	7545	4393	4511
Diffuse Avg	883	1317	1709	2393	2964	2948	2501	1635	1491	1263	966	720
Spokane, WA (Zone 5)												
Direct Avg	1182	2027	3484	4383	4992	5485	8577	7440	5720	4276	1596	1189
Direct Max	4551	7339	8434	10319	11296	12051	12223	11232	9951	8820	5675	5565
Diffuse Avg	1107	1204	1519	2065	2543	2637	1790	1614	1330	989	833	786

Table 6.8 – Monthly statistics for solar radiation (W/m^2) of climatic Zones 4-5

	Jan	Feb	Mar	Apr	May	Jun	Jul	Aug	Sep	Oct	Nov	Dec
Cincinnati, OH (Zone 5)												
Direct Avg	3292	2314	2945	3726	3172	4691	4239	3389	3884	2534	3342	1873
Direct Max	6229	7900	8286	8859	8243	8965	9213	8654	7430	6928	5900	5445
Diffuse Avg	905	1323	1598	2144	2815	2533	2790	2579	1859	1373	935	845
Philadelphia, PA (Zone 5)												
Direct Avg	2841	3398	3819	4023	4031	4463	4703	4587	3998	3869	2565	2025
Direct Max	7288	7798	8420	9542	10074	9209	10086	7938	8101	8306	7087	6547
Diffuse Avg	908	1265	1700	2197	2674	2846	2702	2429	1905	1389	1119	909
Great Falls, MT (Zone 6)												
Direct Avg	2079	3244	4142	4668	5179	6629	7305	6620	6088	3951	2470	2064
Direct Max	5887	7862	10198	9994	11220	13117	12512	11960	10563	8788	6358	6383
Diffuse Avg	803	1092	1661	2252	2421	2621	2212	1893	1374	1154	864	700
Minneapolis, MN (Zone 6)												
Direct Avg	3155	3718	3810	4150	5243	5652	5730	5227	4455	3578	2218	2203
Direct Max	6736	8453	9952	11592	11724	10253	11520	9886	9545	8206	6694	6563
Diffuse Avg	914	1344	1770	2066	2470	2608	2537	2180	1754	1266	951	816
Chicago, IL (Zone 6)												
Direct Avg	2335	2640	2912	4178	5014	5205	5347	4194	4004	3438	2051	1512
Direct Max	6874	6769	9134	9143	10148	9706	9701	9321	7925	8440	6933	5487
Diffuse Avg	956	1406	1945	2122	2539	2690	2604	2422	1861	1353	1054	903
Rochester, NY (Zone 6)												
Direct Avg	1244	2156	2881	3689	4540	5461	5129	4511	3839	2419	1265	968
Direct Max	5287	7978	9132	10321	10137	10935	11100	10159	8498	8591	6785	5199
Diffuse Avg	1145	1588	1831	2315	2427	2610	2527	2345	1944	1485	1119	974
Boston, MA (Zone 6)												
Direct Avg	2862	3307	4054	3831	4513	4623	4772	4674	4188	3910	2382	2425
Direct Max	6675	6931	9618	9929	10617	9229	10334	9275	8669	7787	5889	6457
Diffuse Avg	871	1373	1578	2227	2463	2813	2700	2403	1849	1317	1007	821

Table 6.9 – Monthly statistics for solar radiation (W/m^2) of climatic Zones 5-6

6.3 Building Energy Simulation Descriptions

As mentioned in Chapter 4 – Overview of Computational Case Study Models, the whole building annual energy simulations run using EnergyPlus focus on two reference buildings – a quick-service restaurant and a small commercial office building. These simulations investigate the annual energy efficiency of the air based PV/T solar roof system under various climatic conditions within the United States. The two building types were selected for this study since they are both designed with a Gable roof that can potentially expose half of the roof area to the sun depending on the roof configuration and orientation.

The two reference buildings were modified and equipped with the air based PV/T solar roof system on the south facing roofs to compare the energy performance of the base cases and proposed system under different weather climatic zones. Once the air based PV/T solar roof system is installed, the system is then integrated with the existing HVAC air system loop with air nodes (connections in the air system loop). One of the key elements of this system is to provide the user with input of thermal conversion efficiency. The CFD studies conducted in Chapter 5 – Computational Fluid Dynamics (CFD) Simulations provided analysis that the air based PV/T solar roof system thermal conversion efficiency can be greater than 70% with proper air channel depth, air mass flow rate, and installation of vertical/horizontal baffles to increase the air channel length. Thus, the value of 70% was

used as the input for the thermal conversion efficiency in the whole building annual energy simulations. Further, the inlet velocity input was set to 3.1 m/s.[3]

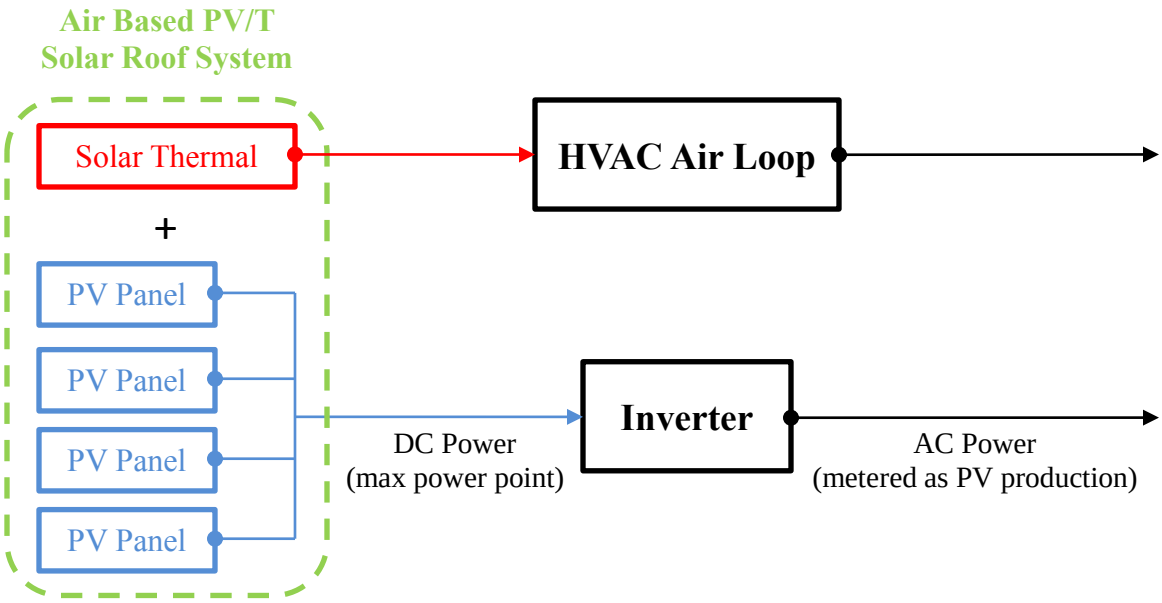

Figure 6.3 – Schematic diagram of air based PV/T solar roof system

Another key element of the air based PV/T solar roof system is the arrangement of the bypass damper. It has the ability to decide if the air should bypass the air channel to better meet the setpoint temperature. In the cases of the two reference buildings, the setpoint temperature is 40℃ (maximum) on the outlet node. This setpoint temperature is the supply air parameters in the HVAC control of the two reference buildings. The air based PV/T solar roof system assumes that it is intended and available for heating when the incident solar radiation on the roof surface is greater than 0.3 W/m^2. Then, the inlet

[3] The inlet area was kept fixed during all of the CFD studies. Hence, with the fixed inlet velocity, the volumetric flow rate was also kept constant throughout the CFD studies.

temperature is compared to the setpoint temperature on the outlet node to determine if heating is beneficial. If the outlet temperature meets the requirement of the existing HVAC controls, the air based PV/T solar roof system is applied to the condition and supplements the air stream. If the outlet temperature does not meet the requirements, then the air is completely bypassed through the system. This will prevent the roof and the attic from heating air during the summer which would cause much higher cooling loads.

The air based PV/T solar roof system also requires installation of PV panels/generators and an inverter. As shown in Figure 6.3, the PV panels collects solar energy and generates direct current (DC) power which runs through an inverter and produces alternating current (AC) power, which is then distributed through the rest of the building. Furthermore, the PV panels are in operation only when the incident solar radiation is greater than 0.3 W/m^2. If the incident solar radiation is less than 0.3 W/m^2, then the PV panels produce no power.

6.4 Energy Performance of the Small Commercial Office Building

Figure 6.4 shows an example of hourly inlet and outlet temperatures of the small office building under the integrated air based PV/T solar roof system. It presents an example of a three day span during the heating season in Flagstaff, AZ. The graph shows that the outlet temperature starts rising once the sun rises and solar radiation is absorbed. It is shown that the outlet temperatures are above or close to 22℃ in the hours between 9am and 5pm. The heating thermostat setpoint temperature of the small commercial office building is set to 21.1℃ during the building's occupied hours that are between 8am and 7pm on weekdays. The heating thermostat setpoint temperature is set to 15.6℃ during

unoccupied hours which include weekends. This is an indication that the air based PV/T solar roof system provides supplemental heating to the air-source heat pump/gas furnace of the small commercial office building during the day when the sun is out. However, the outlet temperatures suggest that the system cannot provide the entire heating load of the building as the outlet temperatures must be at least 35℃ to achieve any physical heating. Thus, the proposed air based PV/T solar roof system can be considered as a low energy solution that supplements the existing HVAC system rather than being responsible for handling the entire heating load of a building.

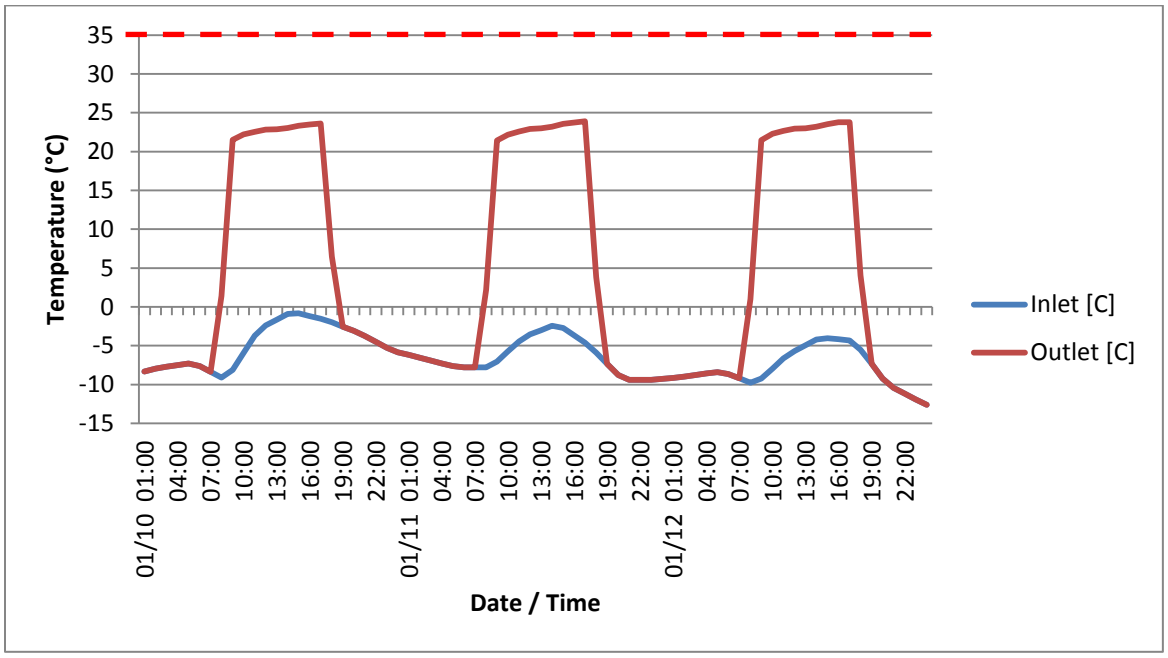

Figure 6.4 – Example of inlet/outlet temperatures of the small commercial office building integrated air based PV/T solar roof system in Flagstaff, AZ (Zone 1)

Figure 6.4 also suggest that rise in temperature within the air channel does not negatively affect the PV panel's electrical conversion efficiency of the air based PV/T solar

roof system. The operating temperature of the PV panel is one of the crucial parameters for determining the electrical conversion efficiency and is defined as the product of ambient air temperature and the level of incident solar radiation. During manufacturing of PV panels, tests are performed to determine the PV panel's tolerance to heat or the maximum power temperature coefficient. This coefficient determines how much power the PV panel will lose when the temperature rises by 1℃ above 25℃[4] [67]. As shown in Figure 6.4, the increased temperature within the air channel is below 25℃ which suggests that it does not impact the maximum power temperature coefficient and the electrical conversion efficiency. As mentioned above, one of the key elements of the air based PV/T solar roof system is the arrangement of the bypass damper. The bypass damper has the ability to decide if the air should bypass through the air channel to better meet the setpoint temperature. This prevents overheating within the air channel during the cooling seasons which will also prevent any negative impact on the electrical conversion efficiency of the PV panel of the air based PV/T solar roof system.

Tables 6.11 – 6.17 present the comparison of the energy performance of a small commercial office building with a conventional HVAC system and integrated air based PV/T solar roof system under six different climatic zones / 28 different cities within the United States. The annual building energy simulations did not show any differences in the electricity consumptions for the interior lights/equipment and gas consumption for the water heater as expected. However, there were slight increases in electricity consumption

[4] The standard test conditions (STC) compares the performance of different PV panels at a temperature of 25℃ and incident solar radiation of 1000 W/m^2 [68].

for cooling and fans. Although the air based PV/T solar roof system is arranged with a bypass damper, the system creates an extra layer of construction on the roof assembly which causes higher roof surface temperatures from the PV and absorber cover and, hence, causes higher cooling loads.

Date Time	Outdoor Air Drybulb Temperature [°C]	Base Case - South Roof Surface Temperature [°C]	Air Based PVT - South Roof Surface Temperature [°C]	Difference [°C]
07/21 12:00	29.4	61.5	61.8	0.3
07/21 13:00	30.3	64.3	65.8	1.5
07/21 14:00	31.0	64.5	67.5	3.0
07/21 15:00	31.2	62.3	66.5	4.2
07/21 16:00	30.8	57.6	63.1	5.5
07/21 17:00	30.1	50.6	57.4	6.8
07/21 18:00	29.1	41.9	49.3	7.4
07/21 19:00	27.7	32.6	40.2	7.6
07/21 20:00	26.3	26.3	32.4	6.1

Table 6.10 – Example of summer design day hourly south roof surface temperature comparison between the base case small commercial office building and the integrated air based PV/T solar roof system in Flagstaff, AZ (Zone 1)

Table 6.10 presents the comparison of the outside south roof surface face temperatures between the base case and the air based PV/T solar roof system during a typical summer design day between 12pm and 8pm in Flagstaff, AZ (Zone 1). The surface temperatures are shown to increase when the air based PV/T solar roof system is installed.

The highest temperature increase was 7.6 ℃ at 7pm. This is an indication that even though the air based PV/T solar roof system is arranged with a bypass damper, the additional roof assembly causes higher conduction heat gain which in turn, results in higher cooling loads for the building.

The annual building simulations showed that the highest increase in the electricity consumption for cooling was shown in Flagstaff, AZ (Zone 1) where the cooling electricity consumption rose from 9.3 GJ to 9.9 GJ (6.3% increase) and the lowest increase was shown in Nashville, TN (Zone 3) where the cooling electricity consumption rose from 25.1 GJ to 25.4 GJ (1.2% increase).

Contrary to the slight increase in electricity consumption for cooling and fans, the annual building energy simulations of the small commercial office building showed significant reductions in carbon dioxide production and gas consumption for heating. Specifically, all of the cities examined showed considerable reductions of over 70% in carbon dioxide production. Further analysis shows that despite differing climate conditions, Zones 1 and 2 have similar reductions in gas consumption for heating and PV electricity production. Similarly, Zones 3 and 4, and Zones 5 and 6 also have similar reductions in gas consumption for heating and PV electricity production despite their different climate conditions. As shown in Figure 6.5, Zones 1 and 2 resulted in the highest gas consumption reduction of 29.2% to 32.6% and Zones 5 and 6 resulted in the lowest gas consumption reduction of 9.7% to 12.2%. The highest decrease in the gas consumption for heating was shown in Albuquerque, NW (Zone 1) where the heating gas consumption dropped from 22.2 GJ to 15.0 GJ (32.6% decrease) and the lowest decrease was shown in Great Falls, MT

(Zone 6) where the heating gas consumption dropped from 82.9 GJ to 74.8 GJ (9.7% decrease).

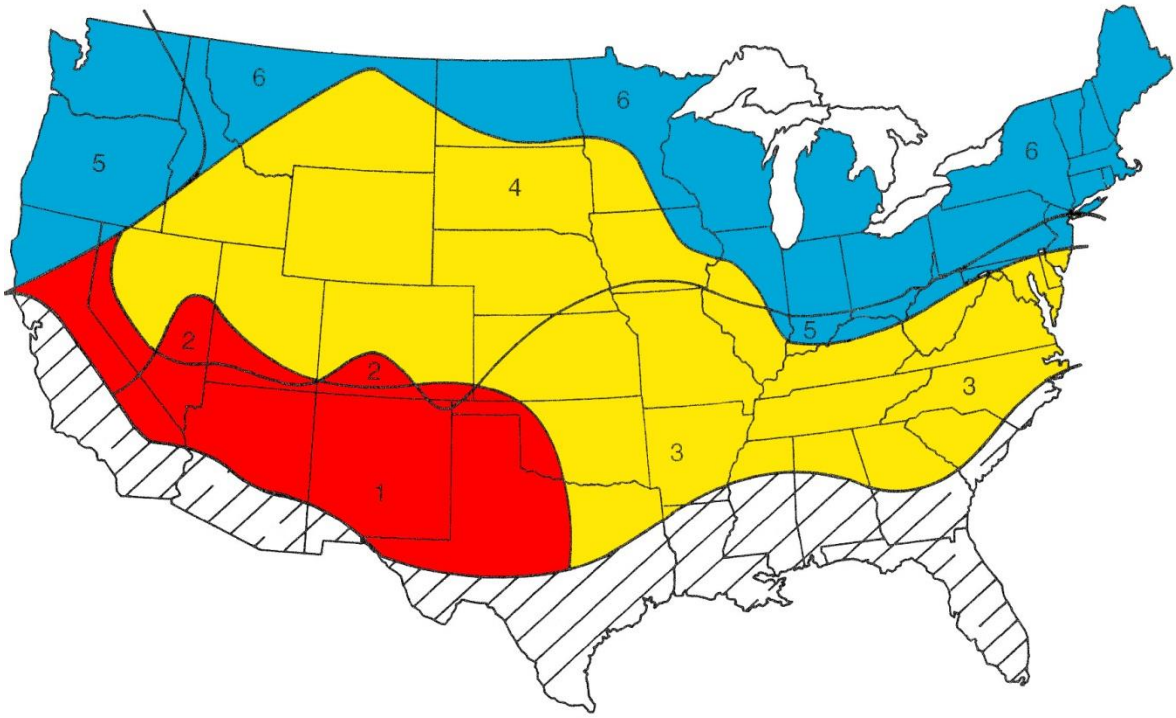

Zones	Mean Daily Solar Radiation (Langley)	Heating: Gas Reduction (%)	Gas: Facility Reduction (%)	PV: Electricity Produced [GJ]
Zone 1 Zone 2	350 ~ 450	29.2 ~ 32.6	15.0 ~ 25.9	266.3 ~ 293.3
Zone 3 Zone 4	250 ~ 350	21.2 ~ 24.1	15.4 ~ 19.5	218.2 ~ 245.6
Zone 5 Zone 6	175 ~ 250	9.7 ~ 12.2	8.0 ~ 10.2	184.0 ~ 215.0

Figure 6.5 – Summary of heating gas reduction (%), facility gas reduction (%), and PV electricity produced (GJ) for small commercial office building with integrated air based PV/T solar roof system

Note that the greatest increase of electricity consumption for cooling and fans was 0.6 GJ under the annual building energy simulations while the gas consumption for heating dropped by at least 8.1 GJ. This suggests the slight increase in electricity consumption for cooling and fans can be offset by the decrease in gas consumption for heating.

As shown in Tables 6.11 – 6.17, the proposed integrated air based PV/T solar roof system produces more annual PV electricity than what is consumed under the conventional HVAC system for the small commercial office building in Zones 1 and 2. The annual PV electricity production slightly decreases in Zones 3 and 4 where the annual PV electricity production is shown to cover between 91.0% ~ 101.2% of the annual electricity consumption under the conventional HVAC system. The annual PV electricity production is lowest in Zones 5 and 6 where the annual PV electricity production is shown to cover between 80.8% ~ 89.5% of the electricity consumption under the conventional HVAC system.

Recall that the whole annual building energy simulations were implemented with the assumption that the proposed air based PV/T solar roof system's thermal efficiency is 70% based on the findings from the previous Chapter 5 – CFD Simulations. Overall, the energy performance of the small commercial office building with integration of the air based PV/T solar roof system definitely presented itself to be beneficial in all climates within the United States. There were no differences in the electricity consumptions for the interior lights/equipment and gas consumption for the water heater, which was expected. However, there were slight increases in electricity consumption for cooling and fans. This is due to the fact that the PV panels and the absorber caused higher south roof surface

temperatures, as shown in Table 6.10. The electricity generated from the PV units nearly offset or produced over 100% of the electricity consumption for all cases thus showing great potential in terms of energy savings. The gas consumption for heating also showed reductions in all climates and the highest savings were shown in Zones 1 and 2 where the mean daily solar radiation values were the highest. This suggests that the gas and electricity savings from the proposed air based PV/T solar roof system is proportional to the mean daily solar radiation as shown in Figure 6.5.

Reno, NV (Zone 1)			
	Base Case (Annual)	Air Based PVT (Annual)	Difference (%)
Electricity: Facility [GJ]	238.2	-28.9	-112.1%
Fans:Electricity [GJ]	42.2	42.4	0.5%
Cooling:Electricity [GJ]	14.3	14.7	3.2%
Gas:Facility [GJ]	46.5	35.3	-24.1%
Heating:Gas [GJ]	34.9	23.7	-32.1%
CO2:Facility [kg]	83,803.2	19,300.1	-77.0%
PV:ElectricityProduced [GJ]	-	267.7	-
Flagstaff, AZ (Zone 1)			
	Base Case (Annual)	Air Based PVT (Annual)	Difference (%)
Electricity:Facility [GJ]	237.0	-31.4	-113.3%
Fans:Electricity [GJ]	45.9	46.1	0.5%
Cooling:Electricity [GJ]	9.3	9.9	6.3%
Gas:Facility [GJ]	52.8	39.5	-25.1%
Heating:Gas [GJ]	41.2	27.9	-32.1%
CO2:Facility [kg]	83,724.4	19,177.0	-77.1%
PV:ElectricityProduced [GJ]	-	269.2	-
Albuquerque, NM (Zone 1)			
	Base Case (Annual)	Air Based PVT (Annual)	Difference (%)
Electricity:Facility [GJ]	244.7	-48.3	-119.7%
Fans:Electricity [GJ]	42.8	43.0	0.5%
Cooling:Electricity [GJ]	20.1	20.6	2.0%
Gas:Facility [GJ]	33.8	26.6	-21.4%
Heating:Gas [GJ]	22.2	15.0	-32.6%
CO2:Facility [kg]	85,376.2	18,058.6	-78.8%
PV:ElectricityProduced [GJ]	-	293.6	-
Santa Fe, NM (Zone 1)			
	Base Case (Annual)	Air Based PVT (Annual)	Difference (%)
Electricity:Facility [GJ]	241.9	-46.0	-119.0%
Fans:Electricity [GJ]	44.5	44.8	0.5%
Cooling:Electricity [GJ]	15.6	16.1	3.2%
Gas:Facility [GJ]	41.1	31.8	-22.6%
Heating:Gas [GJ]	29.5	20.2	-31.5%
CO2:Facility [kg]	84,814.0	19,053.6	-77.5%
PV:ElectricityProduced [GJ]	-	288.7	-

Table 6.11 – Energy performance comparison of small commercial office building with conventional HVAC system and integrated air based PV/T solar roof system, Zone 1

Lubbock, TX (Zone 1)			
	Base Case (Annual)	Air Based PVT (Annual)	Difference (%)
Electricity:Facility [GJ]	243.7	-22.0	-109.0%
Fans:Electricity [GJ]	39.2	39.4	0.5%
Cooling:Electricity [GJ]	22.7	23.1	2.0%
Gas:Facility [GJ]	34.6	27.5	-20.6%
Heating:Gas [GJ]	23.0	15.9	-31.0%
CO2:Facility [kg]	85,068.7	19,019.2	-77.6%
PV:ElectricityProduced [GJ]	-	266.3	-
St. George, UT (Zone 2)			
	Base Case (Annual)	Air Based PVT (Annual)	Difference (%)
Electricity:Facility [GJ]	256.0	-34.7	-113.6%
Fans:Electricity [GJ]	41.0	41.2	0.6%
Cooling:Electricity [GJ]	33.2	33.6	1.0%
Gas:Facility [GJ]	23.9	20.3	-15.0%
Heating:Gas [GJ]	12.3	8.7	-29.2%
CO2:Facility [kg]	88,709.2	18,634.8	-79.0%
PV:ElectricityProduced [GJ]	-	291.3	-
Durango, CO (Zone 2)			
	Base Case (Annual)	Air Based PVT (Annual)	Difference (%)
Electricity:Facility [GJ]	240.9	-28.9	-112.0%
Fans:Electricity [GJ]	46.0	46.2	0.5%
Cooling:Electricity [GJ]	13.2	13.6	3.5%
Gas:Facility [GJ]	57.4	43.1	-24.8%
Heating:Gas [GJ]	45.8	31.5	-31.1%
CO2:Facility [kg]	85,305.0	20,450.9	-76.0%
PV:ElectricityProduced [GJ]	-	270.5	-
Alamosa, CO (Zone 2)			
	Base Case (Annual)	Air Based PVT (Annual)	Difference (%)
Electricity:Facility [GJ]	240.0	-40.7	-117.0%
Fans:Electricity [GJ]	49.1	49.4	0.5%
Cooling:Electricity [GJ]	9.2	9.7	5.9%
Gas:Facility [GJ]	73.2	54.2	-25.9%
Heating:Gas [GJ]	61.6	42.6	-30.8%
CO2:Facility [kg]	85,831.5	19,846.7	-76.9%
PV:ElectricityProduced [GJ]	-	281.5	-

Table 6.12 – Energy performance comparison of small commercial office building with conventional HVAC system and integrated air based PV/T solar roof system, Zones 1-2

Trinidad, CO (Zone 2)			
	Base Case (Annual)	Air Based PVT (Annual)	Difference (%)
Electricity:Facility [GJ]	242.6	-24.9	-110.3%
Fans:Electricity [GJ]	44.1	44.2	0.2%
Cooling:Electricity [GJ]	16.7	17.0	2.4%
Gas:Facility [GJ]	45.3	35.2	-22.2%
Heating:Gas [GJ]	33.7	23.6	-29.8%
CO2:Facility [kg]	85,241.1	20,240.5	-76.3%
PV:ElectricityProduced [GJ]	-	267.9	-
Tulsa, OK (Zone 3)			
	Base Case (Annual)	Air Based PVT (Annual)	Difference (%)
Electricity:Facility [GJ]	245.2	12.1	-95.1%
Fans:Electricity [GJ]	36.9	37.1	0.5%
Cooling:Electricity [GJ]	26.5	26.9	1.5%
Gas:Facility [GJ]	46.0	37.9	-17.6%
Heating:Gas [GJ]	34.4	26.3	-23.6%
CO2:Facility [kg]	86,177.8	20,398.7	-76.3%
PV:ElectricityProduced [GJ]	-	233.7	-
St. Louis, MO (Zone 3)			
	Base Case (Annual)	Air Based PVT (Annual)	Difference (%)
Electricity:Facility [GJ]	241.3	21.6	-91.0%
Fans:Electricity [GJ]	37.5	37.7	0.4%
Cooling:Electricity [GJ]	22.0	22.3	1.4%
Gas:Facility [GJ]	66.8	53.8	-19.5%
Heating:Gas [GJ]	55.2	42.2	-23.6%
CO2:Facility [kg]	85,944.0	21,770.5	-74.7%
PV:ElectricityProduced [GJ]	-	220.2	-
Nashville, TN (Zone 3)			
	Base Case (Annual)	Air Based PVT (Annual)	Difference (%)
Electricity:Facility [GJ]	244.2	17.7	-92.7%
Fans:Electricity [GJ]	37.3	37.5	0.5%
Cooling:Electricity [GJ]	25.1	25.4	1.2%
Gas:Facility [GJ]	49.1	40.1	-18.4%
Heating:Gas [GJ]	37.5	28.5	-24.1%
CO2:Facility [kg]	86,005.8	20,893.8	-75.7%
PV:ElectricityProduced [GJ]	-	226.9	-

Table 6.13 – Energy performance comparison of small commercial office building with conventional HVAC system and integrated air based PV/T solar roof system, Zones 2-3

Atlanta, GA (Zone 3)			
	Base Case (Annual)	Air Based PVT (Annual)	Difference (%)
Electricity:Facility [GJ]	241.0	3.1	-98.7%
Fans:Electricity [GJ]	36.3	36.4	0.5%
Cooling:Electricity [GJ]	23.0	23.4	1.9%
Gas:Facility [GJ]	34.7	29.3	-15.4%
Heating:Gas [GJ]	23.1	17.7	-23.2%
CO2:Facility [kg]	84,154.7	19,971.3	-76.3%
PV:ElectricityProduced [GJ]	-	238.5	-
Charlotte, NC (Zone 3)			
	Base Case (Annual)	Air Based PVT (Annual)	Difference (%)
Electricity:Facility [GJ]	240.6	9.3	-96.1%
Fans:Electricity [GJ]	36.1	36.3	0.5%
Cooling:Electricity [GJ]	22.7	23.1	1.8%
Gas:Facility [GJ]	36.2	30.4	-16.1%
Heating:Gas [GJ]	24.6	18.8	-23.6%
CO2:Facility [kg]	84,085.0	19,732.4	-76.5%
PV:ElectricityProduced [GJ]	-	231.8	-
Boise, ID (Zone 4)			
	Base Case (Annual)	Air Based PVT (Annual)	Difference (%)
Electricity:Facility [GJ]	236.0	1.0	-99.6%
Fans:Electricity [GJ]	40.4	40.5	0.4%
Cooling:Electricity [GJ]	13.9	14.3	3.2%
Gas:Facility [GJ]	61.2	50.7	-17.2%
Heating:Gas [GJ]	49.6	39.1	-21.2%
CO2:Facility [kg]	83,813.8	21,841.1	-73.9%
PV:ElectricityProduced [GJ]	-	235.6	-
Salt Lake City, UT (Zone 4)			
	Base Case (Annual)	Air Based PVT (Annual)	Difference (%)
Electricity:Facility [GJ]	240.3	-2.9	-101.2%
Fans:Electricity [GJ]	41.9	42.1	0.5%
Cooling:Electricity [GJ]	16.6	17.1	2.6%
Gas:Facility [GJ]	55.0	45.7	-16.9%
Heating:Gas [GJ]	43.4	34.1	-21.4%
CO2:Facility [kg]	84,982.0	21,149.2	-75.1%
PV:ElectricityProduced [GJ]	-	243.8	-

Table 6.14 – Energy performance comparison of small commercial office building with conventional HVAC system and integrated air based PV/T solar roof system, Zones 3-4

Denver, CO (Zone 4)			
	Base Case (Annual)	Air Based PVT (Annual)	Difference (%)
Electricity:Facility [GJ]	242.6	-2.3	-101.0%
Fans:Electricity [GJ]	44.1	44.3	0.5%
Cooling:Electricity [GJ]	16.8	17.2	2.4%
Gas:Facility [GJ]	49.1	40.9	-16.7%
Heating:Gas [GJ]	37.5	29.3	-21.9%
CO2:Facility [kg]	85,463.7	20,765.8	-75.7%
PV:ElectricityProduced [GJ]	-	245.6	-
Omaha, NE (Zone 4)			
	Base Case (Annual)	Air Based PVT (Annual)	Difference (%)
Electricity:Facility [GJ]	239.6	17.6	-92.6%
Fans:Electricity [GJ]	39.4	39.5	0.4%
Cooling:Electricity [GJ]	18.5	18.9	2.1%
Gas:Facility [GJ]	83.2	67.9	-18.4%
Heating:Gas [GJ]	71.6	56.3	-21.4%
CO2:Facility [kg]	86,211.4	22,784.6	-73.6%
PV:ElectricityProduced [GJ]	-	222.5	-
Des Moines, IA (Zone 4)			
	Base Case (Annual)	Air Based PVT (Annual)	Difference (%)
Electricity:Facility [GJ]	237.3	19.7	-91.7%
Fans:Electricity [GJ]	39.3	39.4	0.4%
Cooling:Electricity [GJ]	16.3	16.7	2.4%
Gas:Facility [GJ]	90.8	73.4	-19.1%
Heating:Gas [GJ]	79.2	61.8	-21.9%
CO2:Facility [kg]	85,821.6	23,219.1	-72.9%
PV:ElectricityProduced [GJ]	-	218.2	-
Portland, OR (Zone 5)			
	Base Case (Annual)	Air Based PVT (Annual)	Difference (%)
Electricity:Facility [GJ]	226.9	43.7	-80.8%
Fans:Electricity [GJ]	35.9	36.1	0.5%
Cooling:Electricity [GJ]	9.3	9.9	5.8%
Gas:Facility [GJ]	46.3	42.6	-8.0%
Heating:Gas [GJ]	34.7	31.0	-10.7%
CO2:Facility [kg]	79,959.4	23,580.2	-70.5%
PV:ElectricityProduced [GJ]	-	184.0	-

Table 6.15 – Energy performance comparison of small commercial office building with conventional HVAC system and integrated air based PV/T solar roof system, Zones 4-5

Spokane, WA (Zone 5)			
	Base Case (Annual)	Air Based PVT (Annual)	Difference (%)
Electricity:Facility [GJ]	233.5	31.0	-86.7%
Fans:Electricity [GJ]	41.4	41.5	0.4%
Cooling:Electricity [GJ]	10.4	10.8	3.9%
Gas:Facility [GJ]	74.2	67.5	-9.0%
Heating:Gas [GJ]	62.6	55.9	-10.7%
CO2:Facility [kg]	83,643.3	23,679.8	-71.7%
PV:ElectricityProduced [GJ]	-	203.0	-
Cincinnati, OH (Zone 5)			
	Base Case (Annual)	Air Based PVT (Annual)	Difference (%)
Electricity:Facility [GJ]	235.5	43.1	-81.7%
Fans:Electricity [GJ]	36.4	36.6	0.5%
Cooling:Electricity [GJ]	17.3	17.8	2.6%
Gas:Facility [GJ]	58.4	53.3	-8.7%
Heating:Gas [GJ]	46.8	41.7	-10.9%
CO2:Facility [kg]	83,513.8	24,219.6	-71.0%
PV:ElectricityProduced [GJ]	-	193.0	-
Philadelphia, PA (Zone 5)			
	Base Case (Annual)	Air Based PVT (Annual)	Difference (%)
Electricity:Facility [GJ]	235.1	27.7	-88.2%
Fans:Electricity [GJ]	36.5	36.6	0.4%
Cooling:Electricity [GJ]	16.9	17.2	1.9%
Gas:Facility [GJ]	65.7	59.3	-9.7%
Heating:Gas [GJ]	54.1	47.7	-11.8%
CO2:Facility [kg]	83,742.4	22,595.0	-73.0%
PV:ElectricityProduced [GJ]	-	207.9	-
Great Falls, MT (Zone 6)			
	Base Case (Annual)	Air Based PVT (Annual)	Difference (%)
Electricity:Facility [GJ]	235.8	21.5	-90.9%
Fans:Electricity [GJ]	43.4	43.6	0.4%
Cooling:Electricity [GJ]	10.7	11.1	4.2%
Gas:Facility [GJ]	94.5	86.4	-8.6%
Heating:Gas [GJ]	82.9	74.8	-9.7%
CO2:Facility [kg]	85,504.9	23,834.3	-72.1%
PV:ElectricityProduced [GJ]	-	215.0	-

Table 6.16 – Energy performance comparison of small commercial office building with conventional HVAC system and integrated air based PV/T solar roof system, Zones 5-6

Minneapolis, MN (Zone 6)			
	Base Case (Annual)	Air Based PVT (Annual)	Difference (%)
Electricity:Facility [GJ]	235.4	24.7	-89.5%
Fans:Electricity [GJ]	40.2	40.3	0.4%
Cooling:Electricity [GJ]	13.5	13.9	2.8%
Gas:Facility [GJ]	120.1	108.5	-9.6%
Heating:Gas [GJ]	108.5	96.9	-10.6%
CO2:Facility [kg]	86,680.2	24,700.5	-71.5%
PV:ElectricityProduced [GJ]	-	211.2	-
Chicago, IL (Zone 6)			
	Base Case (Annual)	Air Based PVT (Annual)	Difference (%)
Electricity:Facility [GJ]	235.5	32.7	-86.1%
Fans:Electricity [GJ]	38.6	38.8	0.4%
Cooling:Electricity [GJ]	15.2	15.5	2.1%
Gas:Facility [GJ]	85.9	77.4	-9.8%
Heating:Gas [GJ]	74.3	65.8	-11.3%
CO2:Facility [kg]	84,946.4	23,854.4	-71.9%
PV:ElectricityProduced [GJ]	-	203.3	-
Rochester, NY (Zone 6)			
	Base Case (Annual)	Air Based PVT (Annual)	Difference (%)
Electricity:Facility [GJ]	233.4	43.3	-81.4%
Fans:Electricity [GJ]	38.5	38.7	0.4%
Cooling:Electricity [GJ]	13.1	13.5	2.9%
Gas:Facility [GJ]	90.6	81.6	-10.0%
Heating:Gas [GJ]	79.0	70.0	-11.4%
CO2:Facility [kg]	84,465.8	24,394.5	-71.1%
PV:ElectricityProduced [GJ]	-	190.6	-
Boston, MA (Zone 6)			
	Base Case (Annual)	Air Based PVT (Annual)	Difference (%)
Electricity:Facility [GJ]	231.3	24.4	-89.4%
Fans:Electricity [GJ]	37.2	37.3	0.4%
Cooling:Electricity [GJ]	12.4	12.8	3.1%
Gas:Facility [GJ]	72.9	65.5	-10.2%
Heating:Gas [GJ]	61.3	53.9	-12.2%
CO2:Facility [kg]	82,841.9	22,781.4	-72.5%
PV:ElectricityProduced [GJ]	-	207.4	-

Table 6.17 – Energy performance comparison of small commercial office building with conventional HVAC system and integrated air based PV/T solar roof system, Zone 6

6.5 Energy Performance of the Quick-Service Restaurant

The quick-service restaurant was also selected as one of the case study models since this type of building has high electric and gas consumption for refrigeration, food preparation, and high ventilation requirements. In other words, it has higher energy consumption compared to the small commercial office building. Hence, the two types of building will serve as a good comparison of the energy reduction impact of the proposed air based PV/T solar roof system.

Figure 6.6 shows an example of hourly inlet and outlet temperatures of the quick-service restaurant under the integrated air based PV/T solar roof system. It presents an example of a three day span during the heating season in Boston, MA. Similar to Figure 6.4, the graph also shows that the outlet temperature starts rising once the sun rises and solar radiation starts being absorbed. It is shown that the outlet temperatures are above or close to 20℃ in the hours between 10am and 3pm. The heating thermostat setpoint temperature of the quick-service restaurant is set to 21.1℃ (Dining) / 18.9℃ (Kitchen) during the building's occupied hours which are between 7am and 12pm. During the unoccupied hours, both the dining and kitchen's thermostat setpoint temperature is set to 15.6℃. This is an indication that the air based PV/T solar roof system provides supplemental heating to the gas furnace inside the packaged air conditioning unit of the quick-service restaurant for only a few hours of the day when the sun is out during the heating season. Thus, the proposed air based PV/T solar roof system can be considered as a low energy solution that supplements the existing HVAC system rather than being responsible for handling the entire heating load of a building.

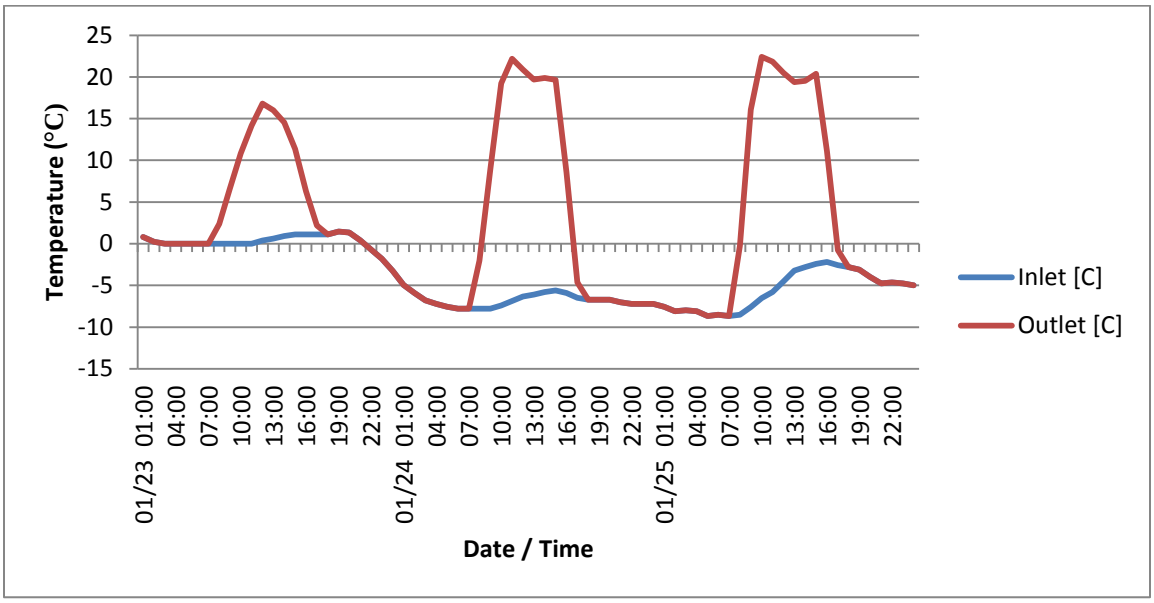

Figure 6.6 – Example of inlet/outlet temperatures of the quick-service restaurant integrated air based PV/T solar roof system in Boston, MA (Zone 6)

Tables 6.22 – 6.28 present the comparison of the energy performance of a quick-service restaurant under the conventional HVAC system and under the integrated air based PV/T solar roof system in six different climatic zones / 28 different cities within the United States. Similar to the small commercial office building, the annual building energy simulations for the quick-service restaurant also did not show much difference in the electricity consumptions for the interior lights/equipment and gas consumption for the interior equipment and the water heater. However, unlike the small office building, the percentage change in the electricity consumption for cooling and fans varied significantly. The electricity consumption percentage change (%) ranges from -3.2% ~ 41.7%. The highest increase in the electricity consumption for cooling was shown in Alamosa, CO (Zone 2) where the cooling electricity consumption rose from 11.8 GJ to 16.8 GJ (41.7%

increase) and the greatest decrease was shown in St. George, UT (Zone 2) where the cooling electricity consumption dropped from 71.3 GJ to 69.0 GJ (3.2% decrease). Nashville, TN (Zone 3) also showed a decrease where the cooling electricity consumption dropped from 50.0 GJ to 49.8 GJ (0.2% decrease) and Flagstaff, AZ (Zone 1) showed an increase where it rose from 12.7 GJ to 17.4 GJ (37.1% increase). 18 different cities (Albuquerque, Lubbock, Trinidad, Tulsa, St. Louis, Atlanta, Charlotte, Boise, Salt Lake City, Denver, Omaha, Des Moines, Cincinnati, Philadelphia, Minneapolis, Chicago, Rochester, and Boston) showed an increase in cooling electricity that ranges between 0.0% ~ 9.0%, and six other cities (Reno, Santa Fe, Durango, Portland, Spokane, and Great Falls) showed an increase that ranged between 10.4% ~ 18.7%.

Flagstaff, AZ (Zone 1)			
	Base Case (Annual)	Air Based PVT (Annual)	Percentage Change (%)
Cooling Coil Total Cooling Energy [GJ]	38.2	58.8	54.0%
St. George, UT (Zone 2)			
	Base Case (Annual)	Air Based PVT (Annual)	Percentage Change (%)
Cooling Coil Total Cooling Energy [GJ]	162.0	155.2	-4.2%
Alamosa, CO (Zone 2)			
	Base Case (Annual)	Air Based PVT (Annual)	Percentage Change (%)
Cooling Coil Total Cooling Energy [GJ]	35.6	57.3	61.0%
Nashville, TN (Zone 3)			
	Base Case (Annual)	Air Based PVT (Annual)	Percentage Change (%)
Cooling Coil Total Cooling Energy [GJ]	163.2	161.9	-0.8%

Table 6.18 – Cooling coil total cooling energy comparison of quick-service restaurant with conventional HVAC system and integrated air based PV/T solar roof system

As mentioned above, the quick-service restaurant's cooling electricity consumption slightly decreased in two cities – St. George, UT (Zone 2) and Nashville, TN (Zone 3). These two cities are the cities with the highest cooling electricity consumption under the base case scenario where St. George consumes 71.3 GJ and Nashville consumes 50.0 GJ. Additional analysis finds that a decrease in the cooling coil energy consumption with the implementation of the air based PV/T system is the main factor that caused the decrease in cooling electricity consumption for these two cities. Table 6.18 summarizes the cooling coil energy consumption of St. George, Nashville and two other example cities, Flagstaff, AZ (Zone 1) and Alamosa, CO (Zone 2). Under the base case scenario, St. George and Nashville is shown to consume a significantly greater amount (over 160 GJ) of cooling coil energy compared to the other two cities. The extreme summer season weather in St. George and Nashville is likely the reason underlying such observation. In other words, the fact that the outdoor temperature on a typical summer day does not cool down significantly after sunset in these two cities results in high consumption of cooling coil energy under the base case that assumes the use of the traditional HVAC system. With the implementation of the air based PV/T solar roof system, the cooling coil energy consumption in Flagstaff and Alamosa increases by over 54%. However, the overall consumption of cooling coil energy was still less than 1/4 of that in St. George and Nashville. This is likely attributable to the additional layer of protection from the exterior environment the PV panel provides. In other words, even though the outdoor temperature remains at a fairly high level after sunset, the extra layer provided by the PV panel better protects the already-cooled air inside the building from escaping. This will likely lead to the consumption of cooling coil energy to

slightly decrease with the implementation of the air based PV/T solar roof system, ultimately leading to a slight decrease in the consumption of cooling electricity.

To further gain understanding of why the cooling electricity consumption under the integrated air based PV/T system decreases in St. George and Nashville, additional analysis on the outdoor air drybulb temperatures on a typical summer day was conducted and a comparison of the cooling coil total cooling energy between the base case and integrated air based PV/T solar roof system was made. Table 6.19 shows an example of hourly outdoor air drybulb temperatures during a three day span in July, and a comparison of cooling coil total cooling energy between the base case and integrated air based PV/T solar roof system in Flagstaff, AZ. The first thing to note is that the outdoor air drybulb temperatures significantly drop in the early morning hours compared to the afternoon hours and the cooling coil is shut down for a periods of time from the evenings until the mornings. With the integration of the air based PV/T solar roof system, cooling coil energy significantly increases throughout the day with the highest increases in the early mornings and late afternoons when solar radiation is absorbed on the roof with increased sunshine. This leads to significantly greater cooling electricity being used during the day time when the air based PV/T solar roof system is implemented compared to when the traditional HVAC system solely exists.

Table 6.20 shows an example of hourly outdoor air drybulb temperatures and a comparison of cooling coil total cooling energy between the base case and integrated air based PV/T solar roof system in St. George, UT. St. George, UT is considered to be a hot desert climate with extreme high temperatures during the summer and the Table 6.20 shows

that the temperatures can rise over 40 ℃ and still remain warm a few hours past midnight. The cooling coil energy is consumed almost all throughout the day with only a few hours of deactivation during the early morning hours. The cooling coil energy consumption comparison between the base case and the integrated air based PV/T solar roof system shows that throughout the day, especially when the sun is out, the integrated air based PV/T solar roof system consumed more energy. This is consistent with the findings in the other 16 cities. However, as soon as the sun set, the cooling coil energy consumption of the air based PV/T solar roof system starts to decrease. This can be attributed to the fact that the air based PV/T solar roof system helps insulate and block the warm/hot night air flow into the building as it has an extra layer of construction on the roof. The highest decrease of cooling coil energy consumption is observed in the early morning hours, right before the activation of the cooling coil, and the late evening hours, right before the deactivation of the cooling coil. A similar effect is found in Nashville, TN where the annual cooling coil energy consumption decreased by 0.8% with the integrated air based PV/T solar roof system. The hourly outdoor air drybulb temperatures and a comparison of cooling coil total cooling energy between the base case and integrated air based PV/T solar roof system in Nashville, TN is shown in Table 6.21.

Flagstaff, AZ (Zone 1)			
Date / Time	Outdoor Air Drybulb Temperature [°C]	Base Case	Air Based PVT
		Cooling Coil Total Cooling Energy [J]	Cooling Coil Total Cooling Energy [J]
07/07 15:00:00	16.5	3,210,112	15,241,522
07/07 16:00:00	15.4	255,574	14,993,028
07/07 17:00:00	14.3	2,187,355	18,391,099
07/07 18:00:00	13.5	0	18,732,759
07/07 19:00:00	13.0	0	16,097,710
07/07 20:00:00	12.4	0	391,512
07/07 21:00:00	11.9	0	0
07/07 22:00:00	11.3	0	0
07/07 23:00:00	10.8	0	0
07/07 24:00:00	10.2	0	0
07/08 01:00:00	9.7	0	0
07/08 02:00:00	9.1	0	0
07/08 03:00:00	8.8	0	0
07/08 04:00:00	8.6	0	0
07/08 05:00:00	8.4	0	0
07/08 06:00:00	9.8	0	0
07/08 07:00:00	12.3	0	8,604,646
07/08 08:00:00	14.7	0	12,268,038
07/08 09:00:00	16.7	218,624	13,844,641
07/08 10:00:00	18.3	9,790,074	15,784,051
07/08 11:00:00	20.0	23,991,283	24,716,619
07/08 12:00:00	21.0	31,781,222	32,315,730
07/08 13:00:00	21.8	32,601,727	33,007,859
07/08 14:00:00	22.5	27,902,024	28,249,029
07/08 15:00:00	22.7	26,488,925	26,846,448
07/08 16:00:00	22.5	25,532,562	25,798,081
07/08 17:00:00	22.3	27,439,022	27,647,689
07/08 18:00:00	21.3	28,418,291	28,588,570
07/08 19:00:00	19.8	23,285,574	23,433,602
07/08 20:00:00	18.4	13,869,367	13,991,972
07/08 21:00:00	17.0	7,487,427	7,599,592
07/08 22:00:00	15.7	457,018	485,765
07/08 23:00:00	14.4	0	0
07/08 24:00:00	12.8	0	0
07/09 01:00:00	11.2	0	0
07/09 02:00:00	9.5	0	0
07/09 03:00:00	8.8	0	0
07/09 04:00:00	8.6	0	0
07/09 05:00:00	8.4	0	0
07/09 06:00:00	10.2	0	0
07/09 07:00:00	13.1	142,926	7,887,552
07/09 08:00:00	16.1	215,332	10,140,696
07/09 09:00:00	18.0	4,630,386	10,475,530
07/09 10:00:00	19.3	10,676,382	11,503,740
07/09 11:00:00	20.6	19,114,492	19,438,393
Total (Percentage Change [%])		**319,695,699**	**466,475,873 (46%)**

Table 6.19 – Example of summer hourly outdoor air drybulb temperature (°C) and cooling coil total cooling energy (J) consumption in Flagstaff, AZ (Zone 1)

St. George, UT (Zone 2)			
Date / Time	Outdoor Air Drybulb Temperature [°C]	Base Case	Air Based PVT
		Cooling Coil Total Cooling Energy [J]	Cooling Coil Total Cooling Energy [J]
07/07 15:00:00	39.8	82,836,417	82,905,018
07/07 16:00:00	40.3	86,128,743	86,184,001
07/07 17:00:00	40.4	93,965,135	94,013,015
07/07 18:00:00	40.0	94,161,388	94,197,708
07/07 19:00:00	38.8	89,735,026	89,770,301
07/07 20:00:00	36.8	78,379,117	73,280,595
07/07 21:00:00	36.0	72,893,765	51,281,039
07/07 22:00:00	34.1	62,961,351	41,039,121
07/07 23:00:00	33.0	55,764,785	34,253,019
07/07 24:00:00	31.1	40,955,098	19,799,400
07/08 01:00:00	30.0	0	0
07/08 02:00:00	28.8	0	0
07/08 03:00:00	28.0	0	0
07/08 04:00:00	26.8	0	0
07/08 05:00:00	26.0	20,915,474	867,481
07/08 06:00:00	24.1	22,144,774	17,285,317
07/08 07:00:00	24.3	28,549,827	28,658,576
07/08 08:00:00	26.9	36,148,261	36,250,825
07/08 09:00:00	29.3	45,080,877	45,180,650
07/08 10:00:00	31.3	53,970,047	54,067,058
07/08 11:00:00	34.5	69,438,517	69,532,405
07/08 12:00:00	37.9	83,888,846	83,972,889
07/08 13:00:00	40.3	91,152,080	91,228,345
07/08 14:00:00	41.0	88,539,343	88,613,214
07/08 15:00:00	42.9	94,665,278	94,739,316
07/08 16:00:00	43.4	97,654,607	97,717,461
07/08 17:00:00	43.0	99,991,784	100,043,477
07/08 18:00:00	42.4	102,589,647	102,637,337
07/08 19:00:00	42.0	101,313,774	101,351,238
07/08 20:00:00	40.1	90,495,781	85,684,026
07/08 21:00:00	38.4	81,562,655	61,042,575
07/08 22:00:00	38.0	76,831,427	55,296,331
07/08 23:00:00	36.1	66,961,160	43,860,599
07/08 24:00:00	35.6	57,084,690	33,932,071
07/09 01:00:00	34.1	0	0
07/09 02:00:00	31.8	0	0
07/09 03:00:00	29.1	0	0
07/09 04:00:00	28.6	0	0
07/09 05:00:00	28.4	29,802,189	9,143,313
07/09 06:00:00	28.6	38,240,907	33,087,050
07/09 07:00:00	28.4	43,395,142	43,481,669
07/09 08:00:00	29.3	44,988,050	45,074,456
07/09 09:00:00	31.7	54,089,352	54,174,700
07/09 10:00:00	34.5	65,638,465	65,723,244
07/09 11:00:00	37.1	79,048,258	79,130,874
Total (Percentage Change [%])		**2,521,962,037**	**2,288,499,714 (-9%)**

Table 6.20 – Example of summer hourly outdoor air drybulb temperature (°C) and cooling coil total cooling energy (J) consumption in St. George, UT (Zone 2)

Nashville, TN (Zone 3)			
Date / Time	Outdoor Air Drybulb Temperature [°C]	Base Case	Air Based PVT
		Cooling Coil Total Cooling Energy [J]	Cooling Coil Total Cooling Energy [J]
07/07 15:00:00	32	111,432,678	111,477,645
07/07 16:00:00	32.6	119,333,909	119,371,590
07/07 17:00:00	31.4	123,388,484	123,461,725
07/07 18:00:00	29.9	117,019,104	117,020,902
07/07 19:00:00	28	107,847,799	107,845,602
07/07 20:00:00	23.8	71,164,278	68,303,387
07/07 21:00:00	21.7	51,503,344	51,517,736
07/07 22:00:00	21.7	41,994,623	40,124,678
07/07 23:00:00	22	36,989,098	33,954,145
07/07 24:00:00	22.2	17,796,594	13,664,101
07/08 01:00:00	22.6	0	0
07/08 02:00:00	23.1	0	0
07/08 03:00:00	23.3	0	0
07/08 04:00:00	23.3	0	0
07/08 05:00:00	23.7	27,791,196	24,692,438
07/08 06:00:00	23.9	50,000,508	50,119,890
07/08 07:00:00	24.2	64,047,698	64,178,239
07/08 08:00:00	25.2	65,176,620	65,272,076
07/08 09:00:00	26.3	77,039,912	77,133,601
07/08 10:00:00	27.7	90,251,790	90,335,901
07/08 11:00:00	28.7	107,448,716	107,519,485
07/08 12:00:00	29.6	122,737,147	122,798,349
07/08 13:00:00	30.4	128,269,634	128,354,663
07/08 14:00:00	31.6	127,185,031	127,257,320
07/08 15:00:00	31.9	129,697,457	129,572,274
07/08 16:00:00	32.7	123,830,108	123,867,147
07/08 17:00:00	32.3	112,188,849	112,216,327
07/08 18:00:00	28.2	111,500,357	111,499,132
07/08 19:00:00	26.1	104,840,290	104,839,887
07/08 20:00:00	25.8	91,679,536	83,928,763
07/08 21:00:00	25.2	82,832,184	76,479,907
07/08 22:00:00	25	71,106,379	62,240,343
07/08 23:00:00	24.6	57,712,585	47,313,588
07/08 24:00:00	24.1	33,473,126	20,193,140
07/09 01:00:00	23.5	0	0
07/09 02:00:00	23.3	0	0
07/09 03:00:00	22.6	0	0
07/09 04:00:00	21.9	0	0
07/09 05:00:00	21	949,210	4,027,510
07/09 06:00:00	21.3	20,104,961	20,141,597
07/09 07:00:00	22.4	34,782,619	34,902,999
07/09 08:00:00	23.8	35,994,857	36,092,715
07/09 09:00:00	24.8	39,511,113	39,601,151
07/09 10:00:00	25.7	43,710,820	43,790,234
07/09 11:00:00	26.5	54,093,059	54,172,303
Total (Percentage Change [%])		**2,806,425,673**	**2,749,282,490 (-2%)**

Table 6.21 – Example of summer hourly outdoor air drybulb temperature (°C) and cooling coil total cooling energy (J) consumption in Nashville, TN (Zone 3)

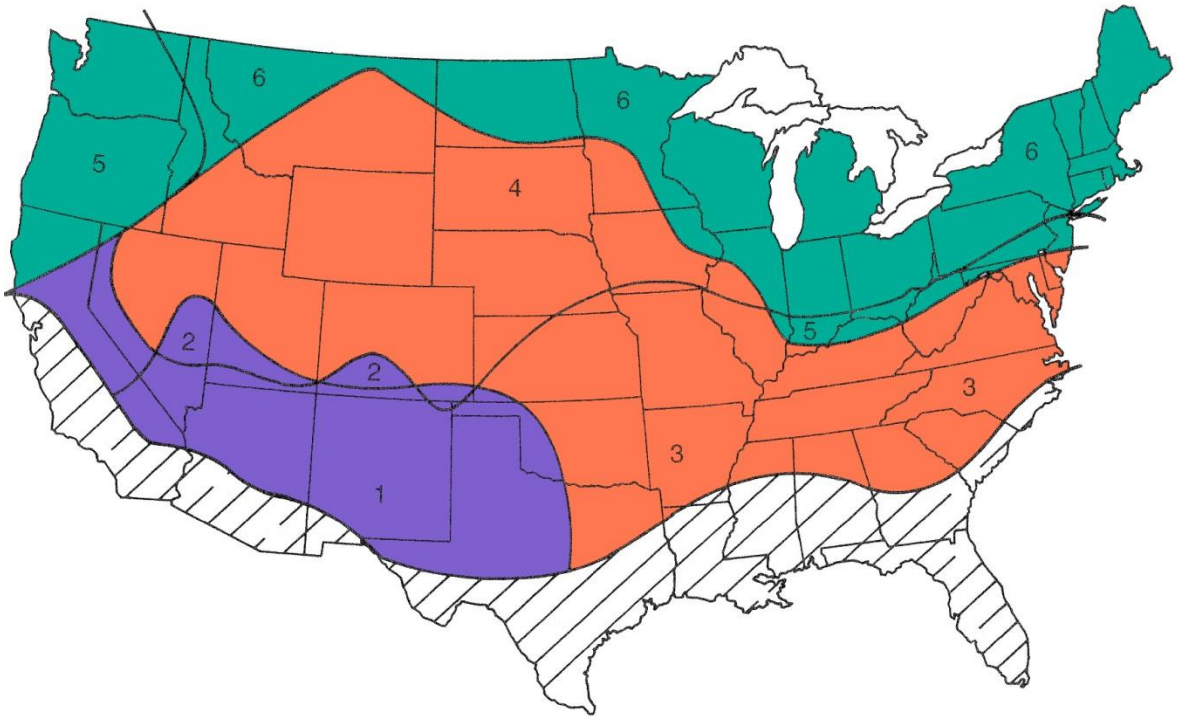

Zones	Mean Daily Solar Radiation (Langley)	Heating: Gas Reduction (%)	Gas: Facility Reduction (%)	PV: Electricity Produced [GJ]
Zone 1 Zone 2	350 ~ 450	37.7 ~ 42.6	6.2 ~ 15.1	222.9 ~ 244.4
Zone 3 Zone 4	250 ~ 350	29.9 ~ 34.9	6.9 ~ 12.4	181.6 ~ 204.4
Zone 5 Zone 6	175 ~ 250	19.2 ~ 24.0	5.9 ~ 8.9	153.2 ~ 178.9

Figure 6.7 – Summary of heating gas reduction (%), facility gas reduction (%), and PV electricity produced (GJ) for quick-service restaurant with integrated air based PV/T solar roof system

Similarly to the small office building, the annual building energy simulations of the quick-service restaurant also showed significant reductions in carbon dioxide production and gas consumption for heating. Specifically, all of the cities examined showed reductions

of over 35% in carbon dioxide production. Further analysis shows that despite differing climate conditions, Zones 1 and 2 have similar reductions in gas consumption for heating and PV electricity production. Similarly, Zones 3 and 4, and Zones 5 and 6 also have similar reductions in gas consumption for heating and PV electricity production despite their different climate conditions. As shown in Figure 6.7, Zones 1 and 2 resulted in the highest gas consumption reduction of 37.7% to 42.6% and Zones 5 and 6 resulted in the lowest gas consumption reduction of 19.2% to 24.0%. The highest decrease in the gas consumption for heating was shown in St. George, UT (Zone 2) where the heating gas consumption dropped from 111.9 GJ to 64.3 GJ (42.6% decrease) and the lowest decrease was shown in Great Falls, MT (Zone 6) where the heating gas consumption dropped from 430.3 GJ to 347.8 GJ (19.2% decrease).

Note that the greatest increase of electricity consumption for cooling and fans was 5.0 GJ in the annual building energy simulation for Alamosa, CO (Zone 2) while the gas consumption for heating dropped by 158.0 GJ. This suggests the slight increase in electricity consumption for cooling and fans can be offset by the significant decrease in gas consumption for heating.

As mentioned in Chapter 4. Overview of Computational Case Study Models, the dimensions of the quick-service restaurant are smaller than the small commercial office building. The surface area of the south-facing roof is also smaller which leads to less electricity produced by the PV/T system when compared to the small commercial office building. The quick-service restaurant requires high electric and gas equipment densities for refrigeration, food preparation, dishwashing, and higher ventilation requirements which

lead to a higher amount of electricity and gas consumption compared to the small office building.

Tables 6.22 – 6.28 show that the base case of quick-service restaurant's annual facility electricity consumption ranged from 674.7 GJ (Portland, OR (Zone 5)) to 741.9 GJ (St. George, UT (Zone 2)), which is about 3 times higher than the electricity consumption of the small commercial office building. Tables 6.22 – 6.28 also show that the proposed integrated air based PV/T solar roof system produced over 30% of the electricity that is consumed by the quick-service restaurant building in Zones 1 and 2. The annual PV electricity production slightly decreases in Zones 3 and 4 where the annual PV electricity production is shown to range between 25.9% ~ 28.9% of the annual electricity consumption under the conventional HVAC system. The annual PV electricity production is lowest in Zones 5 and 6 where the annual PV electricity production is shown to cover between 22.4% ~ 25.8% of the electricity consumption under the conventional HVAC system.

The whole annual building energy simulations showed that the energy performance of the quick-service restaurant with integration of the air based PV/T solar roof system is also beneficial in all climates within the United States. Compared to the small commercial office building, the smaller fraction of PV electricity production of the quick-service restaurant is the result of smaller south facing roof. The quick-service restaurant has much higher ventilation and heating requirements than the small commercial office building and therefore, the heating gas consumption reductions were higher than the small commercial office building. However, the quick-service restaurant's total annual gas consumption reduction was smaller due to the building's larger gas power density. The highest savings

of gas consumption were also shown in Zones 1 and 2 where it has the highest values of mean daily solar radiation. The whole annual building energy simulations of the quick-service restaurant also suggest that the gas and electricity savings from the proposed air based PV/T solar roof system is proportional to the mean daily solar radiation as shown in Figure 6.7.

Reno, NV (Zone 1)			
	Base Case (Annual)	Air Based PVT (Annual)	Difference (%)
Electricity:Facility [GJ]	693.0	472.9	-31.8%
Fans:Electricity [GJ]	78.1	78.1	0.0%
Cooling:Electricity [GJ]	24.2	26.7	10.4%
Gas:Facility [GJ]	919.7	811.1	-11.8%
Heating:Gas [GJ]	265.4	156.8	-40.9%
CO2:Facility [kg]	284,719.9	164,216.1	-42.3%
PV:ElectricityProduced [GJ]	-	222.9	-
Flagstaff, AZ (Zone 1)			
	Base Case (Annual)	Air Based PVT (Annual)	Difference (%)
Electricity:Facility [GJ]	684.3	465.1	-32.0%
Fans:Electricity [GJ]	81.9	82.0	0.1%
Cooling:Electricity [GJ]	12.7	17.4	37.1%
Gas:Facility [GJ]	953.2	831.1	-12.8%
Heating:Gas [GJ]	298.9	176.7	-40.9%
CO2:Facility [kg]	283,486.5	164,645.7	-41.9%
PV:ElectricityProduced [GJ]	-	224.1	-
Albuquerque, NM (Zone 1)			
	Base Case (Annual)	Air Based PVT (Annual)	Difference (%)
Electricity:Facility [GJ]	706.0	463.4	-34.4%
Fans:Electricity [GJ]	79.2	79.3	0.1%
Cooling:Electricity [GJ]	34.3	36.0	4.9%
Gas:Facility [GJ]	839.6	761.0	-9.4%
Heating:Gas [GJ]	185.2	106.6	-42.4%
CO2:Facility [kg]	284,985.5	156,200.3	-45.2%
PV:ElectricityProduced [GJ]	-	244.4	-
Santa Fe, NM (Zone 1)			
	Base Case (Annual)	Air Based PVT (Annual)	Difference (%)
Electricity:Facility [GJ]	696.6	459.4	-34.0%
Fans:Electricity [GJ]	80.9	81.0	0.1%
Cooling:Electricity [GJ]	24.3	27.3	12.3%
Gas:Facility [GJ]	880.4	789.3	-10.3%
Heating:Gas [GJ]	226.0	134.9	-40.3%
CO2:Facility [kg]	283,881.1	159,035.2	-44.0%
PV:ElectricityProduced [GJ]	-	240.3	-

Table 6.22 – Energy performance comparison of quick-service restaurant with conventional HVAC system and integrated air based PV/T solar roof system, Zone 1

Lubbock, TX (Zone 1)			
	Base Case (Annual)	Air Based PVT (Annual)	Difference (%)
Electricity:Facility [GJ]	711.8	490.8	-31.0%
Fans:Electricity [GJ]	75.9	76.0	0.1%
Cooling:Electricity [GJ]	42.1	42.7	1.3%
Gas:Facility [GJ]	825.5	755.1	-8.5%
Heating:Gas [GJ]	171.2	100.7	-41.2%
CO2:Facility [kg]	286,223.6	161,587.6	-43.5%
PV:ElectricityProduced [GJ]	-	221.7	-
St. George, UT (Zone 2)			
	Base Case (Annual)	Air Based PVT (Annual)	Difference (%)
Electricity:Facility [GJ]	741.9	497.2	-33.0%
Fans:Electricity [GJ]	75.8	75.8	0.0%
Cooling:Electricity [GJ]	71.3	69.0	-3.2%
Gas:Facility [GJ]	766.3	718.6	-6.2%
Heating:Gas [GJ]	111.9	64.3	-42.6%
CO2:Facility [kg]	293,422.4	154,804.9	-47.2%
PV:ElectricityProduced [GJ]	-	242.5	-
Durango, CO (Zone 2)			
	Base Case (Annual)	Air Based PVT (Annual)	Difference (%)
Electricity:Facility [GJ]	691.6	470.1	-32.0%
Fans:Electricity [GJ]	81.6	81.6	0.0%
Cooling:Electricity [GJ]	19.8	23.1	17.1%
Gas:Facility [GJ]	965.8	841.5	-12.9%
Heating:Gas [GJ]	311.4	187.2	-39.9%
CO2:Facility [kg]	286,642.4	165,791.1	-42.2%
PV:ElectricityProduced [GJ]	-	225.1	-
Alamosa, CO (Zone 2)			
	Base Case (Annual)	Air Based PVT (Annual)	Difference (%)
Electricity:Facility [GJ]	684.1	455.0	-33.5%
Fans:Electricity [GJ]	83.0	83.1	0.1%
Cooling:Electricity [GJ]	11.8	16.8	41.7%
Gas:Facility [GJ]	1,045.8	887.8	-15.1%
Heating:Gas [GJ]	391.4	233.5	-40.4%
CO2:Facility [kg]	288,257.3	165,180.2	-42.7%
PV:ElectricityProduced [GJ]	-	234.3	-

Table 6.23 – Energy performance comparison of quick-service restaurant with conventional HVAC system and integrated air based PV/T solar roof system, Zones 1-2

Trinidad, CO (Zone 2)			
	Base Case (Annual)	Air Based PVT (Annual)	Difference (%)
Electricity:Facility [GJ]	699.0	478.3	-31.6%
Fans:Electricity [GJ]	80.1	80.1	0.0%
Cooling:Electricity [GJ]	27.3	29.5	7.9%
Gas:Facility [GJ]	892.4	802.7	-10.0%
Heating:Gas [GJ]	238.1	148.4	-37.7%
CO2:Facility [kg]	285,340.6	163,539.7	-42.7%
PV:ElectricityProduced [GJ]	-	223.0	-
Tulsa, OK (Zone 3)			
	Base Case (Annual)	Air Based PVT (Annual)	Difference (%)
Electricity:Facility [GJ]	722.2	527.9	-26.9%
Fans:Electricity [GJ]	72.6	72.7	0.1%
Cooling:Electricity [GJ]	55.6	55.6	0.0%
Gas:Facility [GJ]	875.7	801.0	-8.5%
Heating:Gas [GJ]	221.3	146.7	-33.7%
CO2:Facility [kg]	292,412.3	170,270.5	-41.8%
PV:ElectricityProduced [GJ]	-	194.5	-
St. Louis, MO (Zone 3)			
	Base Case (Annual)	Air Based PVT (Annual)	Difference (%)
Electricity:Facility [GJ]	708.0	524.9	-25.9%
Fans:Electricity [GJ]	72.7	72.7	0.0%
Cooling:Electricity [GJ]	42.4	42.5	0.3%
Gas:Facility [GJ]	971.9	864.3	-11.1%
Heating:Gas [GJ]	317.6	210.0	-33.9%
CO2:Facility [kg]	292,543.5	176,758.5	-39.6%
PV:ElectricityProduced [GJ]	-	183.3	-
Nashville, TN (Zone 3)			
	Base Case (Annual)	Air Based PVT (Annual)	Difference (%)
Electricity:Facility [GJ]	716.5	527.6	-26.4%
Fans:Electricity [GJ]	72.6	72.7	0.1%
Cooling:Electricity [GJ]	50.0	49.8	-0.2%
Gas:Facility [GJ]	890.1	808.9	-9.1%
Heating:Gas [GJ]	235.8	154.6	-34.4%
CO2:Facility [kg]	291,200.5	172,162.4	-40.9%
PV:ElectricityProduced [GJ]	-	188.9	-

Table 6.24 – Energy performance comparison of quick-service restaurant with conventional HVAC system and integrated air based PV/T solar roof system, Zones 2-3

Atlanta, GA (Zone 3)			
	Base Case (Annual)	Air Based PVT (Annual)	Difference (%)
Electricity:Facility [GJ]	710.5	512.2	-27.9%
Fans:Electricity [GJ]	73.0	73.0	0.0%
Cooling:Electricity [GJ]	43.2	43.3	0.3%
Gas:Facility [GJ]	814.3	758.4	-6.9%
Heating:Gas [GJ]	160.0	104.1	-34.9%
CO2:Facility [kg]	285,215.8	167,131.9	-41.4%
PV:ElectricityProduced [GJ]	-	198.6	-
Charlotte, NC (Zone 3)			
	Base Case (Annual)	Air Based PVT (Annual)	Difference (%)
Electricity:Facility [GJ]	708.8	516.4	-27.1%
Fans:Electricity [GJ]	72.7	72.8	0.1%
Cooling:Electricity [GJ]	42.1	42.5	1.1%
Gas:Facility [GJ]	831.3	770.1	-7.4%
Heating:Gas [GJ]	177.0	115.8	-34.6%
CO2:Facility [kg]	285,494.8	168,587.0	-40.9%
PV:ElectricityProduced [GJ]	-	193.0	-
Boise, ID (Zone 4)			
	Base Case (Annual)	Air Based PVT (Annual)	Difference (%)
Electricity:Facility [GJ]	690.3	496.5	-28.1%
Fans:Electricity [GJ]	76.0	76.0	0.0%
Cooling:Electricity [GJ]	23.6	25.7	8.8%
Gas:Facility [GJ]	967.1	868.2	-10.2%
Heating:Gas [GJ]	312.8	213.9	-31.6%
CO2:Facility [kg]	286,274.0	174,451.3	-39.1%
PV:ElectricityProduced [GJ]	-	196.1	-
Salt Lake City, UT (Zone 4)			
	Base Case (Annual)	Air Based PVT (Annual)	Difference (%)
Electricity:Facility [GJ]	699.5	498.7	-28.7%
Fans:Electricity [GJ]	77.8	77.9	0.1%
Cooling:Electricity [GJ]	30.3	32.3	6.7%
Gas:Facility [GJ]	929.2	843.4	-9.2%
Heating:Gas [GJ]	274.9	189.1	-31.2%
CO2:Facility [kg]	287,440.3	170,608.3	-40.6%
PV:ElectricityProduced [GJ]	-	203.0	-

Table 6.25 – Energy performance comparison of quick-service restaurant with conventional HVAC system and integrated air based PV/T solar roof system, Zones 3-4

Denver, CO (Zone 4)			
	Base Case (Annual)	Air Based PVT (Annual)	Difference (%)
Electricity:Facility [GJ]	699.5	497.5	-28.9%
Fans:Electricity [GJ]	79.7	79.7	0.0%
Cooling:Electricity [GJ]	28.4	30.7	8.0%
Gas:Facility [GJ]	914.1	836.4	-8.5%
Heating:Gas [GJ]	259.7	182.1	-29.9%
CO2:Facility [kg]	286,635.1	168,919.8	-41.1%
PV:ElectricityProduced [GJ]	-	204.4	-
Omaha, NE (Zone 4)			
	Base Case (Annual)	Air Based PVT (Annual)	Difference (%)
Electricity:Facility [GJ]	699.6	515.5	-26.3%
Fans:Electricity [GJ]	73.8	73.8	0.0%
Cooling:Electricity [GJ]	33.9	34.8	2.9%
Gas:Facility [GJ]	1,041.3	920.3	-11.6%
Heating:Gas [GJ]	386.9	266.0	-31.3%
CO2:Facility [kg]	293,318.7	179,838.2	-38.7%
PV:ElectricityProduced [GJ]	-	185.2	-
Des Moines, IA (Zone 4)			
	Base Case (Annual)	Air Based PVT (Annual)	Difference (%)
Electricity:Facility [GJ]	693.7	513.4	-26.0%
Fans:Electricity [GJ]	73.3	73.4	0.1%
Cooling:Electricity [GJ]	28.8	30.0	4.2%
Gas:Facility [GJ]	1,076.9	943.1	-12.4%
Heating:Gas [GJ]	422.6	288.8	-31.7%
CO2:Facility [kg]	293,133.4	181,495.1	-38.1%
PV:ElectricityProduced [GJ]	-	181.6	-
Portland, OR (Zone 5)			
	Base Case (Annual)	Air Based PVT (Annual)	Difference (%)
Electricity:Facility [GJ]	674.7	523.9	-22.4%
Fans:Electricity [GJ]	72.3	72.4	0.1%
Cooling:Electricity [GJ]	11.3	13.4	18.7%
Gas:Facility [GJ]	879.5	827.8	-5.9%
Heating:Gas [GJ]	225.2	173.4	-23.0%
CO2:Facility [kg]	276,377.9	182,022.2	-34.1%
PV:ElectricityProduced [GJ]	-	153.2	-

Table 6.26 – Energy performance comparison of quick-service restaurant with conventional HVAC system and integrated air based PV/T solar roof system, Zones 4-5

Spokane, WA (Zone 5)			
	Base Case (Annual)	Air Based PVT (Annual)	Difference (%)
Electricity:Facility [GJ]	681.1	514.5	-24.5%
Fans:Electricity [GJ]	75.7	75.7	0.0%
Cooling:Electricity [GJ]	15.7	18.0	14.3%
Gas:Facility [GJ]	1,024.9	946.5	-7.6%
Heating:Gas [GJ]	370.5	292.2	-21.2%
CO2:Facility [kg]	286,141.6	182,593.4	-36.2%
PV:ElectricityProduced [GJ]	-	169.0	-
Cincinnati, OH (Zone 5)			
	Base Case (Annual)	Air Based PVT (Annual)	Difference (%)
Electricity:Facility [GJ]	697.1	537.8	-22.8%
Fans:Electricity [GJ]	72.5	72.5	0.0%
Cooling:Electricity [GJ]	32.1	33.4	3.8%
Gas:Facility [GJ]	944.9	887.2	-6.1%
Heating:Gas [GJ]	290.6	232.8	-19.9%
CO2:Facility [kg]	287,414.0	183,025.5	-36.3%
PV:ElectricityProduced [GJ]	-	160.6	-
Philadelphia, PA (Zone 5)			
	Base Case (Annual)	Air Based PVT (Annual)	Difference (%)
Electricity:Facility [GJ]	693.3	521.5	-24.8%
Fans:Electricity [GJ]	72.0	72.1	0.1%
Cooling:Electricity [GJ]	29.2	30.2	3.4%
Gas:Facility [GJ]	974.0	901.9	-7.4%
Heating:Gas [GJ]	319.6	247.6	-22.5%
CO2:Facility [kg]	287,660.5	179,440.1	-37.6%
PV:ElectricityProduced [GJ]	-	173.0	-
Great Falls, MT (Zone 6)			
	Base Case (Annual)	Air Based PVT (Annual)	Difference (%)
Electricity:Facility [GJ]	683.3	507.3	-25.8%
Fans:Electricity [GJ]	77.4	77.4	0.0%
Cooling:Electricity [GJ]	16.0	18.8	17.1%
Gas:Facility [GJ]	1,084.7	1,002.1	-7.6%
Heating:Gas [GJ]	430.3	347.8	-19.2%
CO2:Facility [kg]	290,003.6	182,976.1	-36.9%
PV:ElectricityProduced [GJ]	-	178.9	-

Table 6.27 – Energy performance comparison of quick-service restaurant with conventional HVAC system and integrated air based PV/T solar roof system, Zones 5-6

Minneapolis, MN (Zone 6)			
	Base Case (Annual)	Air Based PVT (Annual)	Difference (%)
Electricity:Facility [GJ]	685.7	511.5	-25.4%
Fans:Electricity [GJ]	73.4	73.4	0.0%
Cooling:Electricity [GJ]	21.6	23.1	6.8%
Gas:Facility [GJ]	1,199.3	1,092.1	-8.9%
Heating:Gas [GJ]	545.0	437.8	-19.7%
CO2:Facility [kg]	296,776.5	188,125.3	-36.6%
PV:ElectricityProduced [GJ]	-	175.8	-
Chicago, IL (Zone 6)			
	Base Case (Annual)	Air Based PVT (Annual)	Difference (%)
Electricity:Facility [GJ]	688.4	520.5	-24.4%
Fans:Electricity [GJ]	72.9	73.0	0.1%
Cooling:Electricity [GJ]	24.3	25.5	4.9%
Gas:Facility [GJ]	1,067.3	981.2	-8.1%
Heating:Gas [GJ]	412.9	326.9	-20.8%
CO2:Facility [kg]	290,813.6	184,529.3	-36.5%
PV:ElectricityProduced [GJ]	-	169.2	-
Rochester, NY (Zone 6)			
	Base Case (Annual)	Air Based PVT (Annual)	Difference (%)
Electricity:Facility [GJ]	683.7	526.7	-23.0%
Fans:Electricity [GJ]	72.9	72.9	0.0%
Cooling:Electricity [GJ]	20.0	21.6	7.6%
Gas:Facility [GJ]	1,084.6	993.9	-8.4%
Heating:Gas [GJ]	430.2	339.5	-21.1%
CO2:Facility [kg]	290,132.4	188,530.0	-35.0%
PV:ElectricityProduced [GJ]	-	158.6	-
Boston, MA (Zone 6)			
	Base Case (Annual)	Air Based PVT (Annual)	Difference (%)
Electricity:Facility [GJ]	680.4	509.4	-25.1%
Fans:Electricity [GJ]	72.2	72.2	0.0%
Cooling:Electricity [GJ]	17.2	18.7	9.0%
Gas:Facility [GJ]	1,015.7	929.1	-8.5%
Heating:Gas [GJ]	361.4	274.8	-24.0%
CO2:Facility [kg]	285,408.4	180,572.5	-36.7%
PV:ElectricityProduced [GJ]	-	172.7	-

Table 6.28 – Energy performance comparison of quick-service restaurant with conventional HVAC system and integrated air based PV/T solar roof system, Zone 6

6.6 Cost Benefit Analysis

One way to evaluate the economic merit of the proposed air based PV/T solar roof system is to calculate its payback period. The payback period is the number of years of energy cost savings it takes to recover from the initial investment of integrating the air based PV/T solar roof system into an existing building. The following is an estimate of how much the proposed system would potentially cost and how much money it would save annually. Flagstaff, AZ from Zones 1 and 2, Atlanta, GA from Zones 3 and 4, and Minneapolis, MN from Zones 5 and 6 were chosen for the analysis.

The area of the south facing roof of the quick-service restaurant is 96 m^2 (16 m × 6 m). According to HomeDepot.com, the dimension of a Grape Solar 280-Watt Polycrystalline PV panel is 1.96 m^2 (1.96 m × 1 m) and the price per panel is $400. To cover the south facing roof will require approximately 48 PV panels and the total cost for the PV panels is $19,200 ($400 × 48). Typically, the PV panel is the most expensive portion of the air based PV/T solar roof system. The cost of adding the thermal portion is included under 'installation' in the following estimated breakdown of the building integrated rooftop solar energy system [69]:

(1) PV Panels:	$19,200 [approximately 60% of (4)]
(2) Inverter:	$3,200 [approximately 10% of (4)]
(3) Installation:	$9,600 [approximately 30% of (4)]
(4) Sum of (1),(2),(3) :	$32,000
(5) Taxes:	$3,200 [approximately 10% of (4)]
(6) Total Cost:	**$35,200**

	Quick-Service Restaurant in Flagstaff, AZ (Zone 1)		
	Energy	**Electricity**	**Gas**
(1)	Base Case (Annual Consumption) [GJ]	684.3	953.2
(2)	Air Based PV/T (Annual Consumption) [GJ]	465.1	831.1
(3)	Difference or Savings [GJ] [(1) – (2)]	219.2	122.2
(4)	Conversion to Kilowatt-Hour [kWh]	60,888.9	-
(5)	Conversion to Thousand Cubic Feet of Gas	-	115.8
(6)	Unit Price of Electricity in AZ [$ / kWh]	0.1061	-
(7)	Unit Price of Gas in AZ [$ / Thousand Cubic Feet]	-	9.33
(8)	Annual Savings of Electricity [(4) × (6)]	$6,460	-
(9)	Annual Savings of Gas [(5) × (7)]	-	$1,081
(10)	Total Annual Savings of Electricity and Gas [(8) + (9)]	$7,541	
(11)	Total Cost of Air Based PV/T	$35,200	
(12)	**Estimated Payback Period in Years [(11) / (10)]**	**4.7**	
	Quick-Service Restaurant in Atlanta, GA (Zone 3)		
	Energy	**Electricity**	**Gas**
(1)	Base Case (Annual Consumption) [GJ]	710.5	814.3
(2)	Air Based PV/T (Annual Consumption) [GJ]	512.2	758.4
(3)	Difference or Savings [GJ] [(1) – (2)]	198.3	55.9
(4)	Conversion to Kilowatt-Hour [kWh]	55,093.1	-
(5)	Conversion to Thousand Cubic Feet of Gas	-	53.0
(6)	Unit Price of Electricity in GA [$ / kWh]	0.1001	-
(7)	Unit Price of Gas in GA [$ / Thousand Cubic Feet]	-	8.05
(8)	Annual Savings of Electricity [(4) × (6)]	$5,515	-
(9)	Annual Savings of Gas [(5) × (7)]	-	$427
(10)	Total Annual Savings of Electricity and Gas [(8) + (9)]	$5,942	
(11)	Total Cost of Air Based PV/T	$35,200	
(12)	**Estimated Payback Period in Years [(11) / (10)]**	**5.9**	
	Quick-Service Restaurant in Minneapolis, MN (Zone 6)		
	Energy	**Electricity**	**Gas**
(1)	Base Case (Annual Consumption) [GJ]	685.7	1,199.3
(2)	Air Based PV/T (Annual Consumption) [GJ]	511.5	1,092.1
(3)	Difference or Savings [GJ] [(1) – (2)]	174.2	107.2
(4)	Conversion to Kilowatt-Hour [kWh]	48,397.4	-
(5)	Conversion to Thousand Cubic Feet of Gas	-	101.6
(6)	Unit Price of Electricity in MN [$ / kWh]	0.1014	-
(7)	Unit Price of Gas in MN [$ / Thousand Cubic Feet]	-	11
(8)	Annual Savings of Electricity [(4) × (6)]	$4,908	-
(9)	Annual Savings of Gas [(5) × (7)]	-	$1,118
(10)	Total Annual Savings of Electricity and Gas [(8) + (9)]	$6,026	
(11)	Total Cost of Air Based PV/T	$35,200	
(12)	**Estimated Payback Period in Years [(11) / (10)]**	**5.8**	

Table 6.29 – Summary of the payback period of the air based PV/T solar roof system in Flagstaff, AZ (Zone 1), Atlanta, GA (Zone 3), and Minneapolis, MN (Zone 6)

Tables 6.29 present the summary of the payback period of the proposed air based PV/T solar roof system integrated into a quick-service restaurant in Flagstaff, AZ (Zone 1), Atlanta, GA (Zone 3), and Minneapolis, MN (Zone 6). The unit prices for electricity and gas are the average commercial retail prices per state in August 2013 as provided by the U.S. Energy Information Administration [70][71]. The calculations show that the estimated payback period is 4.7 years in Flagstaff, AZ, 5.9 years in Atlanta, GA, and 5.8 years in Minneapolis, MN.

According to the manufacturer specifications of the Grape Solar 280-Watt Polycrystalline PV panel, there is a 'ten year limited product warranty on materials and workmanship, twenty five year warranty on >80% power output, and ten year warranty on >90% power output' [72]. Other manufactures of PV panels, such as SunPower Corp. [73] and Hanwha SolarOne Co., Ltd. [74], offers similar 25 year warranties on >80% power output. The calculations of the payback period and the warranty information regarding PV panels suggest that the proposed air based PV/T solar roof system can be a good investment as a source of renewable energy solution.

6.7 Summary

This chapter presents the various case studies which compared the annual energy performance, especially the heating performance and PV electricity production, of the air based PV/T solar roof system in six different climatic zones / 28 different cities within the United States. The annual building energy simulations showed that energy savings of gas and electricity consumption can be achieved in two types of buildings when the air based PV/T solar roof system is integrated with the existing HVAC system. The integrated air

based PV/T solar roof system achieved the highest energy savings in climatic Zones 1 and 2 which have the highest mean daily total insolation and are classified as semi-arid and desert climates. Other climatic zones within the United States also achieved gas and electricity energy savings but the annual building energy simulations suggest that gas energy savings is proportional to the mean daily winter insolation, as shown in Figures 6.5 and 6.7.

The building energy simulations also showed slight increases of electricity consumption for cooling and fans in all the case studies for the small commercial office building and most of the case studies for the quick-service restaurant except in St. George, UT and Nashville, TN. The increases of electricity consumption for cooling is due the PV panel and absorber cover of the air based PV/T solar roof system which causes higher roof surface temperatures, hence causing higher cooling loads. An example of the comparison of the outside south roof surface temperatures of the small commercial office building between the base case and integrated air based PV/T solar roof system is shown in Table 6.10. Although the building energy simulation results showed slight increases in the electric consumption for cooling and fans, the decrease in gas consumption for heating was much higher and thus offset the small increase in electric consumption.

The St. George, UT and Nashville, TN accounted for the highest cooling electricity consumption but had slight decreases when comparing the integrated air based PV/T solar roof system to the base case. Further analysis showed that the cooling coil energy consumption decreased in the early morning hours and late evening hours due to installation of the air based PV/T solar roof system which adds an extra layer of

construction on the south facing roof and helps insulate and block the warm/hot night air flow in the building.

The CFD studies presented in Chapter 5 showed that higher thermal efficiency of the air based PV/T solar roof system can be reached by a design that incorporates a shallower air channel depth, lower air mass flow rate, and a longer air channel depth. The annual building energy simulations results presented in this chapter showed that energy saving of gas and electricity can be achieved in various climates within the United States.

The small commercial office building showed that in Zones 1 and 2, an average of 31.1% of heating gas consumption was saved and the highest annual PV electricity at an average of 277.4 GJ was produced. In Zones 3 and 4, an average of 22.6% was saved for heating gas consumption and an average of 231.7 GJ of PV electricity was produced. In Zones 5 and 6, an average of 11% was saved for heating gas consumption and an average of 201.7 GJ of PV electricity was produced, which was lowest between the zones.

As for the quick-service restaurant, Zones 1 and 2 showed an average of 40.7% saving of heat gas consumption and produced an average of 230.9 GJ in PV electricity. In Zones 3 and 4, an average of 32.7% was saved for heating gas consumption and an average of 192.9 GJ of PV electricity was produced. In Zones 5 and 6, an average of 21.3% was saved for heating gas consumption and an average of 167.9 GJ of PV electricity was produced, which was also the lowest between the zones.

A cost benefit analysis is also presented in this chapter to evaluate the economic merit of the proposed air based PV/T solar roof system. Calculations show that the estimated payback period in Flagstaff, AZ (Zone 1), Atlanta, GA (Zone 3), and

Minneapolis, MN (Zone 6) are all less than six years. Considering the fact that the current manufacturer warranties of PV panels are between 10 to 25 years, the short payback periods suggest that the proposed air based PV/T solar roof system can be a good investment as a source of renewable energy solution. The proposed air based PV/T solar roof system is intended for where the PV is not only producing electricity, but also converts solar radiation energy into thermal energy. Considering the fact that the demand for solar heat and solar electricity are often supplementary, a system that simultaneously produces heat and power is a positive aspect of the air based PV/T solar roof system proposed and modeled in this dissertation. However, the annual building energy simulations showed that the outlet temperatures do not meet the required temperatures for heating, as shown in examples of Figure 6.4 and 6.6, Therefore, it is important to note that that the proposed air based PV/T solar roof system should be considered as a low energy solution that supplements the existing HVAC system rather than being responsible for handling the entire heating load of a building.

Chapter 7. Conclusion

An air based photovoltaic thermal (PV/T) solar roof system combines the technologies of electricity generating PV cells and active solar heating to supplement the electricity and heating loads of buildings and potentially reduce energy consumption. Many researchers have investigated the merits of this system but there is a lack of research on the energy efficiency of the proposed air based PV/T solar energy system when applied as a building application in various climates. This study provides information on the analysis of the energy efficiency of an air based PV/T solar roof system when integrated with a building's existing HVAC system in various climates within the United States. Specifically, this study utilized a numerical analysis tool like a computational fluid dynamics (CFD) program to assist in the investigation of detailed fluid flow and heat transfer within the PV/T system. Using the EnergyPlus program, it also performed whole building annual energy simulations using system performance information obtained from the CFD work to obtain a comprehensive insight toward understanding PV/T system performance in various climates within the United States.

The CFD studies showed that having the shallowest air channel depth, within the range provided by the Solar Rating and Certification Corporation (SRCC) and having the lowest air mass flow rate within the range provided by the U.S. Department of Energy (DOE), led to the highest system thermal efficiency. The CFD studies further indicate that different combinations of air channel depth and air mass flow rates result in significant

differences in terms of thermal efficiency which ranged from 13.6% to 47.1% as well as average outlet temperatures which ranged between 25.2℃ to 47.7℃.

Another key parameter that affects the thermal efficiency of the air based PV/T solar roof system is the air channel length. Further CFD studies showed that, with proper air channel depth and air mass flow rate, increasing the distance between the inlet and the outlet by using vertical and horizontal baffles can increase the system's thermal efficiency. Regardless of the baffle orientation and the level of incident solar radiations being absorbed on the air based PV/T solar roof system, the thermal conversion efficiency was shown to ultimately converge to around 70%. This is also an indication that the performance of the proposed air based PV/T solar roof system eventually hits a maximum level, and that the level of incident solar radiation does not play a significant role when the system's thermal efficiency is near the maximum range.

Analyzing the annual energy performance of the air based PV/T solar roof system was conducted by taking the analysis from the CFD studies and inputting the information into two EnergyPlus reference building models, a small commercial office building and a quick-service restaurant. Six different climatic zones were divided within the United States, regarding the amount of insolation and the need for space heating and the local weather information of 28 different cities were used to run the annual building energy simulations. These cities were chosen to represent a wide range of climates in order to test the applicability and performance of the PV/T system under different operating conditions such as exterior temperature and available solar insolation. The results showed that climatic Zones 1 and 2, which have the highest mean daily total insolation, achieved the highest

energy savings. In Zones 1 and 2, the small commercial office building showed an average of 31.1% in heating gas consumption savings and an average of 277.4 GJ in annual PV electricity production. As for the quick-service restaurant, an average of 40.7% of heating gas consumption was saved and an average of 230.9 GJ in PV electricity was produced in Zones 1 and 2. The findings demonstrated that energy savings in gas and electricity consumption can be achieved in both types of buildings and in all the 6 climatic zones within the United States when the air based PV/T solar roof system is integrated with the existing HVAC system. Specifically, the results showed that the heating or gas consumption of a building is positively related to the mean daily winter insolation and significant reductions in gas consumption were achievable in all climates. There were also slight increases of electricity consumption for cooling and fans but the results showed that the small increase can be offset by the significantly larger reduction in gas consumption for heating.

There are some limitations with the EnergyPlus model as it does not include models for charge controllers, batteries, or power-point trackers. The entire electrical system is assumed to operate in ideal ways. PV panels are assumed to always operate at the maximum power point. For a variety of reasons, actual installations of PV panels are often observed to exhibit system-level problems that significantly reduce electricity production. Therefore, the results should be considered a method of bracketing the upper end of electricity production rather than an accurate prediction of what the PV panels will produce in a real installation.

A cost benefit analysis was also performed to evaluate the economic merit of the proposed air based PV/T solar roof system. Calculations showed that the estimated payback period in Flagstaff, AZ (Zone 1), Atlanta, GA (Zone 3), and Minneapolis, MN (Zone 6) are all less than six years. Considering the fact that the current manufacture warranties of PV panels are between 10 to 25 years, the short payback period of the PV panels suggest that the proposed air based PV/T solar roof system can be a good investment as a source of renewable energy solution.

The study suggests that the proposed air based PV/T solar roof system should be considered as a low energy solution. However, it is important to note that it is not intended to handle the entire heating load of a building but rather to supplement the existing HVAC system. The following are the related issues that could build on the results of this study and provide for further lines of research.

Configuration Studies of Integrating the Existing HVAC Air Loop: The proposed air based PV/T solar roof system, within the EnergyPlus model, acts as a preheater of the outside air and is integrated with the existing HVAC air loop. Exploring the option of taking the return air and reheating it through the proposed system may provide additional opportunities to explore energy savings.

Combined Air and Water Heat Transfer: The proposed air based PV/T solar roof system, within the EnergyPlus model, can only be integrated with the existing HVAC air loop. Since there is some equipment within EnergyPlus that operate outside of this EnergyPlus-specific concept of air loop, a model that merges the PV/T output with a heat

pump, a water heater, or an absorption cooling system may provide additional opportunities to explore energy savings.

Development of a More Detailed EnergyPlus Model: The proposed air based PV/T solar roof system, within the EnergyPlus model, is based on user-defined efficiencies and currently has limitations modeling vertical and horizontal baffles within the air channel. A more detailed EnergyPlus model with layer-by-layer descriptions will help provide more detailed information regarding to outlet temperature and fan energy consumption.

CFD Simulations of Inlet Velocity vs. Air Channel Length: Additional CFD simulations of different inlet velocities for differing air channel length will help determine the length requirements for various velocities and performance ceiling levels. Additional simulations will help in producing correlations that might be used to predict the potential performance of a system as a function of inlet velocity, air channel depth, and air channel length.

Configuration Studies of the Roof: This study used a fixed roof definition in examining the thermal efficiency implications of the air based PV/T solar roof system. Studying various roof configurations such as roof slope, different amounts of insulation, and different materials for the vertical and horizontal baffles may be beneficial as the factors may have different effects on the thermal efficiency of the air based PV/T solar roof system.

Experimental Study: Comparison of the CFD studies to measured data from an experimental study would provide further confirmation that the proposed air based PV/T solar roof system is valid. Such validation of the CFD results will also enable researchers to obtain inputs for EnergyPlus without running CFD studies. An experimental study would also assist in further development of the EnergyPlus model for the PV/T system since this system model currently does not provide layer by layer construction analysis.

In summary, this study provided an in-depth analysis of the operating condition design of air based PV/T solar roof systems. There has been a significant amount of research on air based PV/T solar energy systems over the past 30 years including analytical and numerical models, experimental work, and the qualitative evaluation of thermal output. However, there are no studies regarding the energy efficiency of this air based PV/T solar energy system when applied as a building application in various climates. Furthermore, there is a lack of annual building energy simulation data for these systems. This is very important information when attempting to calculate the overall energy savings and payback period. This study helps fill this void.

The overall findings of this dissertation showed that the proposed air based PV/T solar roof system has the potential to save heating gas consumption and produce PV electricity simultaneously. The findings also showed that the proposed system can be beneficial in all the climatic zones throughout the United States. This led to the main conclusion of this study that an air based PV/T solar roof system can be used to supplement the existing HVAC systems in buildings as part of a low energy solution as well as serving as a source of renewable energy.

References

[1] United States Department of Energy (2009). 2008 Buildings Energy Data Book (2011, October), <buildingsdatabook.eere.energy.gov/docs/DataBooks/2008_BEDB_Updated.pdf>.

[2] United States Energy Information Administration (EIA), Annual Energy Review 2009 (2011, October), <www.eia.doe.gov>.

[3] United States Department of Energy (2011). Active Solar Heating (2011, October), <http://www.energysavers.gov/your_home/space_heating_cooling/index.cfm/mytopic=12490>.

[4] United States Department of Energy (2013). Energy Basics – Photovoltaics (2013, January), <http://www.eere.energy.gov/basics/renewable_energy/photovoltaics.html>.

[5] Parker, B.F., Lindley, M.R., Colliver, D.G., and W.E. Murphy (1993). Thermal performance of three solar air heaters. Solar Energy 6, 467–479.

[6] American Society of Heating, Refrigerating and Air-Conditioning Engineers, Inc. (1989). ASHRAE Standard 96-1980 (RA 89): Methods of Testing to Determine the Thermal Performance of Unglazed Flat-Plate Liquid-Type Solar Collectors. Atlanta, GA.

[7] American Society of Heating, Refrigerating and Air-Conditioning Engineers, Inc. (1991). ASHARE Standard 93-1986 (RA 91) – Methods of Testing to Determine the Thermal Performance of Solar Collectors. Atlanta, GA.

[8] Solar Rating and Certification Corporation (2004). Directory of SRCC Certified Solar Collector Ratings, OG 100. Cocoa, Florida: Solar Rating and Certification Corporation.

[9] Charalambous, P., Maidment, G., Kalagirou, S., and K. Yiakoumetti (2007). Photovoltaic thermal (PV/T) collectors: A review. Applied Thermal Engineering 27(2-3), 275-286.

[10] Kalogirou, S. (2004). Solar thermal collectors and applications. Progress in Energy and Combustion Science 30(3), 231-295.

[11] Zondag, H. (2008). Flat-plate PV-Thermal collectors and systems: A review. Renewable and Sustainable Energy Reviews 12(4), 891-959.

[12] EnergyPlus (2012). EnergyPlus Engineering Reference – The Reference to EnergyPlus Calculations.

[13] United States Department of Energy (2013). EnergyPlus Energy Simulation Software (January, 2013), < http://apps1.eere.energy.gov/buildings/energyplus>.

[14] Zondag, H., De Vries, D., Van Helden, W., Van Zolingen, R., and A. Van Steenhoven (2002). The thermal and electrical yield of a PV-Thermal collector. Solar Energy 72(2), 113-128.

[15] Charalambous, P., Maidment, G., Kalagirou, S., and K. Yiakoumetti (2007). Photovoltaic thermal (PV/T) collectors: A review. Applied Thermal Engineering 27(2-3), 275-286.

[16] Zondag, H. (2008). Flat-plate PV-Thermal collectors and systems: A review. Renewable and Sustainable Energy Reviews 12(4), 891-959.

[17] Kim, J., and J. Kim (2012). Comparison of electrical and thermal performances of glazed and unglazed PVT collectors. International Journal of Photoenergy 2012, Article ID 957847, 7 pages.

[18] Bhargava, A., Garg, H., and R. Agarwal (1991). Study of a hybrid solar system – solar air heater combined with solar cells. Energy Conversion and Management 31(5), 471-479.

[19] Sopian, K., Yigit, K., Liu, H., Kakac, S., and T. Veziroglu (1996). Performance analysis of photovoltaic thermal air heaters. Energy Conversion and Management 37(11), 1657-1670.

[20] Garg, H., and R. Adhikari (1999). System performance studies on a photovoltaic/thermal (PV/T) air heating collector. Renewable Energy 16(1-4), 725-730.

[21] Hegazy, A. (2000). Comparative study of the performances of four photovoltaic/thermal solar air collectors. Energy Conversion and Management 41(8), 861-881.

[22] Tonui, J. and Y. Tripanagnostopoulos (2007). Air-cooled PV/T solar collectors with low cost performance improvements. Solar Energy 81(4), 498-511.

[23] Sarhaddi, F., Farahat, S., Ajam, H., Behzadmehr, A., and M. Adeli (2010). An improved thermal and electrical model for a solar photovoltaic thermal (PV/T) air collector. Applied Energy 87(7), 2328-2339.

[24] Prakash, J. (1994). Transient analysis of a photovoltaic-thermal solar collector for co-generation of electricity and hot air/water. Energy Conversion and Management, 35(11), 967-972.

[25] Chen, Y., Galal, K., and A. Athienitis (2010). Modeling, design and thermal performance of a BIPV/T system thermally coupled with a ventilated concrete slab in a low energy solar house: Part 1, BIPV/T system and house energy concept. Solar Energy 84(11), 1908-1919.

[26] Hegazy, A. (1999). Optimum channel geometry for solar air heaters of conventional design and constant flow operation. Energy Conversion and Management 40(7), 757-774.

[27] Garg, H., and R. Adhikari (1997). Conventional hybrid photovoltaic/thermal (PV/T) air heating collectors: steady-state simulation. Renewable Energy 11(3), 363-385.

[28] Candanedo, L., Athienitis, A., Candanedo, J., O'Brien, W., and Y. Chen (2010). Transient and steady state models for open-loop air-based BIPV/T systems. ASHRAE Transactions 116(1), 600-612.

[29] Dubey, S., Sandhu, G., and G. Tiwari (2009). Analytical expression for electrical efficiency of PV/T hybrid air collector. Applied Energy 86(5), 697-705.

[30] Aste, N., Chiesa, G., and F. Verri (2008). Design, development of performance monitoring of a photovoltaic-thermal (PVT) air collector. Renewable Energy 33(5), 914-927.

[31] Zondag, H., Vries, D., Van Hendel, W., Van Zolingen, R., and A. Van Steenhoven (2003). The yield of different combined PV–thermal collector designs. Solar Energy 74(3), 253–269.

[32] Sandnes, B. and J. Rekstad (2002). A photovoltaic/thermal (PV/T) collector with a polymer absorber plate. Experimental study and analytical model. Solar Energy 72(1), 63–73.

[33] Fujisawa, T. and T. Tani (1997). Annual energy evaluation on photovoltaic–thermal hybrid collector. Solar Energy Materials and Solar Cells 47(1–4), 135–148.

[34] Coventry, J. and K. Lovegrove (2003). Development of an approach to compare the 'value' of electrical and thermal output from a domestic PV/thermal system. Solar Energy 75(1), 63-72.

[35] TRNSYS – Transient System Simulation Tool (2013). What is TRNSYS? (2013, March), <http://www.trnsys.com>.

[36] Bloem, J. (2008). Evaluation of a PV-integrated building application in a well-controlled outdoor test environment. Building and Environment 43(2), 205-216.

[37] Bosanac, M., Sorensen, B., Katic, I., Sorensen, H., Nielsen, B., and J. Badran (2003). Photovoltaic/thermal solar collectors and their potential in Denmark. Final Report, EFP Project 1713/00-0014, <http://www.solenergi.dk/rapporter/pvtpotentialindenmark.pdf>.

[38] Kalogirou, S. (2001). Use of TRNSYS for modeling and simulation of a hybrid PV–thermal solar system for Cyprus. Renewable Energy 23(2), 247–260.

[39] King, D., Boyson, W., and J. Kratochvill (2004). Photovoltaic Array Performance Model. Sandia National Laboratory. Albuquerque, NM.

[40] Duffie, J. and W. Beckman (1991). Solar Engineering of Thermal Processes, Second Edition. New York: Wiley-Interscience.

[41] Eicker, U. (2003). Solar Technologies for Buildings. Chichester, UK: John Wiley and Sons, Inc.

[42] ANSYS, Inc. (2011). ANSYS Fluent User's Guide (April, 2013), <http://cdlab2.fluid.tuwien.ac.at/LEHRE/TURB/Fluent.Inc/v140/flu_ug.pdf>.

[43] EnergyPlus (2012). Input Output Reference – The Encyclopedic Reference to EnergyPlus Input and Output.

[44] Perez, R., Ineichen, P., Seals, R., Michalsky, J., and R. Stewart (1990). Modeling daylight availability and irradiance components from direct and global irradiance. Solar Energy 44, 271-289.

[45] Groth, C., and M. Lokmanhekim (1969). Shadow – A new technique for the calculation of shadow shapes and areas by digital computer. 2nd Hawaii International Conference on System Sciences. Honolulu, HI, Jan. 22-24, 1969.

[46] Walton, G. (1983). The Thermal Analysis Research Program Reference Manual. National Bureau of Standards (now National Institute of Standards and Technology - NIST).

[47] King, D. (1996). Photovoltaic Module and Array Performance Characterization Methods for All System Operating Conditions. Sandia National Laboratory. Albuquerque, NM.

[48] Barker, G., and P. Norton (2003). Predicting Long-Term Performance of Photovoltaic Arrays Using Short-Term Test Data and an Annual Simulation Tool. National Renewable Energy Laboratory (NREL). Golden, Colorado.

[49] McClellan, T., and C. Pedersen (1997). Investigation of outside heat balance models for use in a heat balance cooling load calculation. ASHRAE Transactions, 103(2), 469 – 484.

[50] Griffith B., and P. Ellis (2004). Photovoltaic and Solar Thermal Modeling with EnergyPlus Calculation Engine. National Renewable Energy Laboratory (NREL). Golden, Colorado.

[51] United States Department of Energy (2013). EnergyPlus Energy Simulation Software (January, 2013), <http://apps1.eere.energy.gov/buildings/energyplus>.

[52] Chapman, A. (1994). Heat Transfer, Fourth Edition, New York: Macmillan Publishing Company.

[53] Lienhard, J. (1981). A Heat Transfer Texbook. Englewood Cliffs, NJ: Prentice-Hall, Inc.

[54] United States Department of Energy (2013). Building Energy Codes Program – Development (April, 2013), <http://www.energycodes.gov/development>.

[55] Field, K., Deru, M., and D. Studer (2010). Using DOE commercial building for simulation studies. National Renewable Energy Laboratory (NREL). Golden, Colorado.

[56] United States Energy Information Administration (2007). Energy Independence and Security Act of 2007. U.S. Congress. Washington D.C.

[57] Deru, M., Field, K., Studer, D., Denne, K., Griffith, B., Torcellini, P., Liu, B., Halverson, M., Winiarshi, D., Rosenberg, M., Yazdanian, M., Huang, J., and D. Crawley (2011). U.S. Department of Energy Commercial Reference Building Models of the National Building Stock. National Renewable Energy Laboratory (NREL). Golden, Colorado.

[58] Brown, S. (2007). Dedicated Outdoor Air System of Commercial Kitchen Ventilation. ASHRAE Journal 49(7), 24 – 35.

[59] California Energy Commission (2004). Design Guide 2 Improving Commercial Kitchen Ventilation System Performance: Optimizing Makeup Air, Sacramento, CA.

[60] Fisher, D. (2003). Predicting Energy Consumption. ASHRAE Journal 45(6), K8–K13.

[61] Smith, V., Young, R., Spata, A., and D. Fisher (1999). Virtual vs. Real: Modeling the Energy Performance of a Quick-Service Restaurant. AHRAE Transactions 1999, 105.

[62] United States Department of Energy (2013). Building Energy Codes Program – Commercial Prototype Building Models (April, 2013), <http://www.energycodes.gov/development/commercial/90.1_models>.

[63] Crawley, D., Lawrie, L., Winkelmann, F., Buhl, W., Huang, Y., Pedersen, C., Strand, R., Liesen, R., Fisher, D., Witte, M., and J. Glazer (2001). EnergyPlus: creating a

new-generation building energy simulation program. Energy and Buildings 33(4), 319-331.

[64] Jones, I. R. (1974). Solar heating and cooling of buildings technical and economic considerations: A report by TRW. The Workshop on Solar Heating and Cooling of Buildings prepared for the National Science Foundation Research Applied to National Needs Program. Washington D.C., Jun. 17-19, 1974.

[65] Kornher, S., and A. Zaugg (1984). The complete handbook of solar air heating systems. Emmaus, PA: Rodale Press.

[66] EnergyPlus Energy Simulation Software (2013). Weather Data – North and Central America WMO Region 4: USA (September, 2013), <http://apps1.eere.energy.gov/buildings/energyplus/cfm/weather_data3.cfm/region=4_north_and_central_america_wmo_region_4/country=1_usa/cname=USA>.

[67] King, D., Kratochvil, J., and W. Boyson (1997). Temperature coefficients for PV modules and arrays: measurement methods, difficulties, and results. 26th IEEE Photovoltaic Specialists Conference. Anaheim, CA, Sept 29-Oct 3, 1997.

[68] National Renewable Energy Laboratory (NREL) (2013). Renewable Resource Data Center – PVWatts (November, 2013), <http://www.nrel.gov/rredc/pvwatts/changing_parameters.html>.

[69] SolarPower.org (2013). Solar Power Installation Breakdown (November, 2013), <http://solarpower.org/articles/solar-power-installation-breakdown>.

[70] U.S. Energy Information Administration (EIA) (2013). Electric Power Monthly (November, 2013), <http://www.eia.gov/electricity/monthly/epm_table_grapher.cfm?t=epmt_5_6_a>.

[71] U.S. Energy Information Administration (EIA) (2013). Natural Gas Prices (November, 2013), <http://www.eia.gov/dnav/ng/ng_pri_sum_dcu_nus_m.htm>.

[72] Grape Solar (2013). SPECS - 280W POLY GS-P-280-FAB1 (November, 2013), <http://www.grapesolar.com/specs-280w-poly-gs-p-280-fab1.html>.

[73] SunPower Corp. (2013). SunPower Product Warranties and Manuals (November, 2013), <http://us.sunpowercorp.com/support/warranty>.

[74] Hanwha SolarOne Co., Ltd. (2013). Products Warranty (November, 2013), <http://www.hanwha-solarone.com/products/warranty>.